



VCU

Virginia Commonwealth University
VCU Scholars Compass

Theses and Dissertations

Graduate School

2017

Podocyte Dedifferentiation and Glomerular Injury Mediated by Lysosome Dysfunction: Role of Acid Ceramidase

Guangbi Li

Follow this and additional works at: <https://scholarscompass.vcu.edu/etd>

© The Author

Downloaded from

<https://scholarscompass.vcu.edu/etd/5169>

This Dissertation is brought to you for free and open access by the Graduate School at VCU Scholars Compass. It has been accepted for inclusion in Theses and Dissertations by an authorized administrator of VCU Scholars Compass. For more information, please contact libcompass@vcu.edu.

Podocyte Dedifferentiation and Glomerular Injury Mediated by Lysosome Dysfunction: Role of Acid Ceramidase

A dissertation submitted in partial fulfillment of the requirements for the degree of Doctor of
Philosophy at the Virginia Commonwealth University

by

Guangbi Li

Master of Science in Pharmacology and Toxicology
Virginia Commonwealth University, 2015

Advisor: Pin-Lan Li, MD, PhD

Professor, Pharmacology and Toxicology

Virginia Commonwealth University

Richmond, Virginia

December 2017

ACKNOWLEDGMENTS

This dissertation could not be completed without the support and help of departmental leaders, professors, colleagues, classmates and my family. To those whom I have not mentioned by name below, I thank you all for your support, assistance and encouragement throughout my studies over the last 4 years at the Virginia Commonwealth University.

I would like to first express my sincerest thanks to my advisor, Dr. Pin-Lan Li for, providing me with the opportunity to work on this project for my dissertation. I feel I have been so fortunate to work in her laboratory, where she has taught me how to work thoughtfully, how to be productive, and how to commit myself to scientific research. I will never forget this incredible journey as a graduate student in her laboratory that is full of contagious and motivational joy and enthusiasm Dr. Li has brought to me. From the bottom of my heart, I also appreciate her patience, compassion and professionalism as well as new ideas with strong funding support, which make my learning experience joyful, productive and stimulating.

I am very grateful to Dr. Krishna Boini and Dr. Justine Abais-Battad for their guidance and help at beginning of my research in this laboratory. I especially appreciate Mr. Min Xia for teaching me many basic and advanced techniques or skills in kidney studies that ensure the completion of this dissertation. I also really appreciate Dr. Xinxu Yuan and Mrs. Hannah Lohner for their help in cross-breeding and genotyping podocyte-specific *Asah1* gene knockout mice and their littermates, Dr. Qinghua Zhang and Dr. Cai-Xia Li for their help in some confocal microscopy and immunofluorescent staining experiments, and Dr. Joseph Ritter and Miss Sara Dempsey for their helps in tissue lipid measurements and LC-MS/MS analysis of sphingolipids. Moreover, many thanks to other current and past Li lab members, Dr. Owais Bhat, Dr. Yu Chen, Miss Jinni Hong, Dr. Yang Zhang, Dr. Xiang Li, and Dr. Zhida Chen for sharing with me their

expertise and graduate study experience and for making the lab such a wonderful and happy place to work every day.

My sincere thanks to my committee members, Dr. Todd Gehr, Dr. Scott Walsh, Dr. Ningjun Li, and Dr. Joseph Ritter for their constructive criticism and advice in discussing my research proposal and progress as well as guidance and suggestions for the preparation of this dissertation.

I am also deeply grateful to Dr. William Dewey and Dr. Hamid Akbarali, for giving me this wonderful opportunity to be a graduate student in the Department of Pharmacology and Toxicology and for their tremendous support and encouragement during my studies and research. Also, many thanks to all the staff of the Department, especially Mrs. Sheryol Cox, for her kindness and help.

Finally, my greatest thanks go to my parents for their love, understanding and support throughout these years of my graduate study.

TABLE OF CONTENTS

ACKNOWLEDGMENTS.....	II
LIST OF FIGURES.....	VII
LIST OF ABBREVIATIONS.....	IX
ABSTRACT.....	XI

CHAPTER ONE: INTRODUCTION.....	1
1.1 Podocyte dedifferentiation and glomerular diseases.....	1
1.2 Autophagic deficiency and podocyte dedifferentiation	5
1.3 Ceramide metabolism and lysosome-dependent autophagic flux.....	7
1.4 Aims of the study.....	9

CHAPTER TWO: GENERAL METHODS.....	12
2.1 Cell culture.....	12
2.2 Lipid-mediated transfection.....	12
2.3 Nucleofection.....	13
2.4 Western blot analysis.....	13
2.5 Immunofluorescence microscopy.....	14
2.6 GCaMP3 Ca ²⁺ imaging.....	15
2.7 Whole-cell patch clamp recording.....	15
2.8 Isolation of lysosomes from podocytes.....	16
2.9 Whole-lysosome patch clamp recording.....	17
2.10 Podocyte-specific <i>Asah1</i> gene knockout mouse model.....	20
2.11 Mouse genotyping.....	21
2.12 β -galactosidase staining.....	22
2.13 Isolation of glomeruli for LC-MS/MS.....	22
2.14 LC-MS/MS analysis.....	23
2.15 Glomerular isolation and imaging.....	23
2.16 Immunohistochemistry.....	25
2.17 Measurements of urinary protein and albumin excretions.....	26

2.18	Glomerular morphological examination.....	26
2.19	Statistical analysis.....	27
CHAPTER THREE.....		28
<i>Podocyte dedifferentiation induced by lysosome dysfunction and associated autophagic deficiency</i>		
3.1	Enhanced podocyte dedifferentiation by lysosome function inhibition.....	28
3.2	Confocal microscopy of podocyte dedifferentiation during lysosome function inhibition.....	28
3.3	Deficiency of autophagic flux during lysosome function inhibition.....	29
3.4	Attenuation of podocyte dedifferentiation by Sp-1 inhibition of autophagosome formation.....	29
3.5	Failure of Nrf2 gene silencing to alter podocyte dedifferentiation enhanced by lysosome function inhibition.....	30
3.6	No changes in enhanced podocyte dedifferentiation by inhibition of NF-κB-mediated transcriptional regulation.....	31
3.7	Effects of CDK1 inhibition on podocyte dedifferentiation enhancement induced by lysosome dysfunction.....	32
3.8	Reduction of p62 phosphorylation during lysosome function inhibition.....	33
CHAPTER FOUR.....		42
<i>Contribution of altered ceramide metabolism via acid ceramidase (AC) to lysosome dysfunction through reduced TRPML1 channel activity</i>		
4.1	Lysosome trafficking and fusion to autophagosome regulated by AC in podocytes.....	42
4.2	Lysosome trafficking and fusion to MVBs regulated by AC in podocytes.....	43
4.3	TRPML1 channel-mediated Ca ²⁺ release detected by GCaMP3 in podocytes.....	44
4.4	Characterization of lysosome-derived Ca ²⁺ release through TRPML1 channel.....	45
4.5	Inhibition of AC blocked Ca ²⁺ release through TRPML1 channel in podocytes.....	45
4.6	Establishing patch clamp recording using Port-A-Patch.....	46

4.7	Regulation of PANX1 channel activity by adipokines.....	48
4.8	Characterization of enlarged lysosomes isolated from podocytes.....	49
4.9	Enhancement of TRPML1 channel activity by sphingosine.....	50
CHAPTER FIVE.....		66
<i>Albuminuria and podocytopathy induced by podocyte-specific gene deletion of AC α subunit</i>		
5.1	Characterization of podocyte-specific gene deletion of AC α subunit in <i>Asah1^{fl/fl}/Podo^{Cre}</i> mice.....	66
5.2	Ceramide accumulation in glomeruli of <i>Asah1^{fl/fl}/Podo^{Cre}</i> mice.....	67
5.3	Severe proteinuria and albuminuria induced by podocyte-specific gene deletion of AC α subunit.....	68
5.4	Podocyte-specific gene deletion of AC α subunit increased permeability to albumin in isolated glomeruli.....	69
5.5	Undetectable glomerular sclerosis in <i>Asah1^{fl/fl}/Podo^{Cre}</i> mice.....	70
5.6	Hypoalbuminemia and edema induced by podocyte-specific gene deletion of AC α subunit.....	70
5.7	Ultrastructural changes of podocytes in <i>Asah1^{fl/fl}/Podo^{Cre}</i> mice.....	70
5.8	Resistance of podocytopathy in <i>Asah1^{fl/fl}/Podo^{Cre}</i> mice to corticosteroid treatment.....	71
5.9	Dystroglycans in <i>Asah1^{fl/fl}/Podo^{Cre}</i> mice.....	71
CHAPTER SIX: DISCUSSION.....		85
6.1	Enhanced podocyte dedifferentiation associated with autophagic deficiency due to lysosome dysfunction.....	85
6.2	Deficient lysosome trafficking in response to altered ceramide metabolism and associated inhibition of TRPML1 channel activity.....	90
6.3	Severe podocyte dysfunction and albuminuria induced by podocyte-specific gene knockout of acid ceramidase α subunit.....	94
REFERENCES.....		101
VITA.....		126

LIST OF FIGURES

Figure 1. The working hypothesis.....	11
Figure 2. Enhanced podocyte dedifferentiation by lysosome function inhibition.....	34
Figure 3. Confocal microscopy of podocyte dedifferentiation during lysosome Function inhibition.....	35
Figure 4. Deficiency of autophagic flux during lysosome function inhibition.....	36
Figure 5. Attenuation of podocyte dedifferentiation by Sp-1 inhibition of autophagosome formation.....	37
Figure 6. Failure of Nrf2 gene silencing to alter podocyte dedifferentiation enhanced by lysosome function inhibition.....	38
Figure 7. No changes in enhanced podocyte dedifferentiation by inhibition of NF- κ B-mediated transcriptional regulation.....	39
Figure 8. Effects of CDK1 inhibition on podocyte dedifferentiation enhancement induced by lysosome dysfunction.....	40
Figure 9. Reduction of p62 phosphorylation during lysosome function inhibition.....	41
Figure 10. Lysosome trafficking and fusion to autophagosome regulated by acid ceramidase in podocytes.....	52
Figure 11. Lysosome trafficking and fusion to MVBs regulated by acid ceramidase in podocytes.....	53
Figure 12. TRPML1 channel-mediated Ca^{2+} release detected by GCaMP3 in podocytes.....	54
Figure 13. Characterization of lysosome-derived Ca^{2+} release through TRPML1 channel.....	55
Figure 14. Inhibition of AC blocked Ca^{2+} release through TRPML1 channel in podocytes.....	56
Figure 15. Sphingosine induced Ca^{2+} release through TRPML1 channel in podocytes.....	57

Figure 16. Expression of PANXs in cultured podocytes.....	58
Figure 17. Recording and pharmacological inhibition of PANX1 channel activity in podocytes.....	59
Figure 18. Anion permeability of PANX1 channels.....	60
Figure 19. Concentration-dependent enhancement of PANX1 channel activity by visfatin.....	61
Figure 20. Concentration-dependent inhibition of PANX1 channel activity by adiponectin.....	62
Figure 21. Characterization of lysosomes isolated from murine podocytes.....	63
Figure 22. Concentration-dependent activation of TRPML1 channel activity by ML-SA1.....	64
Figure 23. Regulation of TRPML1 channel activity by sphingolipids.....	65
Figure 24. Characterization of <i>Asah1^{fl/fl}/Podo^{Cre}</i> mice.....	73
Figure 25. Confirmation of podocyte-specific expression of Cre recombinase.....	74
Figure 26. Ceramide accumulation in glomeruli of <i>Asah1^{fl/fl}/Podo^{Cre}</i> mice.....	75
Figure 27. Severe proteinuria and albuminuria in <i>Asah1^{fl/fl}/Podo^{Cre}</i> mice.....	76
Figure 28. Development of proteinuria and albuminuria in <i>Asah1^{fl/fl}/Podo^{Cre}</i> mice.....	77
Figure 29. Glomerular permeability to albumin increased in <i>Asah1^{fl/fl}/Podo^{Cre}</i> mice.....	78
Figure 30. Undetectable glomerular morphological changes in <i>Asah1^{fl/fl}/Podo^{Cre}</i> mice under light microscope.....	79
Figure 31. Hypoalbuminemia and edema in <i>Asah1^{fl/fl}/Podo^{Cre}</i> mice.....	80
Figure 32. Ultrastructural changes of podocytes in <i>Asah1^{fl/fl}/Podo^{Cre}</i> mice.....	81
Figure 33. Resistance of podocytopathy in <i>Asah1^{fl/fl}/Podo^{Cre}</i> mice to dexamethasone treatment.....	82
Figure 34. Resistance of podocytopathy in <i>Asah1^{fl/fl}/Podo^{Cre}</i> mice to rapamycin treatment.....	83
Figure 35. Dystroglycans in <i>Asah1^{fl/fl}/Podo^{Cre}</i> mice.....	84

LIST OF ABBREVIATIONS

α -SMA	α -smooth muscle actin
AC	acid ceramidase
ALP	autophagolysosome
AP	autophagosome
ASC	adult stem cell
ASM	acid sphingomyelinase
ATP	adenosine triphosphate
Baf	Baf A1
Bor	Bortezomib
CAEC	coronary arterial endothelial cell
Carm	Carmofur
CASMC	coronary arterial smooth muscle cell
CBX	carbenoxolone
CDK1	cyclin-dependent kinase 1
Cer	ceramide
DEDD	domain-containing DNA-binding protein
DEX	dexamethasone
DG	dystroglycan
DKD	diabetic kidney disease
DYSF	dysferlin
EGFP	enhanced green fluorescent protein
EMT	epithelial-to-mesenchymal transition
ESC	embryonic stem cell
ESRD	end-stage renal disease
FSGS	focal segmental glomerular sclerosis
FSP-1	fibroblast-specific protein 1
GDI	glomerular damage index
GFP	green fluorescent protein
GH	growth hormone
GPEC	glomerular parietal epithelial cell
GPN	glycyl-L-phenylalanine 2-naphthylamide
Hcys	homocysteine
hHcys	hyperhomocysteinemia
HIVAN	HIV-associated nephropathy
lacZ	β -galactosidase

Lamp-1	lysosome-associated membrane protein 1
LC-MS/MS	liquid chromatography tandem mass spectrometry
MCD	minimal change disease
MET	mesenchymal-to-epithelial transition
ML-SA1	mucolipin synthetic agonist 1
MR	membrane raft
MVB	multivesicular body
NAADP	nicotinic acid adenine dinucleotide phosphate
NFκ	nuclear factor κ
Nox	NADHP oxidase
Nrf2	nuclear factor erythroid 2-related factor 2
PANX1	pannexin-1
PAS	periodic acid–Schiff
PBNC	probenecid
P-cad	P-cadherin
PI(3,5)P2	phosphatidylinositol 3,5-bisphosphate
RFP	red fluorescent protein
RO	RO-3306
RPM	Rapamycin
S1P	sphingosine-1-phosphate
siRNA	small interfering RNA
SM	sphingomyelin
SP-1	spaudin-1
Sph	sphingosine
TEM	transmission electron microscopy
TGF-β	transforming growth factor-β
TRPML1	transient receptor potential-mucolipin-1
VAMP-2	vesicle-associated membrane protein 2
V-ATPase	vacuolar-type H ⁺ -ATPase
VPS16	vacuolar protein sorting-associated protein 16
ZO-1	zonula occludens-1

ABSTRACT**PODOCYTE DEDIFFERENTIATION AND GLOMERULAR INJURY MEDIATED BY
LYSOSOME DYSFUNCTION: ROLE OF ACID CERAMIDASE**

By Guangbi Li

A dissertation submitted in partial fulfillment of the requirements for the degree of
Doctor of Philosophy at the Virginia Commonwealth University

Virginia Commonwealth University, 2017

Advisor: Pin-Lan Li, MD, PhD, Professor, Pharmacology and Toxicology

Cell differentiation and senescence in podocytes are attributed to normal autophagy and associated cellular activities. It is possible that derangement of autophagy under different pathological conditions activates or enhances podocyte dedifferentiation leading to glomerular injury and ultimate glomerular disease. To test this hypothesis, we first tested whether autophagic deficiency due to lysosome dysfunction enhances podocyte dedifferentiation and explored the molecular mechanisms by which this lysosome dysfunction trigger or enhance podocyte dedifferentiation. By Western blot and confocal analysis, lysosome inhibition using an inhibitor or siRNA of V-ATPase inhibitor was found to markedly decrease the epithelial markers (P-cadherin and ZO-1) and increase the mesenchymal markers (FSP-1 and α -SMA). This enhancement of podocyte dedifferentiation (formerly referred to as epithelial-mesenchymal transition, EMT) was accompanied by deficient autophagic flux, as demonstrated by marked increases in LC3B-II and p62/Sequestosome 1. However, inhibition of autophagosome formation using spautin-1 (SP-1) significantly attenuated both enhancement of podocyte dedifferentiation and deficiency of autophagic flux. To explore the mechanisms by which deficient autophagic flux enhances podocyte dedifferentiation, we tested the role of accumulated p62 as a signal hub in this process. Neither the nuclear factor erythroid 2-related factor 2 (Nrf2) nor nuclear factor

kappa (NFκ)-light-chain-enhancer pathway regulating p62 function was found to contribute to enhanced dedifferentiation. However, inhibition of cyclin-dependent kinase 1 (CDK1) activity reduced the phosphorylation of p62 and enhanced podocyte dedifferentiation similar to lysosome dysfunction, which indicates that enhanced podocyte dedifferentiation due to lysosome dysfunction may be triggered by accumulation of p62 and associated reduction of p62 phosphorylation. Given the essential role of sphingolipid-ceramide metabolism and transient receptor potential-mucolipin-1 (TRPML1) channel activity in lysosome function, we next sought to test whether altered ceramide metabolism by acid ceramidase (AC) leads to deficient lysosome trafficking and fusion to autophagosome in podocytes and thereby results in autophagic deficiency and podocyte dedifferentiation. Inhibition of AC by a potent and selective inhibitor, carmofur markedly reduced lysosome trafficking and fusion to both autophagosomes and multivesicular bodies (MVBs). Concurrently, enhancement of podocyte AC activity or exposure of podocytes to sphingosine, a product of ceramide metabolism by AC, remarkably increased lysosome trafficking and fusion to autophagosomes and MVBs, indicating that AC activity is critical for lysosome function in podocytes. To further explore the mechanisms by which AC activity contributes to lysosome trafficking, we examined the effects of various sphingolipids related to ceramide metabolism on transient receptor potential-mucolipin-1 (TRPML1) channel, a Ca²⁺ channel essential for lysosome trafficking and function. It was found that sphingomyelin (SM), a precursor for ceramide production blocked TRPML1 channel activity induced by ML-SA1 (a specific TRPML1 agonist), while ceramide had no effects on TRPML1 channel activity induced by ML-SA1. Interestingly, sphingosine, an AC product of ceramide remarkably enhanced TRPML1 channel activity induced by ML-SA1. These results demonstrate that AC product of ceramide, sphingosine may enhance TRPML1 channel activity,

but an upstream sphingolipid, SM may exert inhibitory action on lysosome TRPML1 channel activity. AC may be a key enzyme gating TRPML1 channels by production of sphingosine and changes in upstream substrate SM. These results from *in vitro* cell studies led us hypothesize that a deficient AC activity may induce podocyte injury through lysosome dysfunction, leading to glomerular damage and proteinuria. To test this hypothesis, we generated a mouse colony with podocyte-specific gene deletion of AC α subunit, namely, *Asah1^{fl/fl}/Podo^{Cre}* mice. In these mice, severe proteinuria and albuminuria were shown compared to their littermates, but they were without global and even focal glomerular sclerosis. These mice also had hypoalbuminemia and edema, and under transmission electron microscopy (TEM) ultrastructural changes of podocytes from their glomeruli exhibited diffuse and flat foot process (podocyte effacement), vacuolation, and microvillus formation, which were not observed in their littermates. Treatment of corticosteroids and specific expression patterns of dystroglycans in glomeruli confirmed that albuminuria in these *Asah1^{fl/fl}/Podo^{Cre}* mice may be resistant to corticosteroids. Together, these results from *in vivo* animal studies indicate that podocyte-specific gene deletion of AC α subunit may induce a corticosteroid-resistant minimal change disease (MCD). Based on all results from our *in vitro* and *in vivo* studies, we conclude that the normal lysosome function is essential for maintenance of autophagic flux and podocyte differentiation, which is regulated by a lysosomal AC-mediated signaling pathway through a TRPML1 channel gating mechanism. AC gene defect or deficiency of its activity induces podocyte injury, which is characterized by a corticosteroid-resistant MCD. These findings indicate an important pathological role of AC deficiency and associated lysosome dysfunction in podocytes injury and corticosteroid-resistant MCD, which may help develop novel therapeutic strategies for prevention or treatment of corticosteroid-resistant MCD.

CHAPTER ONE

INTRODUCTION

1.1 Podocyte dedifferentiation and glomerular diseases

Cell differentiation is the process by which a less specialized cell type becomes a more specialized cell type, which is a cell mature process in a variety of differentiable cells. As the representative of immature cells, embryonic stem cells (ESC) are pluripotent cells which give rise to all somatic cell types in the embryo. In adult organisms, the adult stem cells (ASCs) maintain the normal regeneration of many tissues such as blood, skin, intestinal tissues, and renal glomerular or tubular cells. Under different physiological and pathological conditions, ASCs may act as a repair system for human or animal organs, which can replace the loss or dysfunctional specialized cells. Recent studies have suggested that glomerular parietal epithelial cells (GPECs) may serve as progenitor cells for podocytes and thus they may have a potential role in glomerular repair by replacing, in part or completely, the loss of podocyte (1-5). There are evidences that podocytes can derive from GPECs in adolescent mice (1). In certain glomerular diseases, such as focal segmental glomerular sclerosis (FSGS), membrane nephropathy, and aging nephropathy, GPECs were found to express proteins previously considered specific for podocytes (6-8). It has been demonstrated that the therapeutic effect of prednisone, a first line therapeutic glucocorticoid for focal segmental glomerular sclerosis, is attributed to the enhancement of podocyte regeneration by GPECs as a progenitor cells (9).

On the other hand, the reversal of cell differentiation process, namely, cell dedifferentiation, is normally considered as a danger factor under pathological conditions. It is broadly accepted that dedifferentiation is an aberration of the normal development of cell cycle

which results in tumorigenesis and promote fibrosis (10). Consistent with this theory, the transformation into stem cell-like status of podocyte, a highly specialized cell with a unique structure, has been demonstrated as one of the pathogenesises of glomerular disease (11). Since podocytes develop from mesenchymal cells via a mesenchymal-to-epithelial transition (MET), it is hypothesized that podocyte dedifferentiation is the reversal of this process (12). In many previous studies, epithelial-to-mesenchymal transition (EMT) or transdifferentiation was generally used for podocyte phenotype transition upon different pathological stimuli. However, it is recently realized that the traditional definition of a podocyte as an epithelial cell is too simplistic, because the podocyte has features of a partial mesenchymal and partial epithelial cell. Also, podocytes are developmentally derived from mesenchymal stem cells. It is now widely accepted that so called EMT in podocytes are mainly due to reversal of their mesenchymal features, namely, dedifferentiation. However, some researchers suggested that such pathological changes in podocytes can be named as podocyte disease transformation, but this new name of podocyte phenotype transition is not yet widely accepted (11). We are using podocyte dedifferentiation to more accurately represent the reversal of its mesenchymal features observed in our experiments.

In 1980, an *in vitro* model system for studying the glomerular epithelium exposed on the surfaces of kidney slides was described (13). In these studies, an *in vitro* incubation of podocytes at 37°C induced transformation of these cells into a compact group of rounded but viable cells. At lower incubation temperatures, the differentiation process of podocytes was significantly inhibited. This finding was the first direct evidence proving podocyte transformation and potential dedifferentiation, which was followed by many further studies to characterize podocyte

dedifferentiation and to explore the underlying molecular mechanisms. Based on these studies, it has been indicated that the hallmarks of podocyte dedifferentiation includes but is not limited to the suppressed expression of P-cadherin, ZO-1, and nephrin with concomitant upregulation of α -ASM, N-cadherin, SNAIL, SLUG, desmin, fibronectin, and collagen I (14, 15). During dedifferentiation, podocytes lose their highly arborized morphology and adopt a more cobblestone-like morphology. As a result, foot process effacement diminishes the ability of podocytes to restrict urinary protein leaking through glomerular filtration membrane, which may lead to proteinuria, albuminuria and ultimate nephrotic syndrome and other glomerular fibrotic diseases. Concurrently, podocytes with effaced foot processes have less contact with the glomerular basement membrane, making podocyte loss much more likely. Moreover, the increased synthesis of extracellular matrix components such as fibronectin and collagen I due to podocyte effacement may contribute to glomerular basement membrane thickening, leading to glomerulosclerosis. Proteinuria, in particular, albuminuria accelerates kidney disease progression to end-stage renal disease (ESRD) through induction of glomerular and tubular inflammasome activation, increases in chemokines or cytokine production and complement activation, which may lead to inflammatory cells infiltration in the interstitium and sustained fibrogenesis.

Previous studies have demonstrated that podocyte dysfunction and glomerular sclerosis may be due to podocyte dedifferentiation in response to a variety of pathological stimuli and endogenously produced pathogenic factors such as HIV-1 Nef (16-19), transforming growth factor- β (20-22), matrix metalloproteinase-9 (23), Notch-1 (24), RSAD2 (25), integrin-linked kinase (26, 27), PKC- α /PKC- β I (28), NADPH oxidase (29), connective tissue growth factor/ β -catenin (27, 30), PI3-K/ Akt-signaling pathway (31), Rac1/PAK1 signaling (32), high glucose

(30, 33-38), macrophage migration inhibitory factor (39), phosphorylation of caveolin-1 (40), NFATc3 (41), carboxymethyl lysine/ZEB2 (42), and glycogen synthase kinase 3 β (38). It is expected that the progress in understanding of the molecular mechanisms mediating podocyte dedifferentiation under different pathological conditions would tremendously contribute to the development of potential novel therapeutic strategies for patients with various glomerular diseases.

It has been reported that HIV-associated nephropathy (HIVAN) is a leading cause of ESRD in HIV-1 seropositive patients (43). In HIVAN patients, podocytes were found to exhibit a unique phenotype with loss of many differentiation markers, showing more proliferative, dedifferentiable, and dysfunctioning (44-46). These pathological changes of podocytes appear to be a direct result of HIV-1 protein expression, specifically Nef and Vpr (16, 18, 47, 48). Diabetic kidney disease (DKD) is the leading cause of ESRD worldwide, which is considered as a single strongest predictor of the mortality in patients with diabetes (49). Multiple researchers have reported increased expression of Wnt and excessive activation of canonical β -catenin signaling in diabetic glomeruli (50, 51), which are important cell dedifferentiating and proliferative markers. Transgenic mice with podocyte-specific, stabilized β -catenin expression developed basement membrane thickening and mild albuminuria, resembling early changes in human DKD (50). These results suggest that excessive Notch and Wnt activation in DKD diabetic nephropathy is maladaptive, which may contribute to podocyte dedifferentiation and disease progression. In previous studies, we have demonstrated that hHcys induces dedifferentiation of podocytes, which may represent a novel mechanism of hHcys-induced podocyte dysfunction and glomerular sclerosis. As the dominant source of $O_2^{\cdot-}$ in many non-phagocytic cells, especially in the kidney

(52-56), activation of NADHP oxidase (Nox) has been shown to contribute to hHcys-enhanced podocyte dedifferentiation (29). Growth hormone (GH), a hormone regulating cell differentiation and growth, has also been demonstrated to reverse Hcys-induced podocyte dedifferentiation and to ameliorate hHcys-induced glomerular injury (57, 58). These results suggest a crucial role of podocyte dedifferentiation in the sclerogenic mechanism of hHcys during the progression of glomerular injury. However, it remains poorly understood how podocyte dedifferentiation is activated and regulated in response to different pathological stimuli.

1.2 Autophagic deficiency and podocyte dedifferentiation

The term autophagy was first used in 1963 by Christian de Duve, the 1974 Nobel Prize Laureate for his work on lysosomes. It described the phenomenon associated with single- or double-membraned vesicles that contained cytoplasm, including organelles, at various stages of digestion. Since then, at least three forms of autophagy have been reported including chaperone-mediated autophagy, microautophagy, and macroautophagy, which were based on their physiological functions and the mode of cargo delivery to lysosomes. However, many studies have focused on the original concept of de Duve, which likely described macroautophagy. It is a major regulated catabolic mechanism that eukaryotic cells use to degrade long-lived proteins and organelles (59, 60). Therefore, unless there is special definition or description in a study about other two types of autophagy, macroautophagy is often referred to as autophagy in literature.

Autophagy is a basic mechanism of degrading unnecessary or dysfunctional cell components. It is characterized by the engulfment of the targeted components in double-membrane bound autophagosomes followed by their fusion with lysosomes. The contents of

autophagolysosomes are then degraded by lysosomal hydrolases to produce various enzymatic catabolites including amino acids, free fatty acids and others, which are rapidly made available in the cytoplasm for recycling (61). In somatic cells, normal autophagic flux controls the quality of long-lived proteins and organelles. Since misfolded proteins and functionally impaired organelles are targeted and degraded by autophagic flux, their accumulation with toxic effects are prevented (62).

Until the early 1990s, the knowledge of autophagy was limited to understanding of its morphological and biochemical characteristics, but its molecular mechanisms or regulatory pathways were poorly understood. Over the last decade, due to the discovery of yeast autophagy genes (Atg genes) followed by the identification of their mammalian homologues (63-66) numerous studies have been done to elucidate the molecular machinery of this main cellular homeostatic process and its regulatory mechanisms. Also, significant advances have been made to reveal its roles under physiological and pathological conditions (60, 67-77).

While the functions of autophagic flux in somatic cells are well characterized, the role of autophagy in stem cells and dedifferentiated cells is much less understood. In recent studies, autophagy was shown to be involved in the homeostatic control and maintenance of the self-renewal capacity of stem cells. In particular, autophagic flux was demonstrated to participate in stem cell differentiation and somatic reprogramming (78). In this regard, upregulation of autophagy is critically implicated in differentiation of neural stem cells and cardiac stem cells (79-81). Autophagy has also been reported to be rapidly upregulated during early differentiation of mouse embryonic stem cells and human embryonic stem cells, and impaired autophagic flux

led to early embryonic lethality, further confirming a critical role of autophagy in stem cell differentiation (82-86). In podocytes, previous studies have revealed that LC3-I is processed to LC3-II during the podocyte differentiation and recovery from puromycin aminonucleoside-induced nephrosis, which indicates that autophagy plays an important role in podocyte differentiation (87). Recently, our observations revealed that normal expression of CD38, a multifunctional protein involving in a number of signaling pathways, importantly contributes to the differentiation and function of podocytes and the defect of this gene expression may be a critical mechanism inducing podocyte dedifferentiation and consequently resulting in glomerular injury and sclerosis (88). Also, we have found that CD38 controls lysosome function and thus contributes to autophagy maturation in podocytes, which further confirms the vital role of autophagy in maintenance of podocyte differentiation (89). Therefore, autophagic deficiency may be an important mechanism mediating podocyte dedifferentiation under pathological conditions.

1.3 Ceramide metabolism and lysosome-dependent autophagic flux

As a sphingolipid involved in many signaling pathways, ceramide has been reported to inhibit autophagic flux (90, 91). Ceramide production is mainly mediated via the hydrolysis of membrane sphingomyelin by various sphingomyelinases such as acid sphingomyelinase (ASM) or by de novo synthesis via serine palmitoyltransferase and ceramide synthase (92). Subsequently, ceramide is metabolized into sphingosine by various ceramidases such as acid ceramidase (AC), and sphingosine can be further converted to sphingosine-1-phosphate (S1P) via sphingosine kinase (92). In our recent studies, enhanced activity of ASM and associated increase in ceramide production were shown to play a pivotal role in mediating podocyte injury

and glomerulosclerosis during hHcys and obesity (93-95). However, it remains unknown whether altered ceramide metabolism leads to autophagic deficiency and consequent podocyte dedifferentiation under different pathological conditions.

There is considerable evidence that lysosomes have trafficking function within different cells (96-102). Recent studies in our lab also showed that lysosome trafficking is a main regulatory mechanism of autophagic flux, which may depend upon the Ca^{2+} bursts from lysosomes. It has been indicated that although small amounts of Ca^{2+} released from a single lysosome may not be enough to activate global Ca^{2+} release from the sarcoplasmic reticulum (SR), they may be enough to drive the lysosome moving along microtubules to meet with other cellular vesicles such as autophagosomes, endosomes, MVBs, and SR (103-108). This Ca^{2+} -dependent lysosome trafficking was also observed in various types of cells (109-113). In addition to lysosome trafficking, its fusion to cell plasma membrane, endosomes, MVBs, phagosomes, autophagosomes or other organelles is also a Ca^{2+} -dependent event (107, 114-116). It is well known that Ca^{2+} enters lysosomal compartment by $\text{H}^+/\text{Ca}^{2+}$ exchange under resting condition and is released through transient receptor potential-mucolipin-1 (TRPML1) channels in response to endogenously produced nicotinic acid adenine dinucleotide phosphate (NAADP) (103, 107, 108, 117, 118) or other factors like PIPs (PI(3,5)P2) and irons (109, 111, 119). More channels such as two-pore channels may also be implicated in lysosomal Ca^{2+} release, but they may form hybrids with TRPML1 and need accessory proteins to exert their effect (97, 120). More recently, lysosomal TRPML1 channel activity regulated by sphingolipids has been shown to be a key mechanism determining lysosome trafficking. Accumulated sphingomyelin inhibited its activity and reduced lysosomal Ca^{2+} release, leading to failure of lysosome trafficking and

lysosomal storage disease as shown in Niemann-Pick disease (112, 121). Sphingosine, a ceramide metabolite via AC activated TRPML1 channels promoting lysosome Ca^{2+} release and trafficking in some epithelial cells. These results support a scientific premise that lysosome Ca^{2+} bursts through TRPML1 channels may be fine controlled by sphingolipids. Based on these results, we hypothesize that AC-mediated sphingolipid signaling may gate TRPML1 channels in podocytes to control Ca^{2+} -dependent lysosome trafficking to autophagosome that governs autophagic flux. Altered ceramide metabolism due to AC dysfunction inhibits TRPML1 channel activity and lysosome trafficking to autophagosome, leading to autophagic deficiency and consequent podocyte dedifferentiation or dysfunction.

1.4 Aims of the study

The hypothesis to be tested in the present study states that: autophagic deficiency due to lysosome dysfunction contributes to podocyte dedifferentiation leading to glomerular injury and lysosome trafficking to lysosomes is fine controlled by lysosomal AC-mediated signaling pathway that gates TRPML1 channel.

The specific aims are:

1. To determine whether lysosome-mediated autophagic flux serves as a fine control mechanism for differentiation of mouse podocytes and to define the signaling pathways linking autophagy to podocyte differentiation.
2. To determine whether altered ceramide metabolism via AC induces lysosome dysfunction with a focus on deranged lysosome trafficking associated with reduced TRPML1 channel activity.

3. To determine whether derangement of lysosome trafficking results in podocyte dedifferentiation or dysfunction in mice with podocyte-specific AC gene deletion.

The overall hypothesis and the specific aims of this project are schematically represented in

Figure 1.

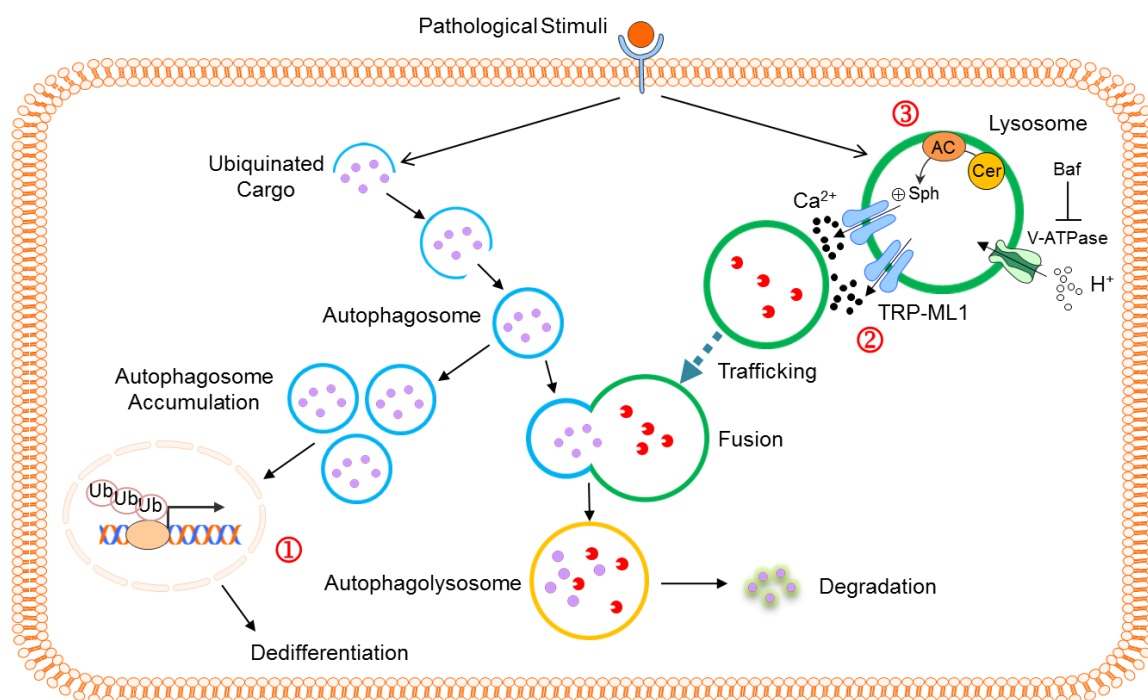


Figure 1. The working hypothesis. Autophagic flux determined by normal lysosome function is crucial for the control of differentiation status in podocytes. If lysosome function is disrupted, podocytes will undergo dedifferentiation. Such lysosome dysfunction may be associated with deficient lysosome trafficking and fusion with autophagosomes (APs), two major processes in autophagic flux. In response to pathological stimuli, lysosome trafficking or fusion to APs is attenuated through abnormal ceramide metabolism and transient receptor potential-mucolipin 1 (TRPML1) channel activity, which may be attributed to acid ceramidase (AC) deficiency and reduced production of sphingosine or sphingosine-1-phosphate (S1P). The dedifferentiated podocytes lose their epithelial properties and gain more mesenchymal features, which increases their migration capability, detachment and interactions with extracellular matrix, leading to glomerular injury and proteinuria.

CHAPTER TWO

GENERAL METHODS

2.1 Cell culture

A conditionally immortalized mouse podocyte cell line, graciously provided by Dr. Paul E. Klotman (Division of Nephrology, Department of Medicine, Mount Sinai School of Medicine, New York, USA), was constructed with a temperature-sensitive variant of the simian virus (SV40) containing a large T antigen (tsA58) inducible by interferon- γ at 33°C, allowing for cellular proliferation. These cells were cultured and maintained on collagen-coated flasks in RPMI 1640 medium supplemented with 10% fetal bovine serum, 10 U/ml recombinant mouse interferon- γ , 100 U/ml penicillin and 100 mg/ml streptomycin. The podocytes were then passaged and allowed to differentiate to a mature cell type at 37°C for two weeks without interferon- γ before use in experiments.

Podocytes were treated with Baf A1 (Baf), a potent vacuolar-type H⁺-ATPase inhibitor, at a concentration of 10 nM for 24 hours. Rapamycin (100 nM), 7-keto (5 μ g/mL), Spautin-1 (2 μ M), Bortezomib (1 nM), and RO-3306 (200 nM) were added to the cells 1 hour prior to Baf treatment. As a selective acid ceramidase inhibitor, Carmofur was used to treat podocytes at a concentration of 10 nM for 24 hours.

2.2 Lipid-mediated transfection

The scrambled RNA, vacuolar H⁺-ATPase siRNA, Nrf2 siRNA, and NF- κ B siRNA were purchased from Qiagen, Valencia, CA, USA. The scrambled RNA was confirmed as non-

silencing double-strand RNA and used as the control in the present study. Podocytes were serum starved for 12 h and then transfected with small interfering RNA (siRNA) or scrambled RNA using siLentFect Lipid Reagent (Bio-Rad, Hercules, CA, USA). After 24 h of incubation at 37°C, the medium was changed, and Baf (10 nM) was added into the medium for indicated time span in different protocols.

2.3 Nucleofection

Podocytes were transfected with GCaMP3-ML1 plasmid directly to the nucleus via nucleofector technology developed by Lonza (Basel, Switzerland). This technology involves the temporary creation of small pores in the membrane through electrical impulses together with cell-specific solutions to deliver substrates through the cytoplasm and into the nuclear membrane. Podocytes were trypsinized, counted, and 1×10^6 cells were gently centrifuged at 90xg for 10 min at RT. Cells were resuspended in SF Cell Line nucleofector solution containing 2 µg plasmid DNA and then transferred into a certified cuvette. The cuvette was placed into the nucleofector system and subject to cell-type specific program DS-150, chosen based on optimization experiments. Nucleofected cells were resuspended with pre-warmed medium and transferred to cultured plates for use in experiments.

2.4 Western blot analysis

Western blot analysis was performed as described previously (57). In brief, homogenates from cultured podocytes were prepared using sucrose buffer containing protease inhibitors. After boiling for 5 min at 95°C in a 5× loading buffer, 20 µg of total proteins were subjected to SDS-PAGE, transferred onto a PVDF membrane and blocked by solution with dry milk. Then, the

membrane was probed with primary antibodies of anti-ZO-1 (1:1000, Invitrogen), anti-P-cadherin (1: 1000, R&D System), anti- α -SMA (1:5000, R&D System), anti-FSP-1 (1:1000, Abcam), anti-LC3B (1:1000, Cell Signaling Technology), anti-LAMP1 (1:1000, Novus Biologicals), mouse anti-p62 (1:5000, Abcam, Cambridge, MA, USA), rabbit anti-phospho-p62 (1:1000, Cell Signaling Technology, Beverly, MA, USA) or anti- β -actin (1:5000, Santa Cruz Biotechnology) overnight at 4 °C followed by incubation with horseradish peroxidase-labeled IgG (1:5000). The immunoreactive bands were detected by chemiluminescence methods and visualized on Kodak Omat X-ray films. Densitometric analysis of the images obtained from X-ray films was performed using the Image J software (NIH, Bethesda, MD, USA).

2.5 Immunofluorescence microscopy

Double-immunofluorescence staining was performed using cultured podocytes on cover slips. After fixation, the cells were incubated with rabbit anti-podocin (1: 200 dilution, Sigma, St. Louis, MO, USA). At the same time, goat anti-FSP-1 (1:50 dilution), goat anti-ZO-1 (1:50 dilution, Santa Cruz Biotechnology Inc, Santa Cruz, CA, USA), goat anti-P-cadherin (1:25 dilution), or mouse anti- α -SMA (1:300 dilution, R&D system, Minneapolis, MN, USA) was added to the cell slides and then incubated overnight at 4°C. For examination of lysosome trafficking and fusion to MVBs, the cells were incubated with rat anti-Lamp-1 (1:200 dilution, Novus Biologicals, Littleton, CO, USA). At the same time, mouse anti-VPS16 (1:100 dilution, Abcam, Cambridge, United Kingdom) or mouse anti-Annexin-II (1:100 dilution, Santa Cruz Biotechnology Inc, Santa Cruz, CA, USA) was added to the cell slides and then incubated overnight at 4°C. After washing, the slides were incubated with corresponding Alex-488-labeled secondary antibody and Alex-555-labeled secondary antibodies and then mounted and subjected

to examinations using a confocal laser scanning microscope (Fluoview FV1000, Olympus, Japan). Frozen mouse kidneys were also fixed in acetone, blocked, and then incubated with the same aforementioned primary antibodies overnight at 4°C. For confirmation of podocyte-specific EGFP expression, frozen kidney sections were only incubated with rabbit anti-podocin 1: 200 (Sigma, St. Louis, MO, USA). After washing, the slides were incubated with corresponding the Alex-555-labeled secondary antibodies and then mounted and subjected to examinations using a confocal laser scanning microscope (Fluoview FV1000, Olympus, Japan). Image Pro Plus software (version 6.0; Media Cybernetics, Bethesda, MD) was used to analyze colocalization, which was expressed as the Pearson correlation coefficient.

2.6 GCaMP3 Ca²⁺ imaging

At 18–24 h after nucleofection with GCaMP3-ML1, podocytes were used for experiments. The fluorescence intensity at 470 nm (F470) was monitored using the EasyRatioPro system. Lysosomal Ca²⁺ release was measured under a ‘low’ external Ca²⁺ solution, which contained 145 mM NaCl, 5 mM KCl, 3 mM MgCl₂, 10 mM glucose, 1 mM EGTA and 20 mM HEPES (pH 7.4). Ca²⁺ concentration in the nominally free Ca²⁺ solution is estimated to be 1–10 μM. With 1 mM EGTA, the free Ca²⁺ concentration is estimated to be < 10 nM based on the Maxchelator software (<http://maxchelator.stanford.edu/>).

2.7 Whole-cell patch clamp recording

Whole-cell planar patch-clamp recordings were performed in cultured murine podocytes. The planar patch-clamp technology combined with a pressure control system (Port-a-Patch, Nanion Technologies) was applied as previously described (122). Ion currents were recorded,

filtered, and analyzed using an Axopatch 200B amplifier, an Axon Digidata 1550B low-noise data acquisition system, and the pClamp10 software (Axon instruments). Seal resistance was higher than 1 G Ω . Internal solution contained 50 mM CsCl, 10 mM NaCl, 60 mM Cs fluoride, 20 mM EGTA, and 10 mM Hepes/CsOH. External solution contained 140 mM NaCl, 4 mM KCl, 1 mM MgCl₂, 2 mM CaCl₂, 5 mM D-Glucose monohydrate, and 10 mM Hepes/NaOH. Seal enhancer contained 80 mM NaCl, 3 mM KCl, 10 mM MgCl₂, 35 mM CaCl₂, and 10 mM Hepes/HCl. Podocytes were stimulated by bath application of compounds.

2.8 Isolation of lysosomes from podocytes

After treatment with Vacuolin-1 (1 μ M) for 2 hours, isolation of lysosomes was performed. After washing podocytes with pre-cooled PBS, pre-cooled homogenization buffer was used for detachment of podocytes by a cell scraper. Cell suspension in glass-grinding vessel was homogenized using a Teflon pestle operated at 900 rotations per minute (rpm). The homogenate was then transferred to a 1.5 ml microfuge test tube and centrifuge at 14,000g for 15 min at 4°C. After centrifuge, the middle part of supernatant was transferred to a 10-ml polycarbonate centrifuge tube. An equal volume of 16 mM CaCl₂ was added to precipitate lysosomes. After being shaken on a rotary shaker at 100 rpm for 5 min at 4°C, supernatant was centrifuged at 25,000g for 15 min at 4°C in an ultracentrifuge. The supernatant was discarded and the pellet was resuspended in one volume of ice cold washing buffer. The suspension was centrifuged at 25,000 g for 15 min at 4°C in an ultracentrifuge. After supernatant being discarded, the pellet containing lysosomes was resuspended in 40 μ l of washing buffer, which was used for whole-lysosome patch clamp recording. All steps were performed on ice to minimize the activation of

damaging from intracellular phospholipases and proteases. Lysosomes was used for electrophysiological recordings within 3 hours of isolation to keep lysosomes fresh.

Homogenization Buffer

Sucrose 0.25 M

Tris 10 mM

Adjust pH to 7.4 with HCl, sterilize by passing through a 0.2 μm filter, prepare 1 ml aliquots, and store at - 20°C for several months. Before use, add 40 μl of Complete Protease Inhibitor Cocktail (final concentration 1 \times) per aliquot of homogenization buffer.

Washing Buffer

KCl 150 mM

Tris 10 mM

Adjust pH to 7.4 with HCl, sterilize by passing through a 0.2 μm filter, prepare 4 ml aliquots, and store at - 20°C for several months. Before use, add 160 μl of Complete Protease Inhibitor Cocktail (final concentration 1 \times) per aliquot of Washing Buffer.

2.9 Whole-lysosome patch clamp recording

For whole-lysosome planar patch recordings, the Port-a-Patch (Nanion Technologies) was used. Lysosomes were enlarged with the treatment of 1 μM vacuolin-1 overnight (102, 119, 123, 124). The planar patch-clamp technology combined with a pressure control system and microstructured glass chips containing an aperture of around 1 μm diameter (resistances of 10-15

M Ω) (Nanion Technologies). Currents were recorded using an EPC-10 patch-clamp amplifier and PatchMaster acquisition software (HEKA). Data were digitized at 40 kHz and filtered at 2.8 kHz. For all planar patch-clamp experiments, salt-agar bridges were used to connect the reference Ag/AgCl wire to the bath solution to minimize voltage offsets. Ag/AgCl-coated electrodes need to be regularly chloridated in bleach solution approximately 15 min until a black AgCl-layer is obvious on the silver wire. Generally, electrodes should be replaced every 2 months.

It is essential to form a high-resistance seal (gigaseal) with the membrane of the lysosome or organelle of interest. Gigaseals are formed usually with the aid of seal enhancer external solution (cytoplasmic side) which contains a high concentration of fluoride, whereas the intralysosomal solution contains a high concentration of Ca²⁺. For tight-seal lysosomal patch-clamp recordings, we added solutions containing high Ca²⁺ (> 60 mM) on one side of the glass chip and solution containing high fluoride at the other side during seal formation. Omitting either of the ions from the respective solutions after seal formation caused loss of seal quality and patch-clamp stability. Inclusion of fluoride improved patch-clamp sealing and stabilized the cell membrane, which resulted in longer, more stable patch-clamp recordings (125).

The membrane potential was held at -60mV, and 500ms voltage ramps from -200 to +100 mV were applied every 5s. All recordings were obtained at room temperature (21-23°C), and all recordings were analyzed using PatchMaster (HEKA) and Origin 6.1 (OriginLab). To dissect lysosomal currents from whole-lysosome planar patch-clamp recording, all currents in the absence of compounds were subtracted from the currents obtained in the presence of compounds

as previously described (102). Liquid junction potential was corrected. The EC50 of graded dose response curves were fitted with the Hill equation.

Standard Intralysosomal Solution

KMSA	70 mM
CaMSA	60 mM
MgCl ₂	2 mM
HEPES	10 mM

Preparation as follows: Adjust pH to 4.6 with MSA, sterilize by passing through a 0.2 μ m filter, prepare 1 ml aliquots, and store at -20°C for several months.

Standard Extralysosomal Solution

KMSA	60 mM
KF	60 mM
HEPES	10 mM

Preparation as follows: Adjust pH to 7.2 with KOH, sterilize by passing through a 0.2 μ m filter, prepare 4 ml aliquots, and store at -20°C for several months.

CaMSA	2 mM
-------	------

Preparation and use as follows: Add CaMSA immediately before starting the measurements to avoid precipitation of CaF₂.

Seal Enhancer Solution

KMSA	60 mM
KF	60 mM
EGTA	10 mM
HEPES	10 mM

Preparation as follows: Adjust pH to 7.2 with KOH, sterilize by passing through a 0.2 μ m filter, prepare 4 ml aliquots, and store at -20°C for several months.

Extralyosomal Bath Solution

KMSA	120 mM
EGTA	10 mM
HEPES	10 mM

Preparation as follows: Adjust pH to 7.2 with KOH, sterilize by passing through a 0.2 μ m filter, prepare 1 ml aliquots, and store at -20°C for several months.

2.10 Podocyte-specific *Asah1* gene knockout mouse model

We developed *Asah1*^{fl/fl}/Podo^{Cre} mice and their littermates including WT/WT and *Asah1*^{fl/fl}/WT mice, which were used for *in vivo* experiments to explore the role of acid ceramidase in podocyte function and integrity. *Asah1* is a mouse code of AC gene. The *Asah1*^{fl/fl} mice were provided by Dr. Erich Gulbins (Department of Molecular Biology, University of Duisburg-Essen); the Podo^{Cre} mice were purchased from Jackson Laboratories (Bar Harbor, ME, USA). To confirm the specificity of *Asah1* gene knockout in podocytes, *Asah1*^{fl/fl}/Podo^{Cre} mice were mated with lacZ/EGFP mice (Jackson Laboratories, Bar Harbor, ME, USA) to produce *Asah1*^{fl/fl}/Podo^{Cre}+lacZ/EGFP mice. Based on previous studies, lacZ/EGFP mice express β -

galactosidase (lacZ) throughout embryonic development and adult stages. Cre excision, however, removes the lacZ gene, which activates expression of the second reporter, enhanced green fluorescent protein (EGFP). To detect the lacZ expression levels in glomeruli, we performed lacZ activity assay in which the expression of lacZ was marked by the dark blue staining. Podocyte-specific expression of EGFP was detected by confocal microscopy. During experiments, all *Asah1^{fl/fl}/Podo^{Cre}* mice and their littermates at different ages or with different treatments were placed in metabolic cages and urine samples were collected for 24 hours before collecting blood samples, sacrificing, and harvesting tissues for analysis. The Institutional Animal Care and Use Committee of Virginia Commonwealth University approved all animal protocols.

2.11 Mouse genotyping

Each mouse used in the in vivo studies was genotyped for the *Asah1^{fl/fl}* gene and Cre recombinase gene to confirm podocyte-specific gene deletion of acid ceramidase α subunit prior to use in experiments. Briefly, genomic DNA extracted from the tail was subjected to PCR amplification using taq DNA polymerase (Invitrogen, Inc., Grand Island, NY). Using a Bio-Rad iCycler, PCR was performed using a validated protocol provided by Jackson Laboratories: denaturing the DNA at 94°C for 3 min, followed by a first round of 12 cycles: 94°C for 20 sec, 64°C for 30 sec (-0.5°C per cycle), 72°C for 35 sec, and then a second round of 25 cycles: 94°C for 20 sec, 58°C for 30 sec, 72°C for 35 sec, and a final extension step at 72°C for 2 min. The *Asah1^{WT}* and *Asah1^{fl/fl}* genes were detected using primers of 5'-ACAACTGTGTAGGATTCACGCATTCTCC-3' and 5'-TCGATCTATGAAATGTCGCTGTCGG-3'. The internal control gene was detected using

primers of 5'-CTAGGCCACAGAATTGAAAGATCT-3' and 5'-GTAGGTGGAAATTCTAGCATCATCC-3'. The Cre recombinase gene was detected using primers of 5'-GCGGTCTGGCAGTAAAACTATC-3' and 5'-GTGAAACAGCATTGCTGTCACTT-3'. The PCR products were separated by gel electrophoresis on a 3% agarose gel, visualized by ethidium bromide fluorescence, and compared to a 100 bp DNA ladder (New England Biosystems, Ipswich, MA).

2.12 β -galactosidase staining

β -galactosidase staining was performed on 8- μ m cryosections of mouse kidneys as described previously (126). Briefly, adult mice were perfused with 4% paraformaldehyde. Tissues were resected and frozen in liquid nitrogen. Eight-micrometer cryosections were cut and postfixed with 4% paraformaldehyde for 5 min. The sections were then incubated overnight at 30°C with X-gal staining solution (1 mg/ml X-gal, 5 mM potassium ferricyanide, 5 mM potassium ferrocyanide, 2 mM MgCl₂ in phosphate-buffered saline [PBS]), washed with PBS, dehydrated through grades of ethanol and xylene, and mounted.

2.13 Isolation of glomeruli for LC-MS/MS

For quantitation of ceramide and its products, *Asah1*^{fl/fl}/*Podo*^{Cre} mice and their littermates were used to isolate glomeruli of the kidney as described previously (127, 128). In brief, the mice were anesthetized with 2% isoflurane and then the kidneys were perfused with ice-cold PBS and harvested. After blood samples were taken, the mice were euthanized. The harvested kidneys were hemisected on a sagittal plane and the renal cortex was separated from the medulla, chopped into fine pieces, and passed through filters with decreasing pore sizes from 150 to 106

μm (USA standard sieve numbers 100 and 140, respectively; Thermo Fisher Scientific, Waltham, MA) into a petri dish. The glomeruli were captured on a 70 μm cell strainer (BD Biosciences, San Jose, CA), then washed off from the sieve with ice-cold Hank's solution containing 6% BSA, and pelleted for later use to measure ceramide and sphingosine levels by liquid chromatography tandem mass spectrometry (LC-MS/MS).

2.14 LC-MS/MS analysis

Glomeruli were isolated from mice as described above. After homogenization of glomeruli, 10 ng C12 ceramide was added to homogenate reaction mixture to act as an internal standard. Then, the mixture was separated in chloroform/methanol/water (2:2:1.8). After evaporation with nitrogen and reconstitution with ethanol/formic acid (99.8:0.2), the samples were ready for LC-MS/MS assay. The separation of ceramide was performed on a Shimadzu SCL HPLC system (Kyoto, Japan) with a C18 Nucleosil AB Column (Macherey-Nagel, Duren, Germany). MS detection was carried out using an Applied Bio systems 3200 Q trap with a turbo V source for TurbolonSpray (Ontario, Canada). The concentrations of total ceramide, including C14, C16, C18, C20, C22, and C24 ceramide, and sphingosine were calculated after normalization with glomerular numbers of each sample. The fragment ion obtained with the highest mass-to-charge ratio (m/z 264) was selected for quantitative MS detection in the multiple reaction monitoring mode.

2.15 *In vitro* measurement of glomerular permeability

The glomerular permeability was measured as previously described (129). The mice were anesthetized with 2% isoflurane. FITC-dextran (250 kDa; Sigma-Aldrich, St. Louis, MO) at a

dose of 75 mg/kg in a 0.9% NaCl solution was injected into the femoral vein. Other fluorescently labeled Cy3, Cy5, and rhodamine high-molecular weight dextrans work equally as well. After 3–5 min, the kidneys were harvested and placed in ice-cold isotonic HBSS (Life Technologies, Grand Island, NY) containing 6% BSA (Sigma-Aldrich) and 10 mM HEPES (Sigma-Aldrich), pH 7.4. Then, glomeruli were isolated as previously described (127, 128). Briefly, the kidney was hemisected on a sagittal plane and the renal cortex was separated from the medulla, chopped into fine pieces, and passed through stainless steel filters with decreasing pore sizes from 150 to 106 μm (USA standard sieve No. 100 and No. 140, respectively, Thermo Fisher Scientific, Waltham, MA) into a petri dish. The glomeruli were captured on a 70- μm cell strainer (BD Bioscience, San Jose, CA) and washed off of the sieve with ice-cold Hank's solution containing 6% BSA. The mixture was transferred to a 15-ml tube and stored on ice before the experiment.

A small aliquot (50–100 μl) of the isolated glomeruli was loaded onto a coverslip, precoated with poly-l-lysine hydrobromide (10 mg/ml, Sigma-Aldrich), which formed the bottom of a fluid exchange chamber (RC-24, Warner Instruments, Hamden, CT). The inflow line to the chamber was attached to two peristaltic pumps so that the bath could be rapidly exchanged in less than 10 s. The effluent was collected through a vacuum line. The isolated glomeruli were imaged using a fluorescent microscope (Nikon TS-100, Nikon Instruments, Melville, NY) equipped with a high-sensitivity camera and a 175-Wt Xenon Arc Lamp (Intracellular Imaging, Cincinnati, OH) and filter wheel (Excitation/emission: 480/510–550 μm). The glomeruli were observed using a low-numerical aperture $\times 5$ lens (Nikon Instruments, Melville, NY) with a large depth of field ($>50 \mu\text{m}$) so that the fluorescence signal from the entire glomerulus could be collected. Approximately 30 glomeruli/field were selected for study based on their

morphological appearance. A recording area slightly larger than the circumference of the glomeruli was defined using Image 1 fluorescent imaging software (Incyte, Cincinnati, OH) so that all of the label remains in the recorded volume when the glomeruli expand following a reduction in the oncotic pressure of the bath. Glomeruli poorly labeled or too bright with intensities near the saturation level of the camera were not chosen for permeability measurements.

Fluorescent intensities were individually recorded, and the values are expressed as the percentage of the control intensity measured at time 0 for each glomerulus. There was more variation in the time course of the changes in fluorescent intensity between glomeruli than between mice of a given strain, so we typically averaged all the individual data and expressed the results as number of glomeruli studied per strain or group. After selection of the glomeruli to be studied, the chamber was perfused at 0.5 ml/min with a solution containing 6% BSA, and baseline fluorescent signals were continuously recorded using a high speed wavelength switching fluorescent microscopic system. The bath solution was then switched to one containing 4% BSA and the fluorescent signals from the glomeruli were recorded for an additional 3-5 minutes. The initial fluorescence value (time 0) was converted to 100%, and the subsequent values were expressed as a percentage of the initial value.

2.16 Immunohistochemistry

Kidneys were embedded with paraffin and 5 mm sections were cut from the embedded blocks. After heat-induced antigen retrieval, washing with 3% H₂O₂, and 30 min blocking with fetal bovine serum, slides were incubated with primary antibody diluted in PBS with 4% fetal

bovine serum. Anti- α -dystroglycan antibody and anti- β -dystroglycan antibody were used as primary antibodies in this study. After incubation with primary antibody overnight, the sections were washed in PBS and incubated with biotinylated IgG (1:200) for 1 h and then with streptavidin-HRP for 30 min at room temperature. Fifty microliters of DAB were added to each kidney section and stained for 1 min. After washing, the slides were counterstained with hematoxylin for 5 min. The slides were then mounted and observed under a microscope in which photos were taken (130).

2.17 Measurements of urinary protein and albumin excretions

Total urinary protein excretion was determined spectrophotometrically using the Bradford assay (Sigma), and urinary albumin excretion was measured using a commercially available mouse albumin ELISA kit (Bethyl Laboratories, Montgomery, TX).

2.18 Glomerular morphological examination

Renal tissues were fixed with a 10% formalin solution, paraffin-embedded, and stained with periodic acid–Schiff (PAS). Renal morphology was observed using a light microscope, and glomerular sclerosis was assessed semiquantitatively and expressed as glomerular damage index (GDI) (131, 132). Fifty glomeruli per slide were counted and scored as 0, 1, 2, 3, or 4, according to 0, <25, 25–50, 51–75, or >75% sclerotic changes, respectively, across a longitudinal kidney section. The GDI for each mouse was calculated by the formula $((N1 \times 1) + (N2 \times 2) + (N3 \times 3) + (N4 \times 4))/n$, where N1, N2, N3, and N4 represent the numbers of glomeruli exhibiting grades 1, 2, 3, and 4, respectively, and n is the total number of glomeruli scored.

2.19 Statistical analysis

All results were expressed as the arithmetic mean \pm SEM; n represents the number of independent experiments. Data obtained from multiple animal or experimental groups were tested for significance using one- or two-way ANOVA, and a paired and unpaired Student's t-test was used for two animal or experimental groups. The glomerular damage index was analyzed for statistical significance using a nonparametric Mann-Whitney rank sum test and a χ^2 test was used to determine the significance of ratio and percentage data. Results with $p < 0.05$ were considered statistically significant.

CHAPTER THREE

Podocyte dedifferentiation induced by lysosome dysfunction and associated autophagic deficiency

3.1 Enhanced podocyte dedifferentiation by lysosome function inhibition

To determine whether lysosome function inhibition has effects on podocyte dedifferentiation, Western blot analysis was performed before and after inhibition of lysosome function by either Baf A1 (Baf), a well-known lysosome function inhibitor through its inhibitory effect on V-ATPase or siRNA of this enzyme. As shown in Fig. 2A and 2B, when podocytes were treated with Baf, the epithelial markers P-cad and ZO-1 decreased significantly, while the mesenchymal markers FSP-1 and α -SMA increased markedly. Similarly, V-H-ATPase siRNA transfection (siv-A) decreased P-cad and ZO-1 but increased FSP-1 and α -SMA significantly in podocytes (Fig. 2C and 2D). It is clear that the ratio of epithelial markers vs. mesenchymal markers was significantly reduced during lysosome function inhibition, suggesting a large enhancement of dedifferentiation in podocytes.

3.2 Confocal microscopy of podocyte dedifferentiation during lysosome function inhibition

The effects of lysosome functional inhibition on podocyte dedifferentiation were further detected using confocal microscopy. As shown in Fig. 3A, under basal condition podocytes were enriched with P-cadherin and ZO-1. When these podocytes were treated with Baf, both P-cadherin and ZO-1 fluorescent staining were significantly reduced. As shown in overlaid cell images (OL in left panels of Fig. 3A), there were much less co-localized signals of podocin

with ZO-1 or P-cad in Baf-treated podocytes compared with control podocytes. In contrast, FSP-1 and α -SMA staining increased by Baf as shown by enhanced co-localization of podocin with both markers (right panels of Fig. 3A). In podocytes transfected with V-ATPase siRNA (siv-A), detected epithelial marker and mesenchymal marker stainings were similar to that shown in Baf-treated podocytes, decreases in epithelial marker and increases in mesenchymal markers (Fig. 3B).

3.3 Deficiency of autophagic flux during lysosome function inhibition

Given the role of autophagy in podocyte differentiation, we tested whether enhanced podocyte dedifferentiation due to lysosome function inhibition is associated with deficient autophagy. Fig. 4A shows representative gel documents of Western blot using antibodies against LC3B, Lamp-1 and p62. Under basal condition and co-treatment of podocytes with rapamycin (RPM, an autophagy inducer) or 7-keto (an autophagy stimulator), the protein levels of both LC3B-II and p62 (two autophagosome markers) significantly increased by Baf, while Lamp-1, a lysosome membrane marker was not changed. As shown in Fig. 4B, lysosome function inhibition mainly increased LC3II because the ratio of LC3B-II vs. LC3B-I was largely increased by Baf, which were similar under control condition and with stimulation of autophagosome formation by RPM or 7-keto. The increased LC3BII level was accompanied by accumulation of p62 in podocytes (Fig. 4C). However, the Lamp-1 level was not significantly changed by Baf (Fig. 4D).

3.4 Attenuation of podocyte dedifferentiation by Sp-1 inhibition of autophagosome formation

To further determine the role of autophagosome accumulation in podocyte dedifferentiation enhanced by lysosome function inhibition, we examined the effects of selective autophagosome formation inhibitor, Sp-1 on Baf-enhanced podocyte dedifferentiation. As shown in Fig. 5A, a representative Western blot gel document showed that Baf dramatically increased the LCB-II level. In the presence of Sp-1, the effects of Baf on the LCBII level were largely weakened. As summarized in Fig. 5B, the ratio of LC3B-II vs. LC3B-I was significantly increased by Baf. However, this increase in Baf-induced autophagosome accumulation was significantly attenuated by Sp-1. Moreover, Baf-induced p62 accumulation was markedly inhibited by Sp-1 as shown in Western gel document (Fig. 5C). Densitometric analysis showed that lysosome function inhibition by Baf led to a significant accumulation of p62 in podocytes, which was remarkably lessened by Sp-1 (Fig. 5D). As shown in Fig. 5E, interestingly, enhanced podocyte dedifferentiation by Baf as shown by decrease in P-cad and increase in α -SMA was obviously attenuated by Sp-1. The ratio of P-cad to α -SMA, a podocyte dedifferentiation index, significantly decreased in Baf-treated podocytes. In the presence of Sp-1, P-cadherin to α -SMA ratio was significantly reduced (Fig. 5F).

3.5 Failure of Nrf2 gene silencing to alter podocyte dedifferentiation enhanced by lysosome function inhibition

Mechanistically, we first tested the possibility of p62-regulated Nrf2 signaling pathway to participate in the enhancement of podocyte dedifferentiation by lysosome function inhibition. Fig. 6A shows representative Western blot gel documents illustrating the changes in P-cad, α -SMA and p62 induced by Baf before and after Nrf2 gene silencing (siNrf). The level of P-cad was markedly decreased, while p62 increased in Baf-treated podocytes. These Baf-induced

changes in podocyte dedifferentiation markers in associated with increase in p62 were not altered by Nrf2 gene silencing. As shown in Fig. 6B, Baf significantly decreased the ratio of P-cad and α -SMA, a podocyte dedifferentiation index. However, Nrf2 gene silencing did not alter the ratio of P-cad to α -SMA. In addition, Baf-induced significant accumulation of p62 was also not altered by Nrf2 siRNA (Fig. 6C).

3.6 No changes in enhanced podocyte dedifferentiation by inhibition of NF- κ B-mediated transcriptional regulation

Given the role of NF- κ B-mediated transcriptional regulation in cell dedifferentiation and its association with p62, we tested whether inhibition of its activity alters podocyte dedifferentiation enhanced by lysosome function inhibition. Representative Western blot gel documents in Fig. 7A showed that the level of P-cad remarkably decreased, but p62 was increased in Baf-treated podocytes. These Baf-induced changes in podocyte dedifferentiation markers as well as p62 were same before and after treatment with a NF- κ B inhibitor, Bortezomib (Bor). As summarized in Fig. 7B, Baf significantly decreased the ratio of P-cad vs. α -SMA, the podocyte dedifferentiation index, which was not altered by pharmacological inhibition of NF- κ B activity. Furthermore, Baf-induced significant accumulation of p62 remained same even though NF- κ B activity was inhibited (Fig. 7C). We also inhibited NF- κ B-mediated transcriptional regulation by gene silencing to further confirm whether this transcription factor is involved in Baf-enhanced podocyte dedifferentiation. As shown in Fig. 7D, 7E and 7F, the effect of NF- κ B gene silencing (siNF- κ B) on Baf-enhanced podocyte dedifferentiation was similar to its pharmacological inhibition, without effects on decreases in the ratio of P-cad vs. α -SMA and p62 accumulation in podocytes.

3.7 Enhancement of podocyte dedifferentiation by inhibition of CDK1

Another signaling pathway being tested is whether inhibition of CDK1 activity and expression alters Baf-induced enhancement of dedifferentiation in podocytes. It has been reported that phosphorylation of p62 regulates exit from cell cycle or cell arrest during cell mitosis and that reduced phosphorylation of p62 leads to a faster exit from cell mitosis, controlling cell dedifferentiation and tumorigenesis (133). In Fig. 8, panel A shows representative Western blot gel documents, depicting that the level of P-cad remarkably decreased, but α -SMA and p62 increased in Baf-treated podocytes. Similar to Baf, CDK1 inhibitor, a quinolinyl thiazolinone derivative, RO-3306 (RO) also decreased the level of P-cad markedly, but increased α -SMA and p62 in podocytes. In the presence of RO, Baf-induced changes in podocyte dedifferentiation markers were almost same as that observed in the absence of RO. However, RO was without effect on p62 level before and after stimulation of Baf. Fig. 8B presents summarized results showing that the ratio of P-cad to α -SMA was significantly reduced by both Baf and RO. Moreover, the inhibition of CDK1 by RO had no effect on the p62 level in podocytes under control condition and upon Baf treatment (Fig. 8C). To further confirm the role of CDK1 in enhancement of podocyte dedifferentiation, we used its siRNA to test whether gene silencing of CDK1 alters podocyte dedifferentiation. As shown in Fig. 8D, 8E and 8F, CDK1 siRNA (siCDK1) had similar effects on podocyte dedifferentiation to CDK1 inhibitor-RO, enhancing podocyte dedifferentiation under control condition without further influence on Baf-induced enhancement of podocyte dedifferentiation. It was also without effects on p62 levels in podocytes with or without treatment of Baf.

3.8 Reduction of p62 phosphorylation during lysosome function inhibition

Further experiments were designed to determine whether reduced p62 phosphorylation occurs due to lysosome function inhibition. As shown in Fig. 9A, Western blot gel documents show that CDK1 inhibitor RO markedly decreased phosphorylated p62 even though it had no effect on total p62 level in podocytes. However, Baf mainly led to p62 accumulation, but it had no effect on phosphorylation of p62. By calculation, the ratio of phosphorylated p62 to total p62 was found reduced significantly by both RO and Baf, suggesting that the relative reduction of phosphorylated p62 may be involved in the control of podocyte dedifferentiation (Fig. 9B). We also conducted additional experiments to silence CDK1 gene in order to confirm the role of decreased phosphorylated p62 in podocyte dedifferentiation. As presented in Fig. 9C, similar to RO, CDK1 siRNA reduced phosphorylated p62, but had no effects on total p62 level. As summarized in Fig. 9D, this CDK1 siRNA reduced the ratio of phosphorylated p62 to total p62, which was similar to the effects of Baf.

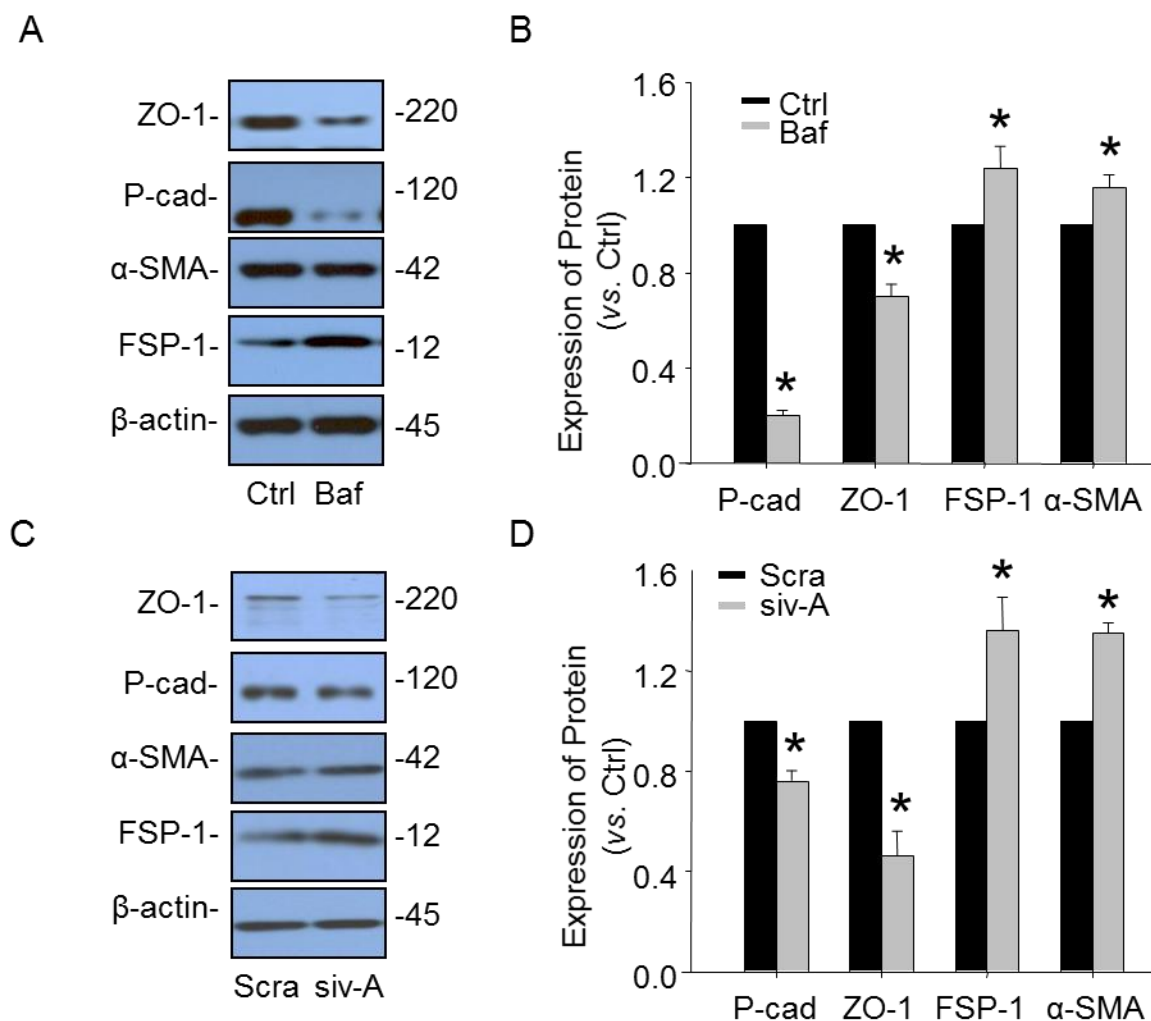


Fig. 2. Enhanced podocyte dedifferentiation by lysosome function inhibition. Podocytes were stimulated by Baf (5 μ M) for 12 hours or transfected with v-Ca²⁺-ATPase siRNA (10 nM) for 24 hours. A. Representative gel documents showing the expression of ZO-1 and P-cadherin (P-cad) as epithelial markers and the expression of α -SMA and FSP-1 as mesenchymal markers in different groups. B. Summarized data showing the expression of ZO-1 and P-cadherin as epithelial markers and the expression of α -SMA and FSP-1 as mesenchymal markers, quantitated as a ratio of detected specific protein band vs. β -actin as loading control (n=3-5). C. Representative gel documents showing the expression of ZO-1 and P-cadherin as epithelial markers and the expression of α -SMA and FSP-1 as mesenchymal markers in different groups. D. Summarized data showing the expression of ZO-1 and P-cadherin as epithelial markers and the expression of α -SMA and FSP-1 as mesenchymal markers, quantitated as a ratio of detected specific protein band vs. β -actin as loading control (n=3-5). * P<0.05 vs. Ctrl. Ctrl: Control; Baf: Baf; Scra: scramble RNA; siv-A: V-H-ATPase siRNA.

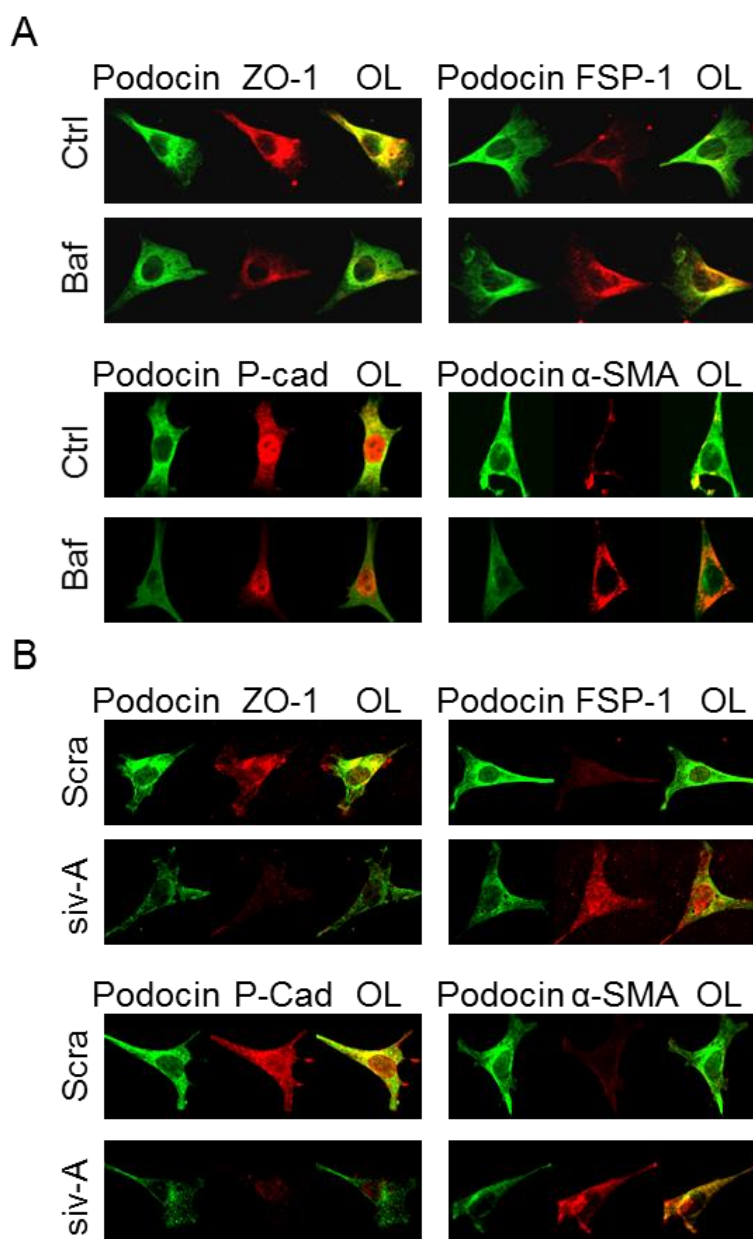


Fig. 3. Confocal microscopy of podocyte dedifferentiation during lysosome function inhibition. A. Images showing double-immunostained podocytes for epithelial markers, P-cadherin (p-cad) and ZO-1 (Alex555, red color) or mesenchymal markers, α -SMA and FSP-1 (Alex555, red color) with podocyte marker, podocin (Alex488, green color) in different groups (n=5). B. Images showing double-immunostained podocytes for epithelial markers, P-cadherin and ZO-1 (Alex555, red color) or mesenchymal markers, α -SMA and FSP-1 (Alex555, red color) with podocyte marker, podocin (Alex488, green color) in different groups (n=4). Ctrl: Control; Baf: Baf; Scra: scramble RNA; siv-A: V-H-ATPase siRNA; OL: Overlaid.

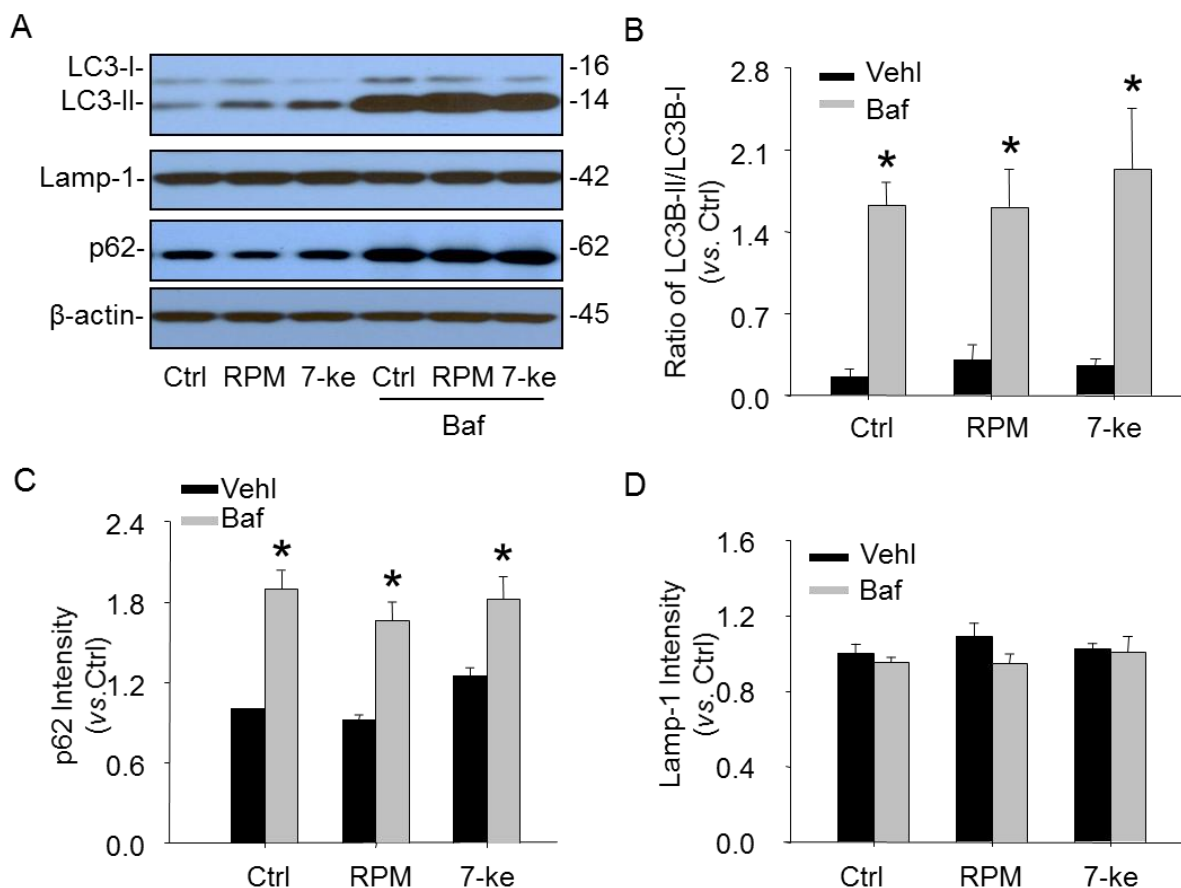


Fig. 4. Deficiency of autophagic flux during lysosome function inhibition. Podocytes were cultured for 24 hrs with rapamycin (100 nM) or 7-keto cholesterol (5 μ g/ml) in the absence or presence of Baf A1 (10 nM). A. Representative gel documents showing the expression of LC3B-I, LC3B-II, p62 as autophagosome markers and Lamp-1 as lysosome marker in different groups. B. Summarized data showing expression of LC3B-I and LC3B-II, quantitated as a ratio of LC3B-II band over LC3B-I band (n=4). C. Summarized data showing expression of p62, quantitated as a ratio of detected specific protein band vs. β -actin as loading control (n=4). D. Summarized data showing expression of Lamp-1, quantitated as a ratio of detected specific protein band vs. β -actin as loading control (n=4). * $P < 0.05$ vs. Ctrl: Control; Baf: Baf; VehI: vehicle; RPM: Rapamycin; 7-Keto: 7-Ketocholesterol.

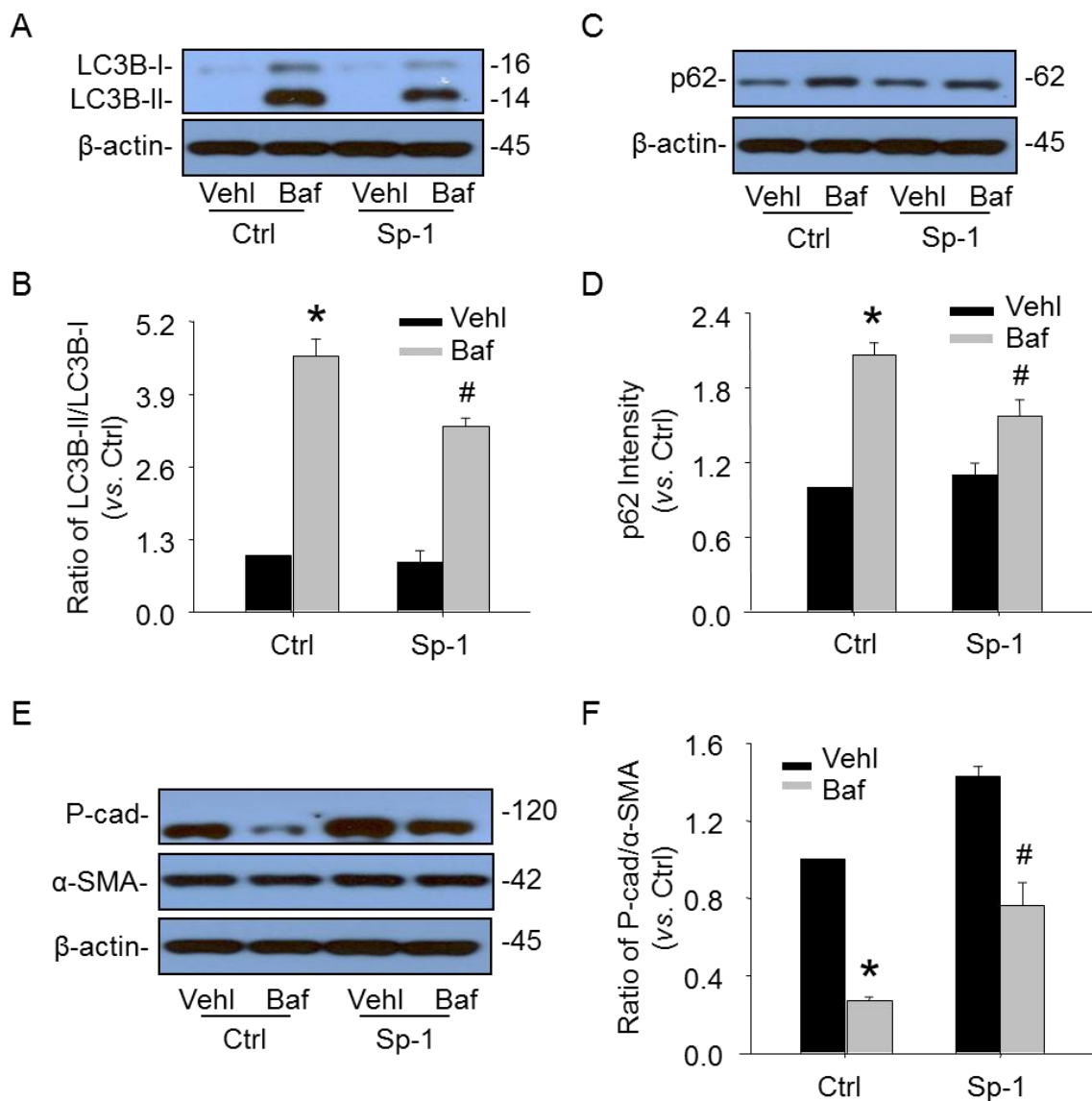


Fig. 5. Attenuation of podocyte dedifferentiation by Sp-1 inhibition of autophagosome formation. A. Representative gel documents showing the expression of LC3B-I and LC3B-II as autophagosome markers in different groups. B. Summarized data showing expression of LC3B-I and LC3B-II, quantitated as a ratio of LC3B-II band over LC3B-I band (n=3). C. Representative gel documents showing the expression of p62 as autophagosome marker in different groups. D. Summarized data showing expression of p62, quantitated as a ratio of detected specific protein band vs. β -actin as loading control (n=3). E. Representative gel documents showing the expression of P-cadherin, α -SMA in different groups. F. Summarized data showing expression of P-cadherin and α -SMA, quantitated as a ratio of P-cadherin band over α -SMA band (n=3-4). * $P < 0.05$ vs. Ctrl; # $P < 0.05$ vs. Baf. Ctrl: Control; Baf: Baf; Vehl: Vehicle; Sp-1: Spautin-1.

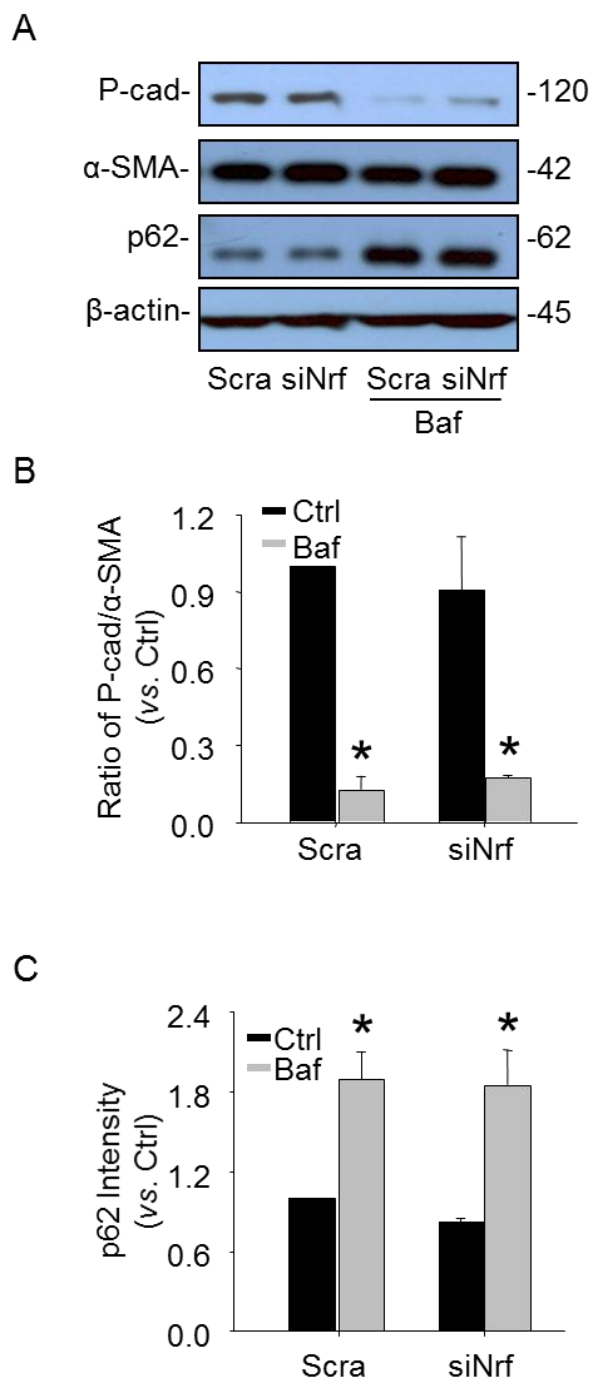


Fig. 6. Failure of Nrf2 gene silencing to alter podocyte dedifferentiation enhanced by lysosome function inhibition. A. Representative gel documents showing the expression of P-cadherin, α -SMA and p62 in different groups. B. Summarized data showing expression of P-cadherin and α -SMA, quantitated as a ratio of P-cadherin band over α -SMA band (n=3-4). C. Summarized data showing expression of p62, quantitated as a ratio of detected specific protein band vs. β -actin as loading control (n=3-4). * P<0.05 vs. Ctrl. Ctrl: Control; Baf: Baf; Scra: scramble RNA; siNrf: Nrf2 siRNA.

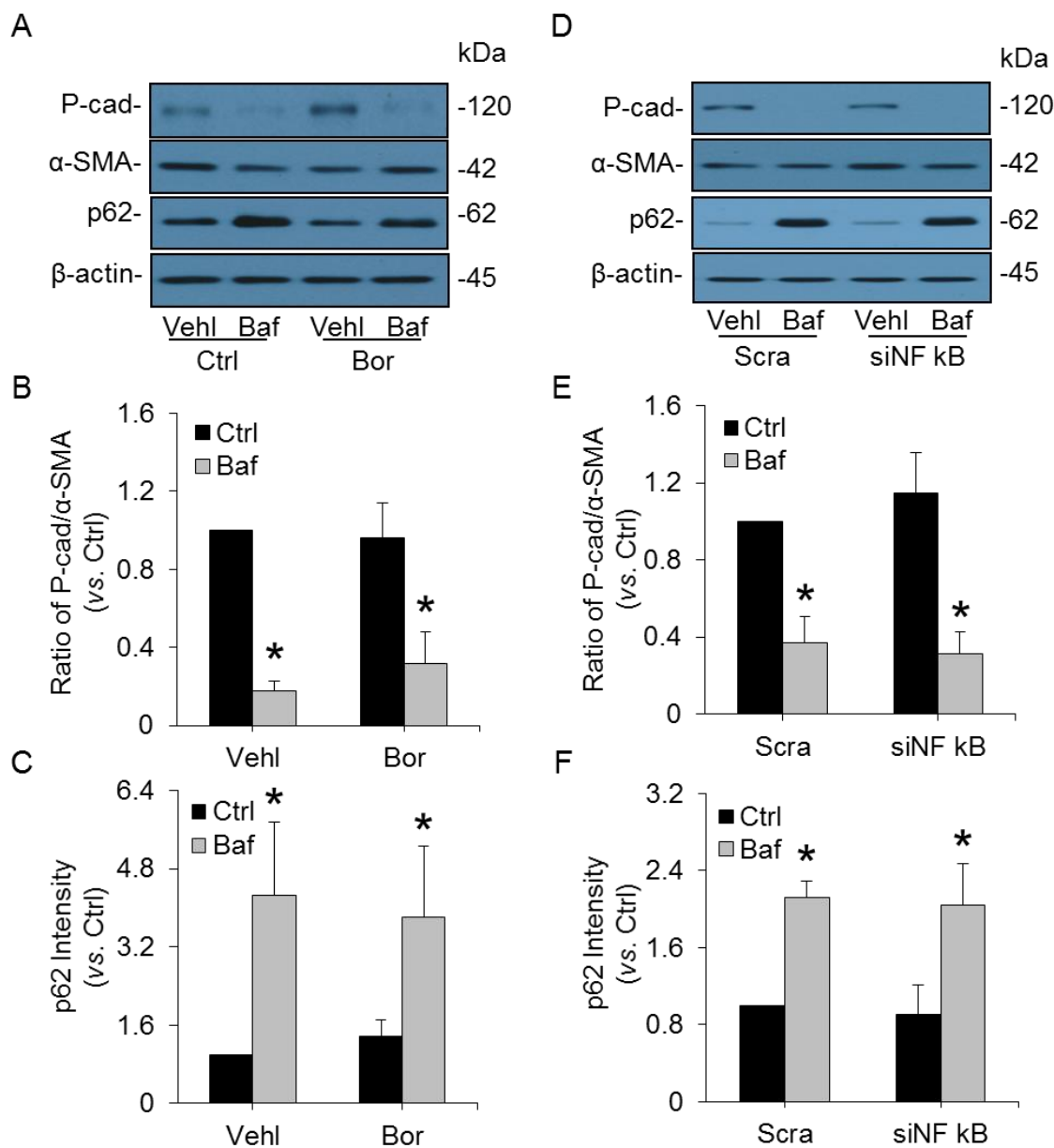


Fig. 7. No changes in enhanced podocyte dedifferentiation by inhibition of NF- κ B-mediated transcriptional regulation. A. Representative gel documents showing the expression of P-cadherin, α -SMA and p62 in different groups. B. Summarized data showing expression of P-cadherin and α -SMA, quantitated as a ratio of P-cadherin band over α -SMA band (n=5). C. Summarized data showing expression of p62, quantitated as a ratio of detected specific protein band vs. β -actin as loading control (n=5). D. Representative gel documents showing the expression of P-cadherin, α -SMA and p62 in different groups. E. Summarized data showing expression of P-cadherin and α -SMA, quantitated as a ratio of P-cadherin band over α -SMA band (n=5). F. Summarized data showing expression of p62, quantitated as a ratio of detected specific protein band vs. β -actin as loading control (n=4). * P<0.05 vs. Ctrl. Ctrl: Control; Baf: Baf; Bor: Bortezomib; Scra: scramble RNA; siNF κ B: NF κ B siRNA.

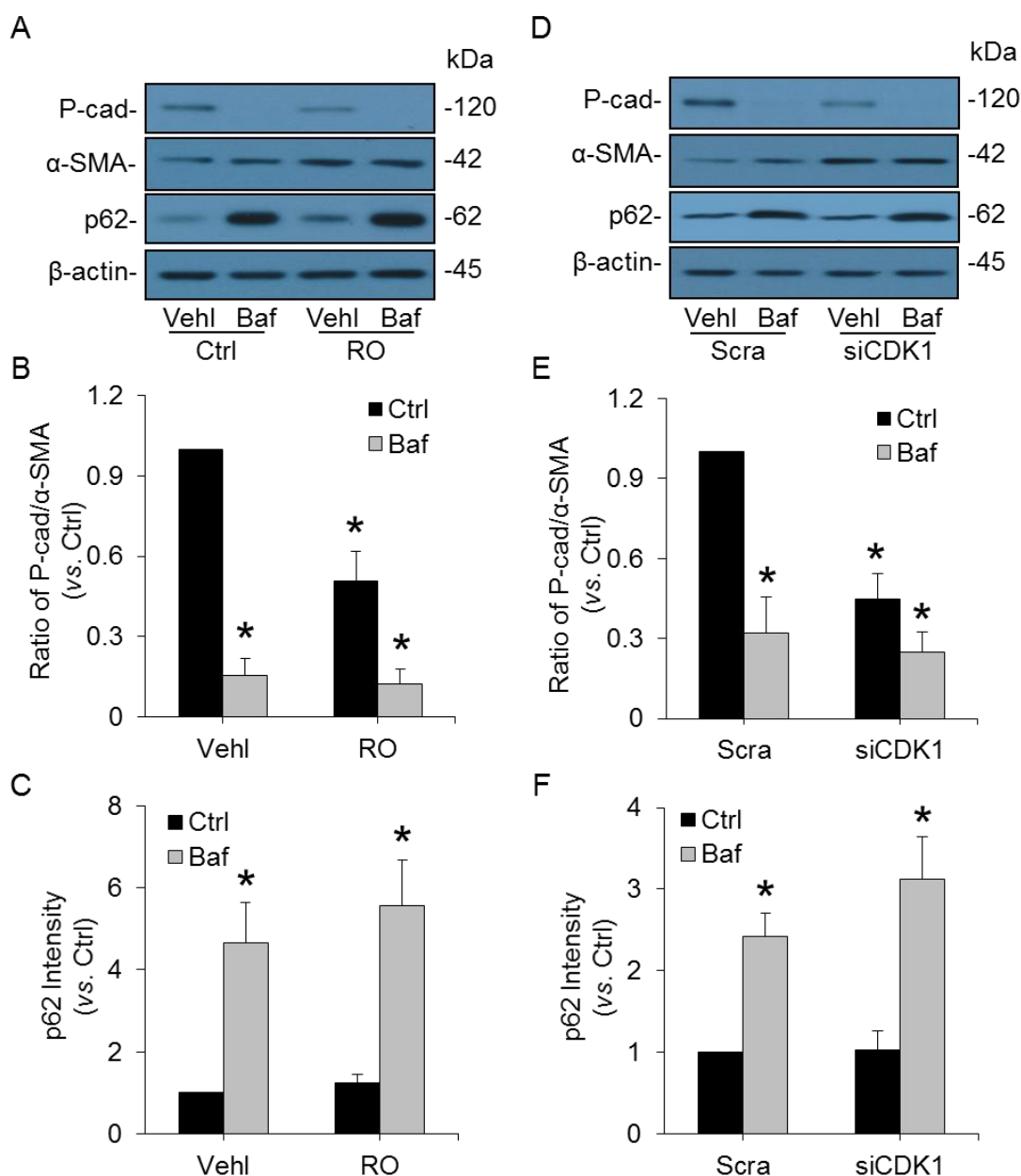


Fig. 8. Enhancement of podocyte dedifferentiation by inhibition of CDK1. A. Representative gel documents showing the expression of P-cadherin, α -SMA and p62 in different groups. B. Summarized data showing expression of P-cadherin and α -SMA, quantitated as a ratio of P-cadherin band over α -SMA band (n=5). C. Summarized data showing expression of p62, quantitated as a ratio of detected specific protein band vs. β -actin as loading control (n=9). D. Representative gel documents showing the expression of P-cadherin, α -SMA and p62 in different groups. E. Summarized data showing expression of P-cadherin and α -SMA, quantitated as a ratio of P-cadherin band over α -SMA band (n=5). F. Summarized data showing expression of p62, quantitated as a ratio of detected specific protein band vs. β -actin as loading control (n=7). * P<0.05 vs. Ctrl. Ctrl: Control; Baf: Baf; RO: RO-3306; Scra: scramble RNA; siCDK1: CDK1 siRNA.

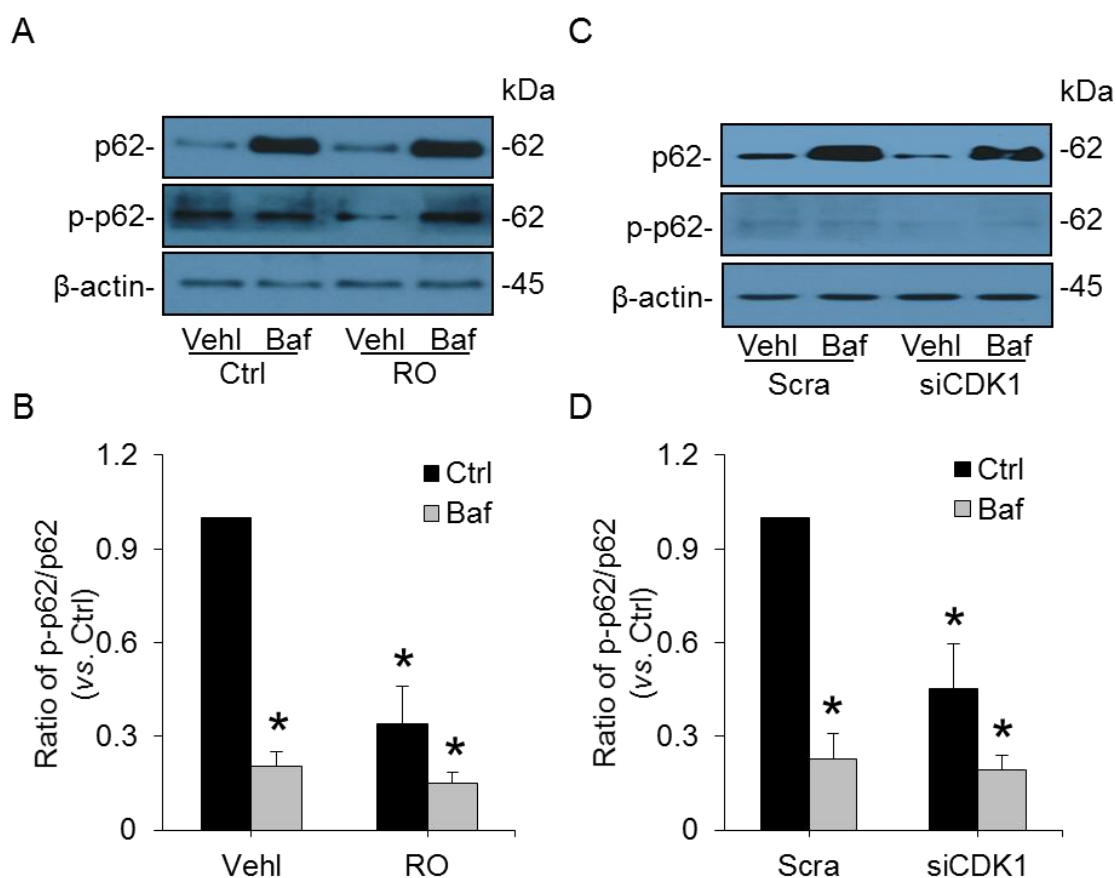


Fig. 9. Reduction of p62 phosphorylation during lysosome function inhibition. A. Representative gel documents showing the expression of p62 and p-p62 in different groups. B. Summarized data showing expression of p62 and p-p62, quantitated as a ratio of p-p62 band over p62 band (n=5). C. Representative gel documents showing the expression of p62 and p-p62 in different groups. D. Summarized data showing expression of p62 and p-p62, quantitated as a ratio of p-p62 band over p62 band (n=4). * P<0.05 vs. Ctrl. Ctrl: Control; Baf: Baf; RO: RO-3306; Scra: scramble RNA; siCDK1: CDK1 siRNA.

CHAPTER FOUR

Contribution of altered ceramide metabolism via acid ceramidase to lysosome dysfunction through reduced TRPML1 channel activity

4.1 Lysosome trafficking and fusion to autophagosome regulated by acid ceramidase in podocytes

The results presented in chapter 3 confirmed that normal lysosome function is essential to the autophagic flux and thereby for podocyte differentiation. Pharmacological and genetic interventions to induce lysosome dysfunction led to accumulation of autophagosomes and thereby activated podocyte dedifferentiation. The next question we tried to answer is whether there is any physiological regulatory system that regulates lysosome functions in podocytes and thereby controls the differentiation of dedifferentiation of these cells. In previous studies from our laboratory and by others, ceramide metabolism in lysosomes was been demonstrated to play an important role in the control of lysosome function including the lysosome fusion to membrane, organelles and Ca^{2+} release (112, 121, 134-136). Therefore, we hypothesized that ceramide production or metabolism may contribute to the regulation of lysosome function, autophagic flux and differentiation of podocytes. A deficiency of ceramide metabolism may result in increased level of ceramide in these cells and thereby cause lysosome dysfunction, autophagic deficiency and dedifferentiation.

To test this hypothesis, we directly observed the role of acid ceramidase, an enzyme for catabolism of ceramide to produce sphingosine in the lysosome trafficking and fusion to autophagosome in living podocytes. In these experiments, both LC3B-GFP and Lamp-1-RFP

gene constructs were introduced into podocytes to visualize lysosome (red puncta) and autophagosome (green puncta). Co-localization of LC3B-GFP and Lamp-1-RFP yields yellow puncta, indicating the fusion of lysosome and autophagosome. As shown in Fig. 10, only a few yellow puncta were detected in living podocytes under control condition. When podocytes were treated with an autophagy activator, rapamycin, which has been reported to enhance the entire autophagic process including autophagosome formation and autophagic flux, the number of yellow puncta markedly increased and the co-localization coefficient of LC3B-GFP with Lamp-1-RFP was significantly increased, indicating enhanced fusion of autophagosomes and lysosomes. On the contrary, the fusion of lysosome and autophagosome was blocked by Baf A1, a V-ATPase inhibitor. Similarly, inhibition of AC activity by carmofur markedly decreased the yellow puncta in these living podocytes. These results suggest that lysosome AC activity is indeed involved in the regulation of lysosome trafficking and fusion to autophagosomes.

4.2 Lysosome trafficking and fusion to MVBs regulated by acid ceramidase in podocytes

We also used another marker to measure lysosome trafficking in podocytes, which was to observe the trafficking of lysosome and fusion to multivesicular bodies (MVBs), which represents another important lysosome function in the regulation of intracellular vesicle trafficking or exosome excretion (137-139). In these experiments, we observed the trafficking and fusion of lysosomes to MVBs in podocytes using confocal microscopy. As shown in Fig. 11A, colocalization of MVB marker, VPS16 (Alex 488, green fluorescence) and lysosome marker, Lamp-1 (Alex 555, red fluorescence) yielded yellow puncta, indicating the fusion of lysosome and MVB. Compared with vehicle group, podocytes with inhibition of AC by carmofur also markedly inhibited lysosome trafficking and fusion to MVB. However, such

inhibition was totally reversed by pretreatment of podocytes with AC inducer genistein or sphingosine, an AC product of ceramide. Similarly, colocalization of another MVB marker Annexin-II (Alex 488, green fluorescence) and Lamp-1 (Alex 555, red fluorescence) was remarkably decreased by carmofur. Moreover, enhancement of AC activity by genistein or addition of sphingosine totally reversed the reduction of lysosome trafficking and fusion to MVB in podocytes (Fig. 11B).

4.3 TRPML1 channel-mediated Ca^{2+} release detected by GCaMP3 in podocytes

To explore the mechanisms by which ceramide metabolism regulates lysosome trafficking, we performed another series of experiments to address the role of lysosome Ca^{2+} release in the regulation of lysosome trafficking. The scientific premise of these experiments is that TRPML1 channel-mediated Ca^{2+} release may be an important driving force for lysosome trafficking, which was demonstrated by a number of previous studies (112, 140, 141). We measured lysosomal Ca^{2+} release in intact podocytes using GCaMP3, a single-wavelength genetically encoded Ca^{2+} indicator, to the cytoplasmic amino terminus of TRPML1 (Fig. 12A). When transfected into podocytes, GCaMP3-TRPML1 (GCaMP3-ML1) was mainly localized in lysosomes. To determine the specificity of the GCaMP3-ML1 fluorescence signal, we tested a specific TRPML1 channel agonist ML-SA1 and found that GCaMP3 fluorescence (F470) responded to ML-SA1 in podocytes. As shown in Fig. 12B, confocal microscopy detected that ML-SA1 remarkably increased GCaMP3 fluorescence in podocytes compared with control condition. Maximal response of GCaMP3 to Ca^{2+} signals was induced by ionomycin, a selective calcium ionophore. These data confirmed the specificity of GCaMP3-ML1 fluorescence as Ca^{2+} responsive signal in podocytes.

4.4 Characterization of lysosome-derived Ca^{2+} release through TRPML1 channel

Next, we investigated whether TRPML1 channel-mediated Ca^{2+} release detected by GCaMP3 is derived from lysosomes in podocytes. A fluorescent microscopic imaging system with high speed wave-length switching was used to dynamically and continuously monitor the GCaMP3 fluorescence signal in podocytes. The representative curves of GCaMP3 fluorescence recording are shown in Fig. 13A. To induce Ca^{2+} release from lysosomes, we used glycy-L-phenylalanine 2-naphthylamide (GPN), a cathepsin C substrate that induces osmotic lysis of lysosomes, which can be used to test whether emptying lysosome Ca^{2+} storage can reduce or abolish GCaMP3 detected Ca^{2+} signals. It was found that early addition of GPN triggered a remarkable increase in GCaMP3 fluorescence in podocytes, which was followed by a much lower GCaMP3 fluorescence signal induced by late addition of ML-SA1 (Fig. 13A). On the other hand, early addition of ML-SA1 induced a rapid increase in GCaMP3 fluorescence and a following addition of GPN only induced a small GCaMP3 fluorescence signal in podocytes (Fig. 13B). These data confirmed that the resource of TRPML1 channel-mediated Ca^{2+} release detected by GCaMP3 was lysosomes in podocytes, which is dependent on lysosome Ca^{2+} stores.

4.5 Inhibition of AC blocked Ca^{2+} release through TRPML1 channel in podocytes

To determine the role of AC in the regulation of TRPML1 channel activity in podocytes, carmofer was used to inhibit AC activity before addition of ML-SA1, a potent synthetic agonist for TRPML1 channel, to Ca^{2+} -free external solution. As shown in Fig. 14, ML-SA1 induced rapid elevation of GCaMP3 fluorescence in podocytes after treatment with vehicle. However, pre-treatment with carmofer totally blocked ML-SA1-induced Ca^{2+} release through TRPML1

channel in podocytes, indicating that normal function of AC is essential for TRPML1 channel activity in podocyte lysosomes.

To further confirm this view, sphingosine or sphingosine-1-phosphate (S1P) as AC metabolites of ceramide was used to treat podocytes during GCaMP3 fluorescence recording. As shown in Fig. 15, it was found that sphingosine triggered remarkable increase in lysosome Ca^{2+} as shown by increased GCaMP3 fluorescence in podocytes. On the other hand, S1P had no effects on TRPML1 channel activity in podocytes. Considering that sphingosine is AC product of ceramide, these data demonstrate that activation of AC and consequent production of sphingosine contribute to TRPML1 channel-mediated Ca^{2+} release from lysosome in podocytes.

4.6 Establishing patch clamp recording using Port-A-Patch

To directly record lysosome Ca^{2+} channels or TRPML1 channels, the Port-A-Patch system- a novel automatic patch clamp technique was used for whole-lysosome patch clamping. At beginning, to establish an appropriate condition for podocyte patch clamping using this new system, we first performed whole-cell patch clamp experiments on the cell membrane of cultured podocytes. Using pannexin-1 (PANX1) channel, an ATP release channel as a prototype channel in podocyte, we successfully tested this new patch clamping system in podocytes and then extend such channel recording system into lysosomes.

We first characterized the expression of PANX1 in murine podocytes. Western blot analysis demonstrated that PANX1 was highly expressed in cultured murine podocytes, while both PANX2 and PANX3 were undetectable in these cells (Figs. 16A and 16B). Using real time

RT-PCR, we found high level of PANX1 mRNA in podocytes (data not shown). Also, abundant expression of PANX1 was confirmed in renal glomeruli of C57BL/6J WT mice using immunohistochemistry (Fig. 16C). However, we failed to observe the immunohistochemical staining of PANX2 or PANX3 in renal glomeruli of these mice. In addition, using confocal microscopy it was found that red fluorescence of PANX1 highly colocalized with green fluorescence of podocin (Fig. 16D) or nephrin (Fig. 16E) in podocytes in vitro or in vivo, which further confirmed the expression of PANX1 in podocytes.

After confirmation of pannexin-1 (PANX1) channel expression in podocytes, we next confirmed the activity of PANX1 as a large transmembrane channel in podocytes. Fig. 17A shows representative recordings of this large voltage-gated outward current at holding potentials from -70 to 80 mV under the $\text{Cs}^+_{\text{in}}/\text{Na}^+_{\text{out}}$ gradient of the cells. Fig. 17B summarizes the relationship of holding potential and channel current amplitude. It is clear that the channel currents increased with the elevation of holding potential and the whole-cell current was $\sim 283.9 \pm 10.9$ pA/pF at +80 mV. Pharmacologically, these podocyte membrane currents were blocked with selective PANX1 inhibitors, carbenoxolone (CBX) and probenecid (PBNC) by $81.0 \pm 2.6\%$ and $73.8 \pm 2.1\%$ of control, respectively. The sensitivity of whole-cell currents to CBX and PBNC was well detected at negative voltage, signifying the voltage-gated property of these currents and further demonstrating the contribution of PANX1 to these currents.

As another important nature of PANX1, anion permeability was also determined by the substitution of extracellular chloride for a carrying anion for PANX1 currents. During whole-cell current recording, 140 mM NaCl, 4 mM KCl, 1 mM MgCl_2 , and 2 mM CaCl_2 were substituted

for 140 mM Na-aspartate, 4 mM K-aspartate, 1 mM Mg-aspartate², 2 mM Ca-aspartate. As shown in Fig. 18A, the replacement of chloride with aspartate (131 Da) remarkably decreased the whole-cell currents and shifted the reversal potential of PANX1 channel to the right. Similar data was obtained when we replaced chloride with gluconate (195 Da) in the external solution (Fig. 18C). Restoration of extracellular chloride totally recovered the whole-cell currents and the reversal potential of PANX1 channel in podocytes. Summarized data demonstrated significant decrease in whole-cell currents by chloride replacement (Fig. 18B and Fig. 18D). Altogether, these observations confirmed that PANX1 is a voltage-gated transmembrane channel with anion permeability in podocytes.

4.7 Regulation of PANX1 channel activity by adipokines

Given the stimulatory role of extracellular ATP in inflammation and chronic low-grade inflammation as a hallmark of obesity, we tested whether visfatin, a pro-inflammatory adipokine from fat cells activates PANX1 channel activity to release ATP. As shown in Fig. 19A, addition of visfatin into the bath solution remarkably increased whole-cell PANX1 currents. Summarized data showed that visfatin at 0.25-1 $\mu\text{g}/\text{mL}$ significantly enhanced PANX1 channel activity in a dose-dependent manner (Fig. 19B). When podocytes were pretreated with CBX, visfatin-induced enhancement of PANX1 channel activity was almost completely blocked (Fig. 19C and Fig. 19D).

Since previous studies have reported that adiponectin, a protective adipokine, can increase intracellular ATP content, further experiments were designed to determine whether these channels can be inhibited by adiponectin. As shown in Fig. 20A, the representative recordings

showed that addition of adiponectin into the extracellular solution remarkably decreased whole-cell currents of PANX1. Fig. 20B summarizes the results showing that adiponectin at 2.5-10 $\mu\text{g/mL}$ significantly inhibited the PANX1 channel activity in a dose-dependent manner. When the dose of adiponectin reached 10 $\mu\text{g/mL}$, the activity of PANX1 channel decreased to $29.4\pm 5.3\%$ of control, a level similar to the effects of CBX and PBNC.

These experiments demonstrate that podocytes express PANX1 channels on their cell membrane, which may be important for the regulation of ATP release under different physiological and pathological conditions. Importantly, we found that a Port-A-Patch system can be used to automatically patch clamp podocytes for recording of podocytes. To our knowledge, these results represent the first use of Port-a-Patch for podocyte PANX1 channels recording to show the regulatory action of adipokines on the activity of this channel. Importantly, the establishment of such cell patching and recording system provides an important tool for us to study intracellular organellar channels given the potential for automatic patching of single lysosome without use of glass pipettes.

4.8 Characterization of enlarged lysosomes isolated from podocytes

For patch clamp studies of single lysosomes from podocytes using the Port-A-Patch system, we need to isolate and purify lysosomes from these cells. To isolate lysosomes, we first treated podocytes with vacuolin-1 to enlarge lysosomes and then isolated enlarged lysosomes from podocytes for whole-lysosome patch clamp recording. As shown in Fig. 21A, a lysosome isolated from podocytes was confirmed by differential interference contrast (DIC) microscopy compared to podocytes in size. Isolated lysosomes loaded with LysoTracker were also confirmed

with green fluorescence that indicates the low pH of lysosome lumen. In addition, the purity of isolated lysosomes was confirmed by flow cytometry. Fig. 21B showed that isolated lysosomes loaded with LysoTracker shifted to the area with high fluorescence intensity. Quantification of the data in Fig. 21B indicated very high purity of isolated lysosomes.

After confirmation of integrity and purity of isolated lysosomes, the whole-lysosome patch clamp approach was adopted to characterize the properties of TRPML1 channel in isolated lysosomes. As shown in Fig. 22, bath application of ML-SA1 induced TRPML1 channel-mediated Ca^{2+} releasing current from lysosome in a dose-dependent manner. In the presence of 20 μM ML-SA1 in the bath solution, the whole-lysosome current was -333.18 ± 18.83 pA at -200 mV with positive reversal potentials. These data demonstrated the normal function of TRPML1 channel in isolated lysosomes from podocytes.

4.9 Enhancement of TRPML1 channel activity by sphingosine

To further confirm the role of AC in TRPML1 channel-mediated Ca^{2+} release from lysosomes, the effects of sphingolipids associated with AC, sphingomyelin (SM), ceramide (Cer), and sphingosine (Sph), on TRPML1 channel currents were tested by whole-lysosome patch clamp recording. As shown in Fig. 23, ML-SA1-induced Ca^{2+} enhancement through TRPML1 channels was blocked by sphingomyelin. On the other hand, ceramide had no effects on TRPML1 channel-mediated Ca^{2+} currents induced by ML-SA1. Sphingosine, the AC product of ceramide, was found to enhance TRPML1 channel activation in the presence of ML-SA1. These results imply that inhibition of AC may reduce sphingosine production, thereby decreasing TRPML1 channel activity. It is also possible that reduction of AC activity induces ceramide

accumulation in lysosomes, which in turn results in sphingomyelin increase, thereby suppressing TRPML1 channel activity. This effect of sphingolipids on TRPML1 channel activity may be a cellular mechanistic basis for their regulation of lysosome trafficking, which can be toward autophagosomes, MVBs, or SRs (89, 120, 141, 142).

LC3-II-GFP/Lamp-1-RFP

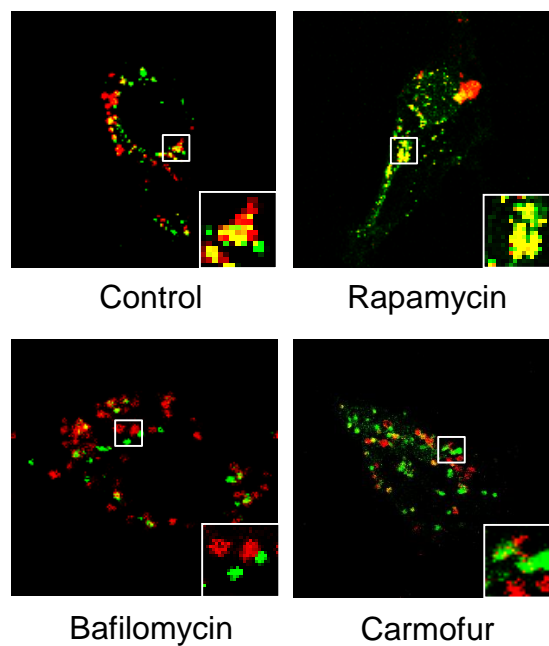


Fig. 10. Lysosome trafficking and fusion to autophagosome regulated by acid ceramidase in podocytes. Representative images showing the colocalization of LC3B-GFP and Lamp-1-RFP in podocytes of various treatment groups (n=3). Veh1: vehicle; Baf: Baf A1; Carm: Carmofur; RPM: rapamycin.

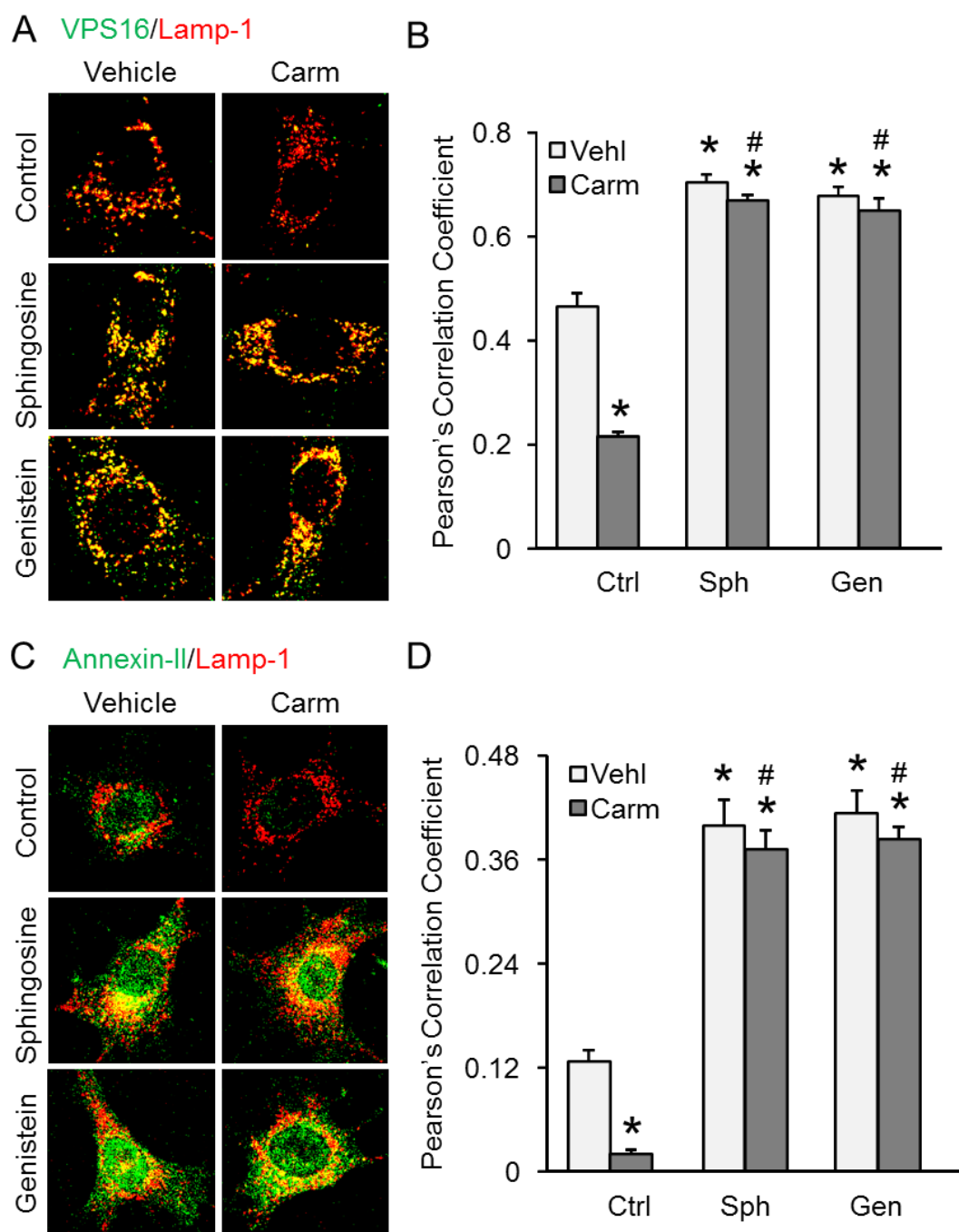


Fig. 11. Lysosome trafficking and fusion to MVBs regulated by acid ceramidase in podocytes. A. Representative images showing the colocalization of VPS16 (green fluorescence) and Lamp-1 (red fluorescence) in podocytes of various treatment groups. B. Summarized data of colocalization coefficients of VPS16 and Lamp-1 in podocytes of various treatment groups (n=4). C. Representative images showing the colocalization of Annexin-II (green fluorescence) and Lamp-1 (red fluorescence) in podocytes of various treatment groups. D. Summarized data of colocalization coefficients of Annexin-II and Lamp-1 in podocytes of various treatment groups (n=4). * P<0.05 vs. Ctrl-Vehl. # P<0.05 vs. Ctrl-Carm. Ctrl: Control; Carm: Carmofur; Sph: sphingosine; Gen: Genistein.

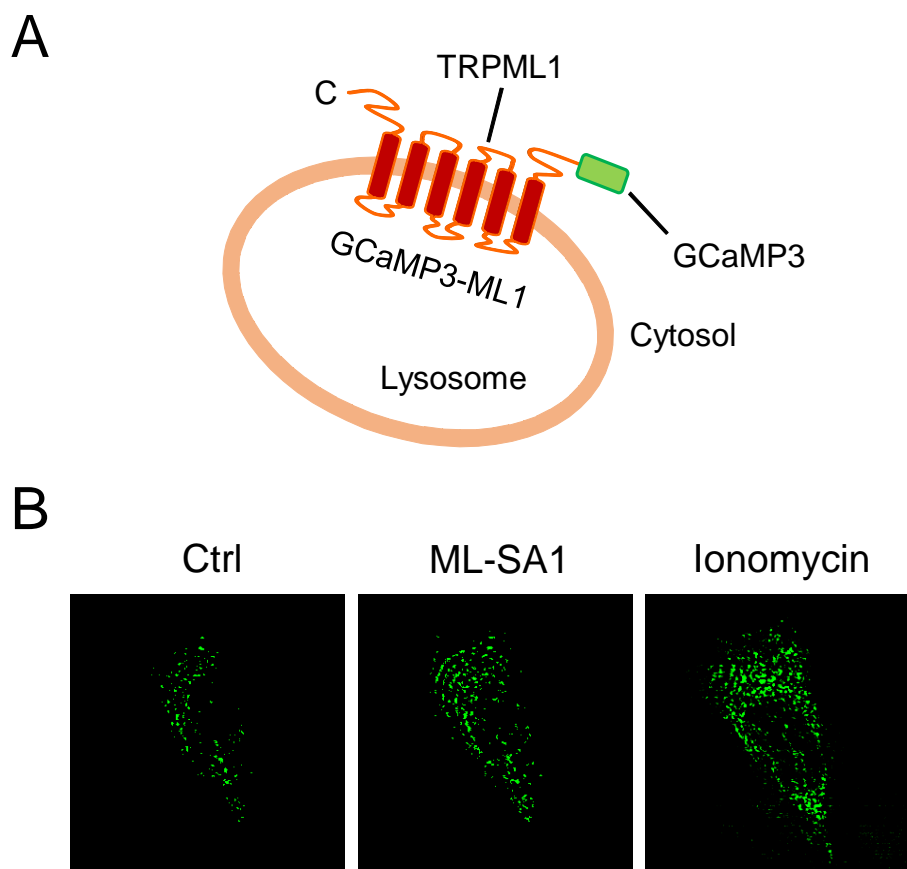


Fig. 12. TRPML1 channel-mediated Ca^{2+} release detected by GCaMP3 in podocytes. A. GCaMP3-TRPML1 (GCaMP3-ML1) fusion strategy. GCaMP3 is fused to the N-terminus of TRPML1. **B.** Representative micrographs showing the changes of GCaMP3 fluorescence upon bath application of ML-SA1 and ionomycin to GCaMP3-ML1-transfected podocytes.

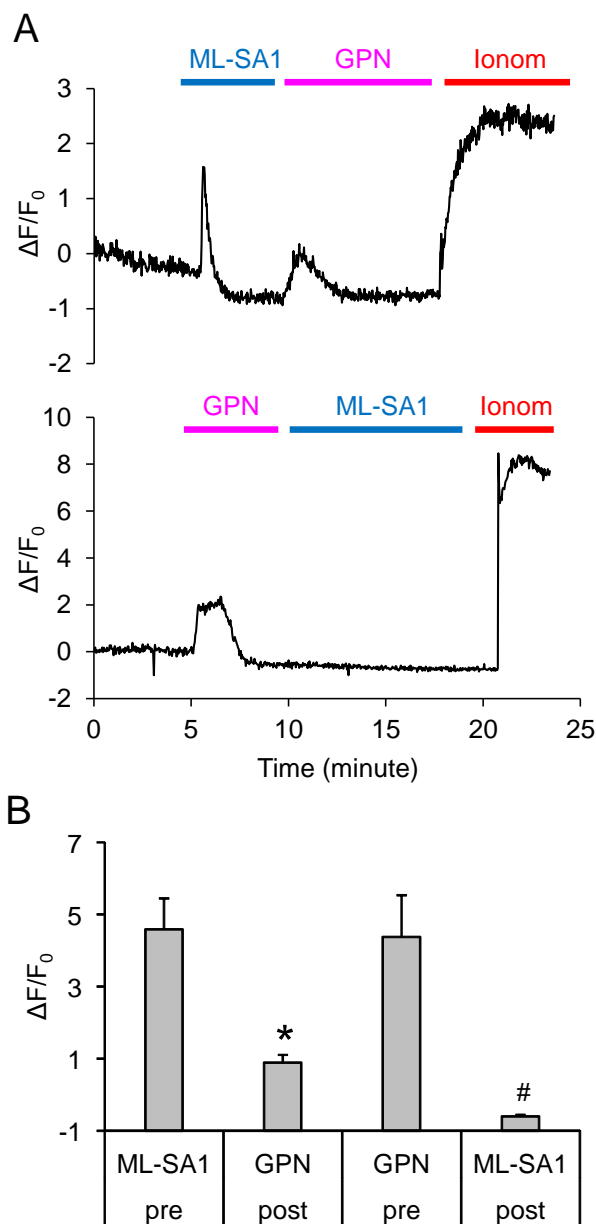


Fig. 13. Characterization of lysosome-derived Ca²⁺ release through TRPML1 channel.

A. ML-SA1 (20 μM) induced rapid increases in GCaMP3 fluorescence (measured as change of GCaMP3 fluorescence ΔF over basal fluorescence F₀; ΔF/F₀) in podocytes transfected with GCaMP3-ML1. Subsequent application of GPN (200 μM) induced smaller responses. On the other hand, ML-SA1 induced small responses in GCaMP3-ML1-expressing podocytes that had received an application of GPN. Maximal responses were induced by ionomycin (1 μM) application. B. Summarized data showing ML-SA1-induced responses in podocytes transfected with GCaMP3-ML1 after pretreatment with GPN and GPN-induced responses in podocytes transfected with GCaMP3-ML1 after pretreatment with ML-SA1. * P<0.05 vs. pre-treatment with ML-SA1. # P<0.05 vs. pre-treatment with GPN. GPN: glycyl-L-phenylalanine 2-naphthylamide; Ionom: ionomycin.

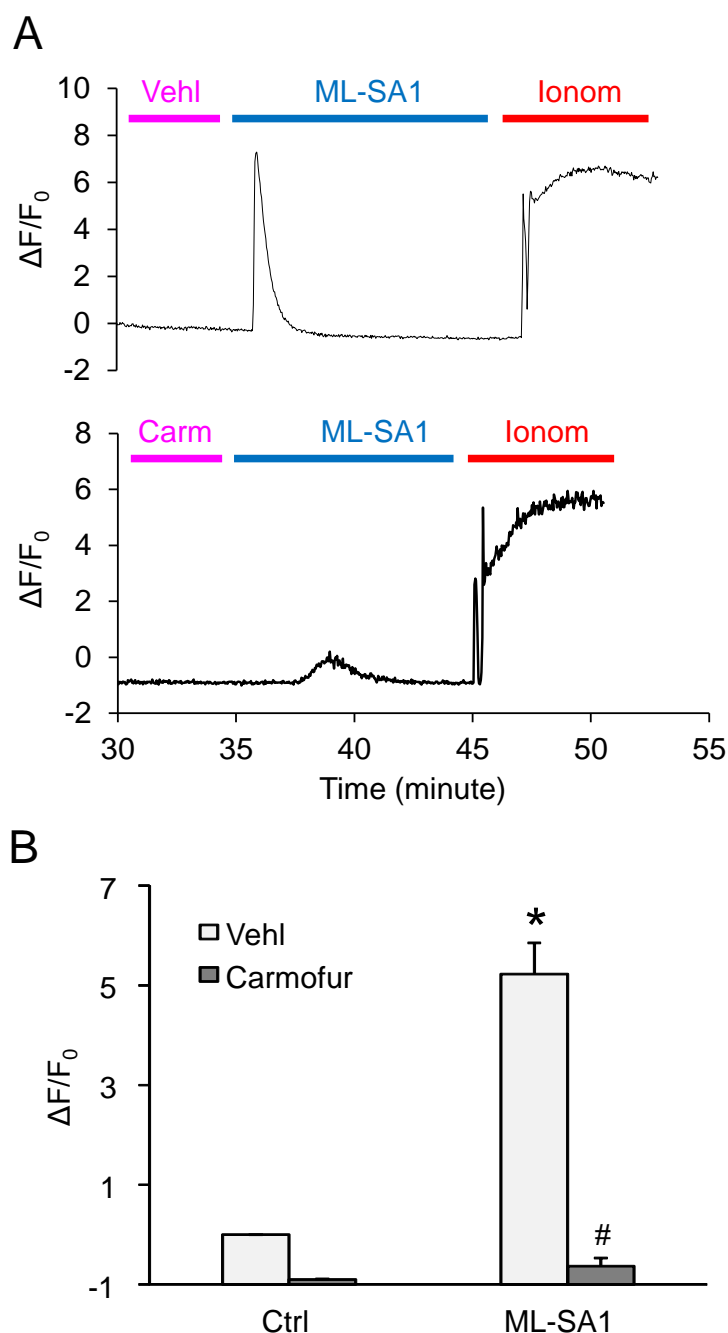


Fig. 14. Inhibition of AC blocked Ca²⁺ release through TRPML1 channel in podocytes. A. ML-SA1 (20 μM) induced rapid increases in GCaMP3 fluorescence (measured as change of GCaMP3 fluorescence ΔF over basal fluorescence F_0 ; $\Delta F/F_0$) in podocytes transfected with GCaMP3-ML1 after pre-treatment with vehicle. On the other hand, ML-SA1 induced small responses in GCaMP3-ML1-expressing podocytes after pre-treatment with Carmofur. Maximal responses were induced by ionomycin (1 μM) application. B. Summarized data showing ML-SA1-induced responses in podocytes transfected with GCaMP3-ML1 after pretreatment with vehicle and ML-SA1-induced responses in podocytes transfected with GCaMP3-ML1 after pretreatment with Carmofur. * $P < 0.05$ vs. Vehl-Ctrl. # $P < 0.05$ vs. Vehl-ML-SA1. Ctrl: control; Vehl: vehicle; Ionom: ionomycin; Carm: Carmofur.

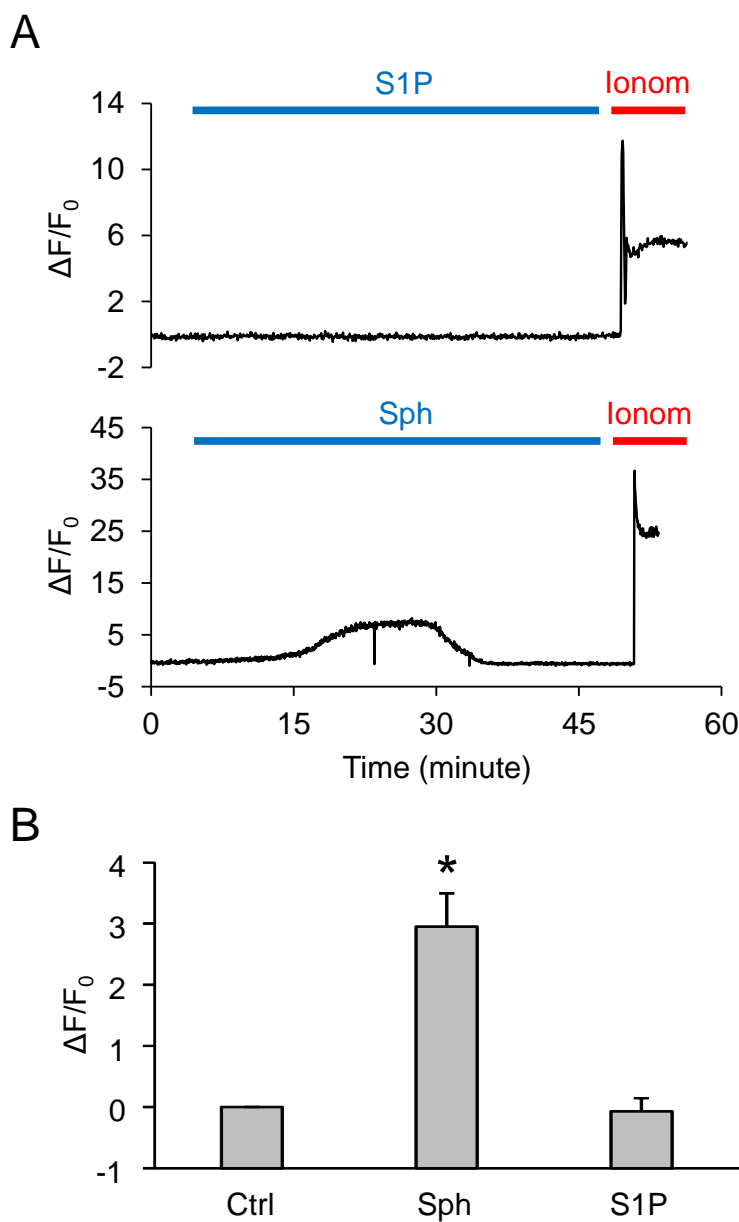


Fig. 15. Spingosine induced Ca^{2+} release through TRPML1 channel in podocytes. A. Spingosine ($20 \mu\text{M}$) induced remarkable increases in GCaMP3 fluorescence in podocytes transfected with GCaMP3-ML1. On the other hand, S1P had no effects on GCaMP3 fluorescence in GCaMP3-ML1-expressing podocytes. Maximal responses were induced by ionomycin ($1 \mu\text{M}$) application. B. Summarized data showing responses in podocytes transfected with GCaMP3-ML1 induced by spingosine and S1P. * $P < 0.05$ vs. Ctrl. Ctrl: control; Sph: spingosine; S1P: spingosine-1-phosphate.

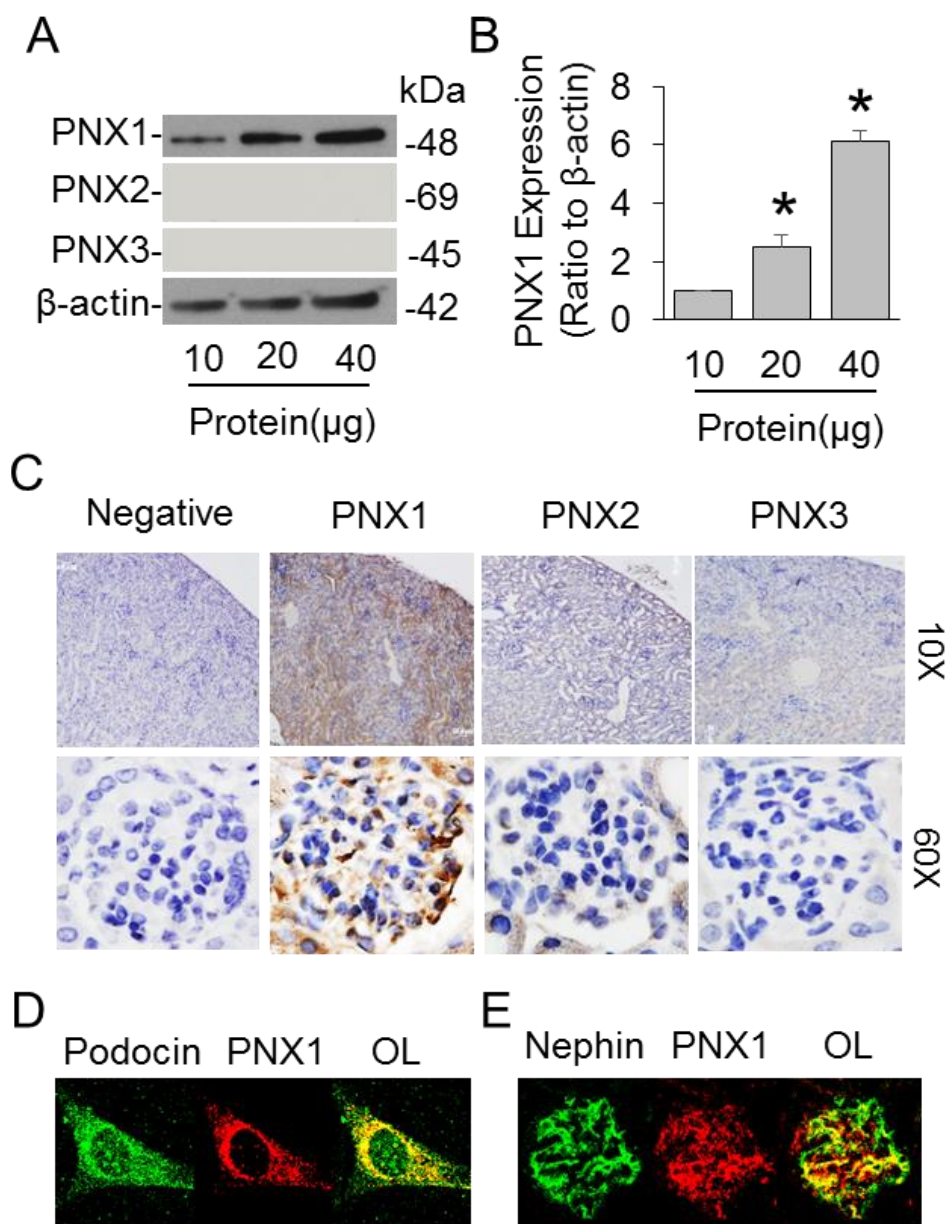


Fig. 16. Expression of PANXs in cultured podocytes. A. Representative Western blot gel documents and summarized data showing the expressions of PANX1, PANX2, and PANX3 in cultured podocytes. B. Summarized data showing the expressions of PANX1 in cultured podocytes (n=4). C. Immunohistochemical staining of PANX1, PANX2, and PANX3 in glomeruli from mice (n=4-5). D. Representative image of confocal microscopy showing the colocalization of podocin and PANX1 in cultured podocytes (n=4). E. Representative image of confocal microscopy showing the colocalization of nephrin and PANX1 in glomeruli from mice (n=6). * $p < 0.05$ vs. 10 μ g protein group. PANX: pannexins; OL: overlay.

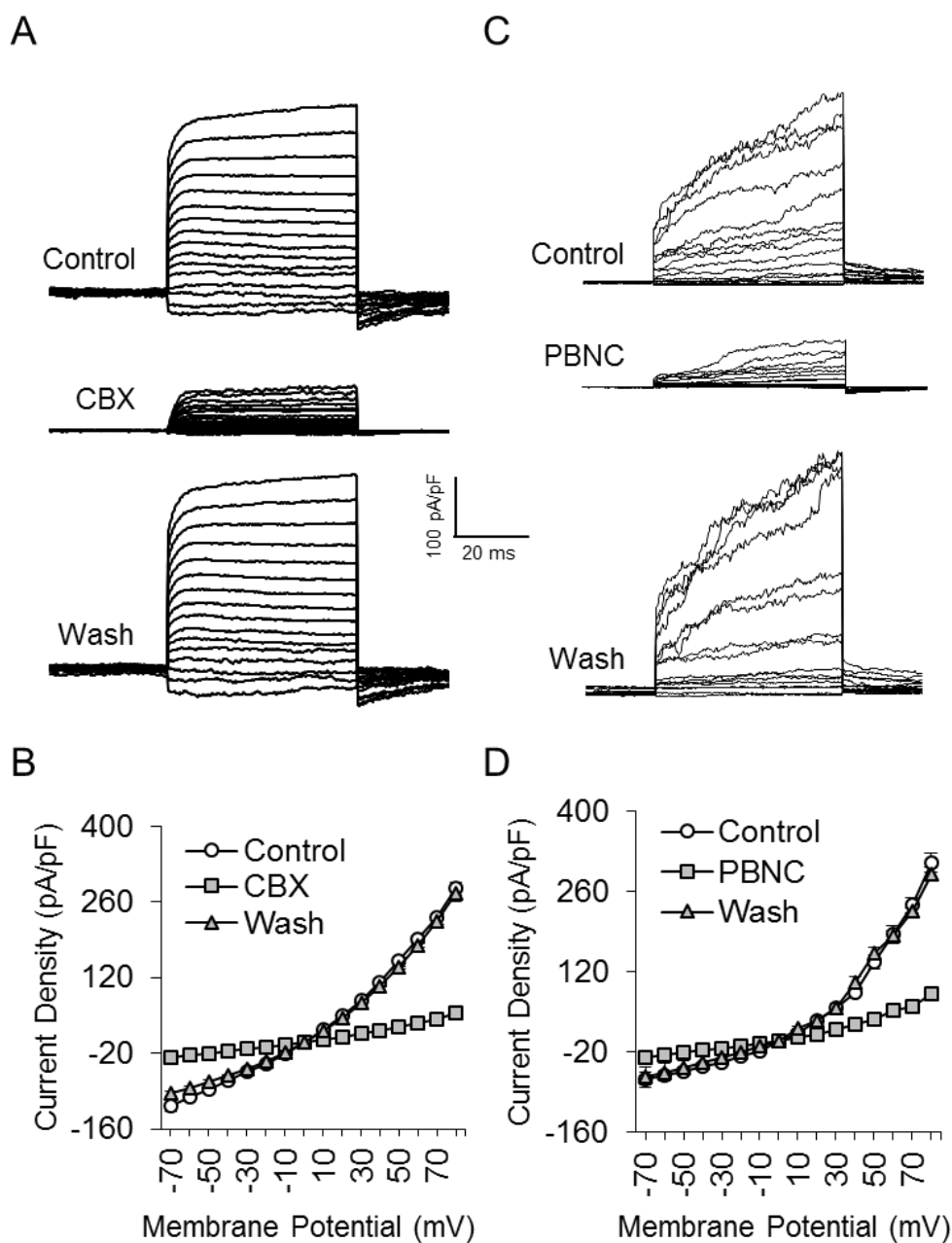


Fig. 17. Recording and pharmacological inhibition of PANX1 channel activity in podocytes. Podocytes were held at -50 mV and polarized by 100 ms voltage pulses between -70 and 80 mV. A. Representative whole-cell currents of podocytes with or without CBX. B. I-V curves of steady-state currents of podocytes with or without CBX (25 μ M) (n=10). C. Representative whole-cell currents of podocytes in the presence or the absence of PBNC. D. I-V curves of steady-state currents of podocytes in the presence or the absence of PBNC (1 mM) (n=12). CBX: carbenoxolone; PBNC: probenecid.

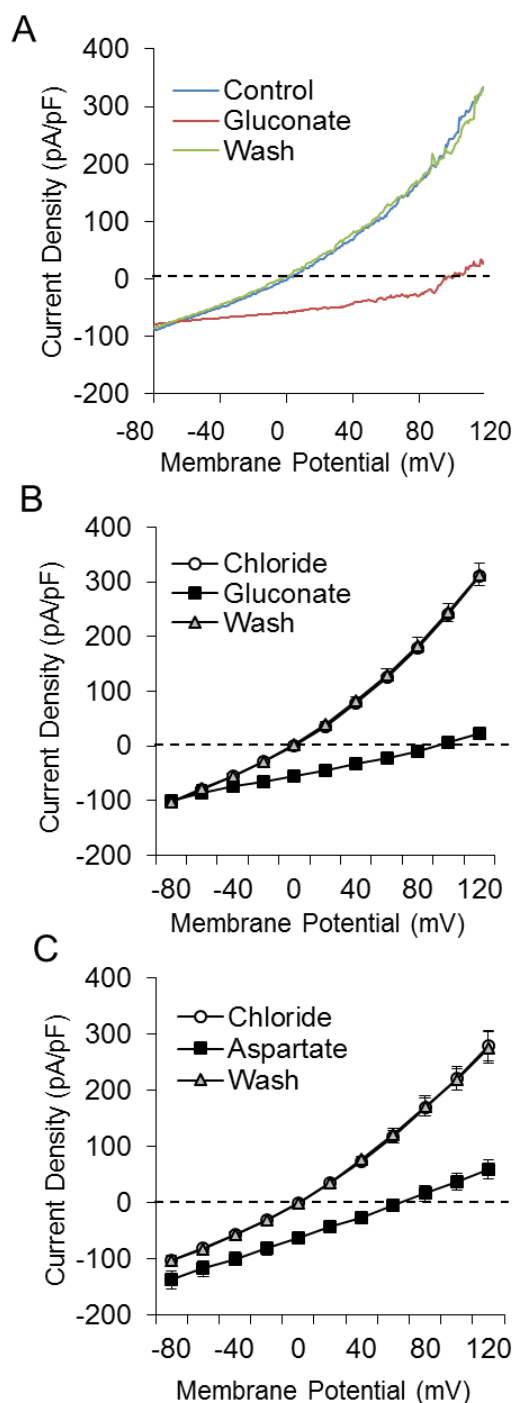


Fig. 18. Anion permeability of PANX1 channels. PANX1 currents in podocytes were recorded with different anion in the external solution. A. Representative whole-cell currents of podocytes with chloride or aspartate in the external solution. B. I-V curves illustrating shifts of PANX1 current reversal potentials upon replacement of extracellular chloride with aspartate (n=5). C. Representative whole-cell currents of podocytes with chloride or gluconate in the external solution. D. I-V curves illustrating shifts of PANX1 current reversal potentials upon replacement of extracellular chloride with gluconate (n=8).

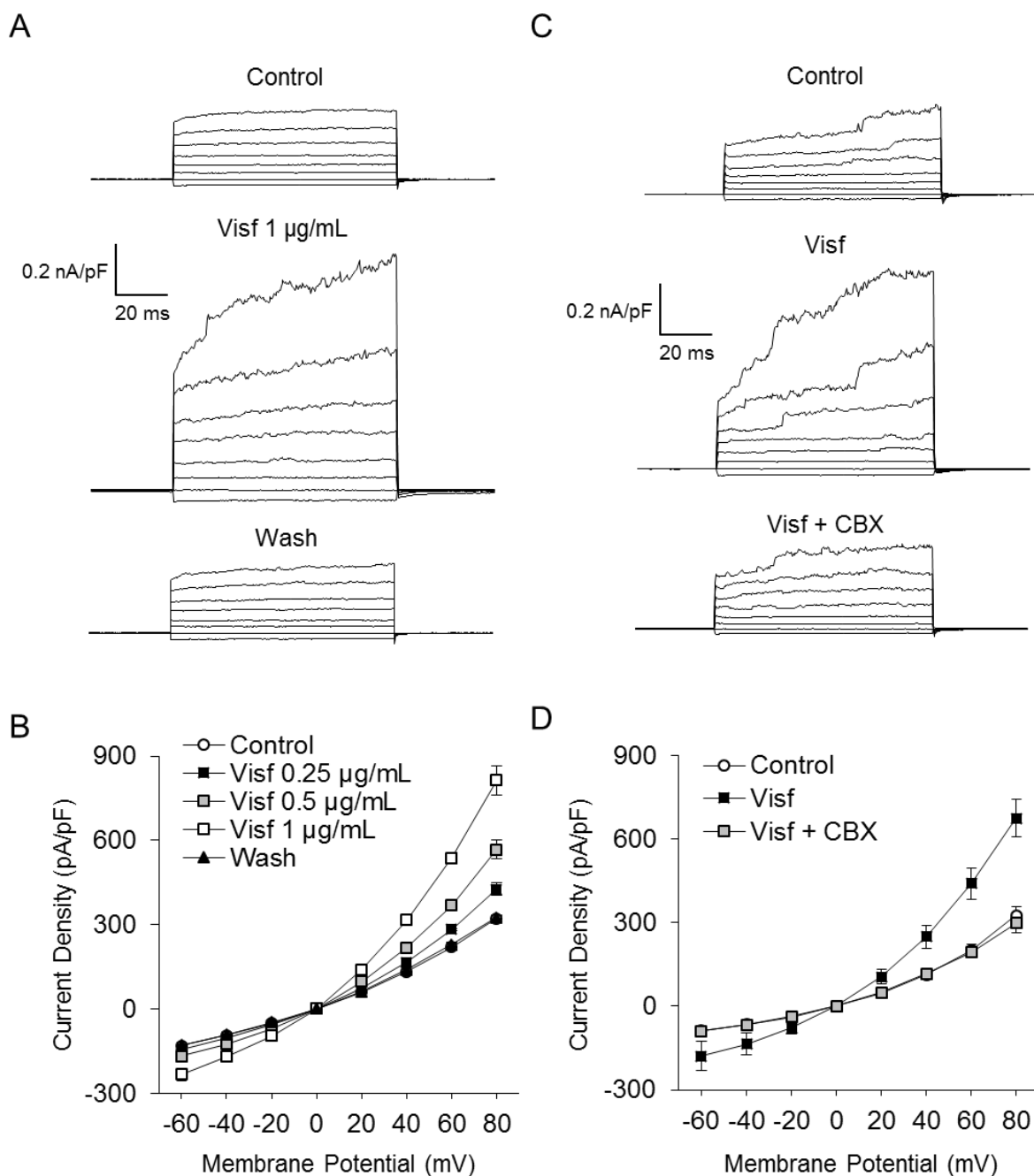


Fig. 19. Concentration-dependent enhancement of PANX1 channel activity by visfatin.

A. Representative whole-cell currents of podocytes with or without visfatin in the external solution. B. I-V curves of steady-state currents of podocytes with or without visfatin in 3 doses (0.25, 0.5, and 1 $\mu\text{g/mL}$) in the external solution (n=9). C. Representative whole-cell currents of podocytes before and after addition of visfatin to the external solution with CBX. D. I-V curves of steady-state currents of podocytes before and after addition of visfatin to the external solution with CBX (n=6). The responses were statistically distinguishable ($P < 0.05$ vs. Control group). Visf: visfatin; CBX: carbenoxolone.

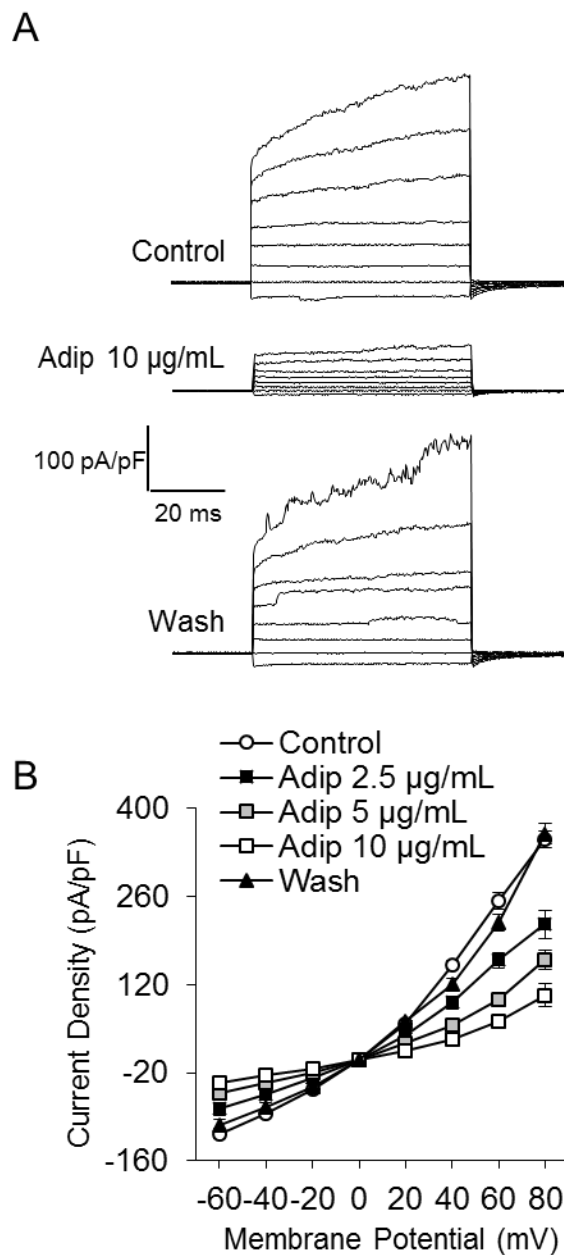


Fig. 20. Concentration-dependent inhibition of PAXX1 channel activity by adiponectin. A. Representative whole-cell currents of podocytes with or without adiponectin in the external solution. B. I-V curves of steady-state currents of podocytes with or without adiponectin in 3 doses (2.5, 5, and 10 $\mu\text{g}/\text{mL}$) in the external solution ($n=9$). The responses were statistically distinguishable ($P<0.05$ vs. Control group). Adip: adiponectin.

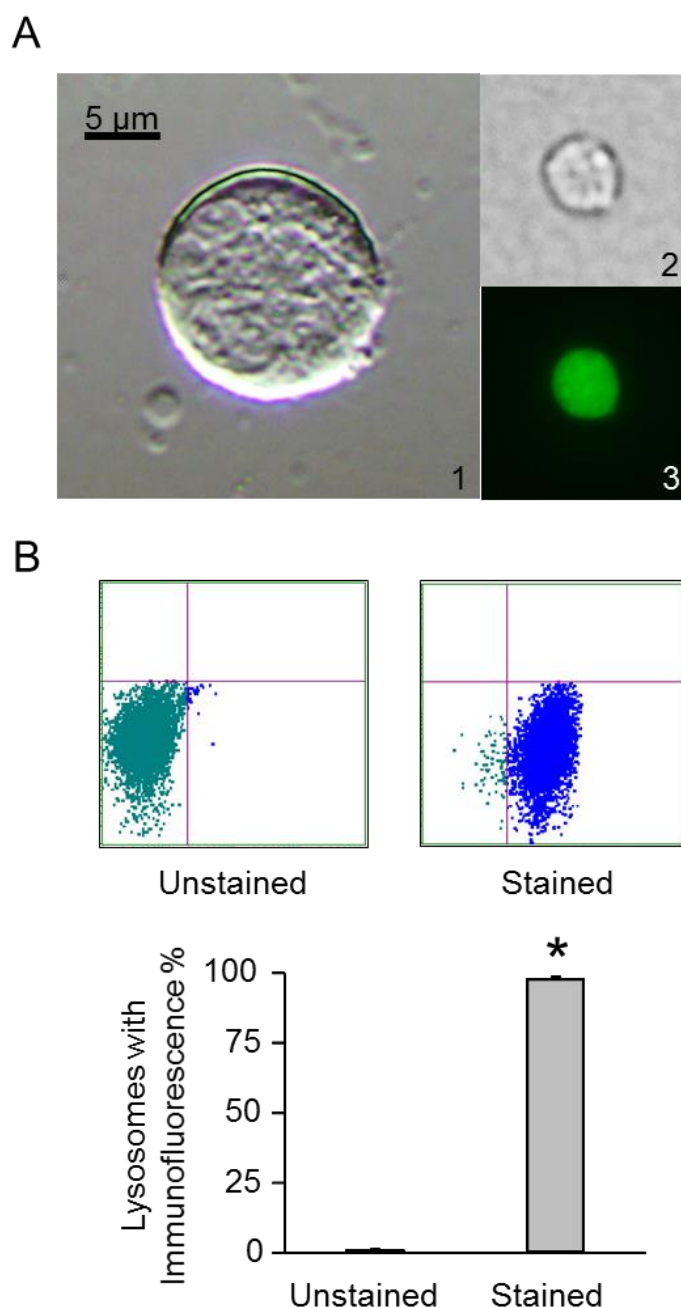


Fig. 21. Characterization of lysosomes isolated from murine podocytes. A. Representative images of (1) DIC picture of suspended podocyte, (2) DIC picture of isolated lysosome, and (3) isolated lysosome stained with LysoTracker. B. Purity of isolated lysosomes detected by flow cytometry (n=5). * P<0.05 vs. Unstained group.

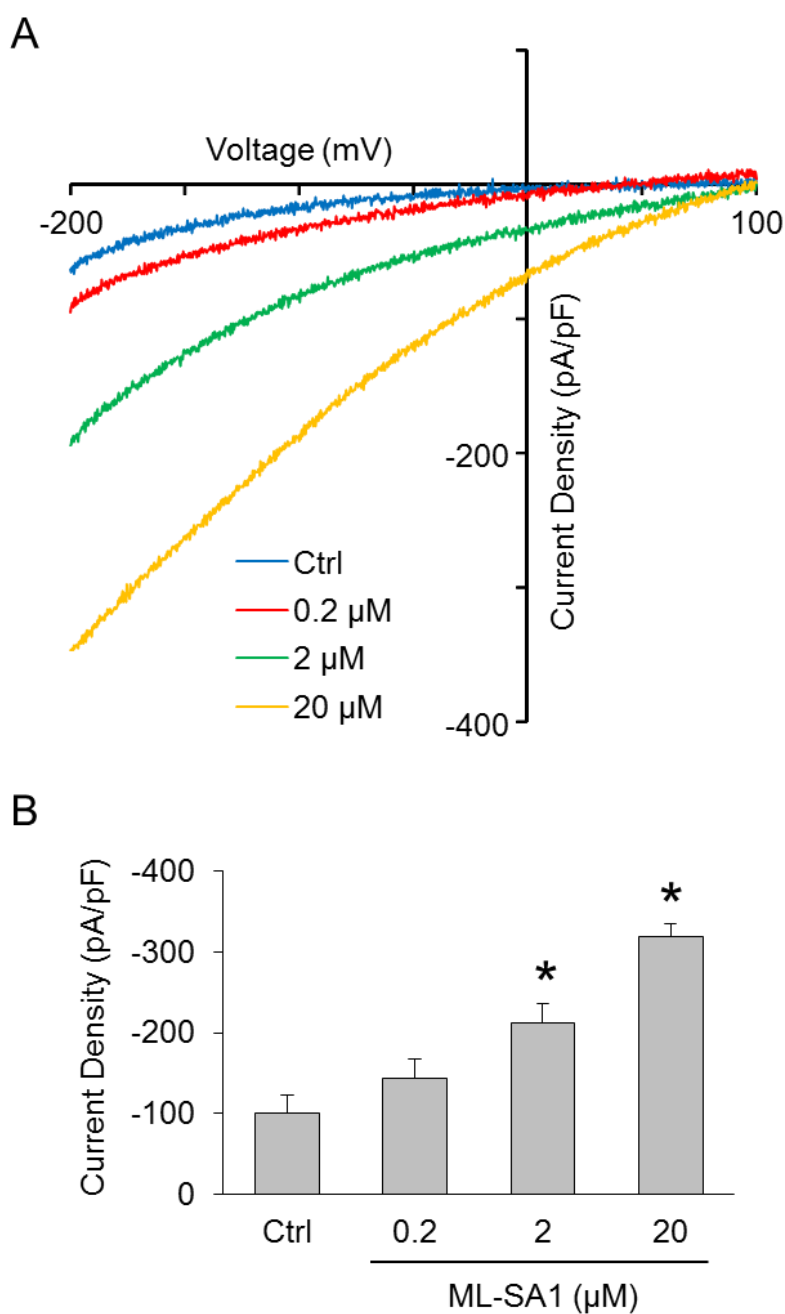


Fig. 22. Concentration-dependent activation of TRPML1 channel activity by ML-SA1. A. Representative whole-lysosome currents enhanced by ML-SA1. B. ML-SA1 enhanced TRPML1 channel activity in a concentration-dependent manner (n=5). * P<0.05 vs. Control group. Ctrl: control.

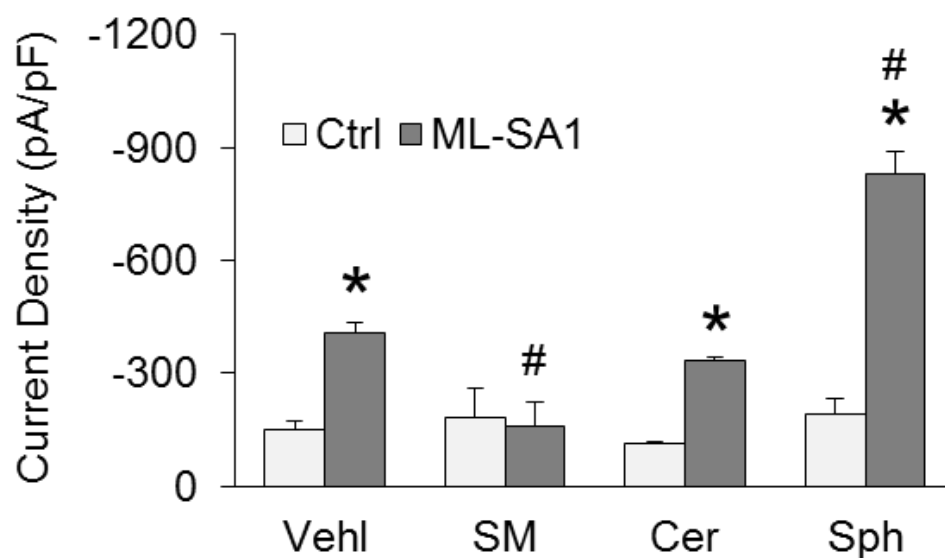


Fig. 23. Regulation of TRPML1 channel activity by sphingolipids. Summary of the effects of various sphingolipids on whole-lysosome currents (n=5). * P<0.05 vs. Ctrl-Vehl group. # P<0.05 vs. ML-SA1-Vehl group. Ctrl: control; Vehl: vehicle; SM: sphingomyelin; Cer: ceramide; Sph: sphingosine.

CHAPTER FIVE

Albuminuria and podocytopathy induced by podocyte-specific gene deletion of AC α subunit

5.1 Characterization of podocyte-specific gene deletion of AC α subunit in *Asah1^{fl/fl}/Podo^{Cre}* mice

To further investigate the physiological relevance of AC inhibition or ceramide metabolism in podocytes to glomerular function, we developed a mouse model with podocyte-specific AC gene knockout, which is named as *Asah1^{fl/fl}/Podo^{Cre}* mouse colony (*Asah1* is AC gene code in mice). These mice and their littermates were characterized by several genetic, molecular and biochemical approaches. As shown in Fig. 24A, by PCR genotyping, detection of both homozygous floxed gene *Asah1* and Cre recombinase gene was considered as homozygous mice with Cre expression. If neither floxed *Asah1* gene nor Cre recombinase gene were detected, the mice were wild type (WT/WT). If only floxed *Asah1* gene was detected without Cre recombinase gene, the mice were *Asah1* flox control without podocyte specific deletion (*Asah1^{fl/fl}/WT*). Confocal microscopy showed no colocalization of podocyte marker podocin (green fluorescence) and AC α subunit (red fluorescence) in glomeruli of *Asah1^{fl/fl}/Podo^{Cre}* mice, compared to WT/WT and *Asah1^{fl/fl}/WT* mice, which indicates podocyte-specific gene deletion of AC α subunit in glomeruli of *Asah1^{fl/fl}/Podo^{Cre}* mice (Fig. 24B).

To further confirm the tissue specific *Asah1* gene deletion in podocytes, *Asah1^{fl/fl}/Podo^{Cre}* mice were mated with lacZ/EGFP mice to produce *Asah1^{fl/fl}/Podo^{Cre}+lacZ/EGFP* mice. Based on previous studies, lacZ/EGFP mice with floxed lacZ express β -galactosidase (lacZ product)

throughout embryonic development and adult stages which is driven by CMV promoter. Cre excision, however, removes the lacZ gene, which activates expression of the second reporter, enhanced green fluorescent protein (EGFP). To detect podocyte-specific expression of β -galactosidase, the hydrolysis of X-gal to produce a blue color was analyzed. As shown in Fig. 25A, the hydrolysis of X-gal in glomeruli was shown by the dark blue staining in the glomeruli of lacZ/EGFP mice. However, the dark blue staining in glomeruli of mice with positive expression of *Asah1*^{fl/fl}/Podo^{Cre} and lacZ/EGFP genes was much weaker compared with only lacZ/EGFP mice because Cre recombinase removed lacZ gene in podocytes. The dark blue staining was undetectable in glomeruli of *Asah1*^{fl/fl}/Podo^{Cre} mice due to the lack of lacZ gene.

Using confocal microscopy, we also analyzed the expression of EGFP in the glomeruli of *Asah1*^{fl/fl}/Podo^{Cre} mice and their littermates. While the green fluorescence emitted by EGFP was undetectable in *Asah1*^{fl/fl}/Podo^{Cre} or lacZ/EGFP mice, colocalization of EGFP (green fluorescence) and podocin (red fluorescence) was remarkable in glomeruli of *Asah1*^{fl/fl}/Podo^{Cre}+lacZ/EGFP mice (Fig. 25B). This is because expression of EGFP was activated when two types of mouse strains were crossbred. Altogether, these results from different characterizing protocols confirm podocyte-specific deletion of AC gene in *Asah1*^{fl/fl}/Podo^{Cre} mice.

5.2 Ceramide accumulation in glomeruli of *Asah1*^{fl/fl}/Podo^{Cre} mice

To confirm whether podocyte-specific gene deletion of AC α subunit results in remarkable changes of ceramide and sphingosine in podocytes, glomeruli of WT/WT, *Asah1*^{fl/fl}/WT, and *Asah1*^{fl/fl}/Podo^{Cre} mice were isolated for sphingolipid measurement by liquid chromatography

tandem mass spectrometry (LC-MS/MS). Fig. 26A shows the representative MS chromatography of ceramide in standard and extracts of sphingolipids from glomeruli of mice with different genotypes. Seven clear peaks of corresponding to C12, C14, C16, C18, C20, C22, and C24 ceramides were detected. Total ceramide level and C16 ceramide, the main substrate of AC, were analyzed after normalization by glomerulus numbers collected during glomeruli isolation from mice. It was found that both total ceramide and C16 ceramide level were much higher in glomeruli of *Asah1^{fl/fl}/Podo^{Cre}* mice, compared with WT/WT and *Asah1^{fl/fl}/WT* mice (Fig. 26B and Fig. 26C). On the other hand, there were no significant differences in glomerular sphingosine level among mice with different genotypes (Fig. 26D).

5.3 Severe proteinuria and albuminuria induced by podocyte-specific gene deletion of AC α subunit

To determine whether podocyte-specific gene deletion of AC α subunit induce podocyte dysfunction and glomerular injury, we measured urinary protein and albumin excretion per 24 hours of WT/WT, *Asah1^{fl/fl}/WT*, and *Asah1^{fl/fl}/Podo^{Cre}* mice. As shown in Fig. 27, severe proteinuria and albuminuria were found in *Asah1^{fl/fl}/Podo^{Cre}* mice compared with WT/WT and *Asah1^{fl/fl}/WT* mice. To confirm the age at which the podocyte dysfunction and glomerular injury were developed in *Asah1^{fl/fl}/Podo^{Cre}* mice, measurements of urinary protein and albumin excretion were performed on WT/WT and *Asah1^{fl/fl}/Podo^{Cre}* mice at different ages. No significant differences were found in urinary protein and albumin excretion between 4-week-old WT/WT and *Asah1^{fl/fl}/Podo^{Cre}* mice. However, when mouse age reached 6 weeks, urinary protein and albumin excretions of *Asah1^{fl/fl}/Podo^{Cre}* mice were significantly higher than WT/WT mice. After mouse age reaching 8 weeks, severe proteinuria and albuminuria were found in

Asah1^{fl/fl}/Podo^{Cre} mice compare with WT/WT mice (Fig. 28). These data indicate that podocyte-specific gene deletion of AC α subunit induces serious podocytopathy, leading to proteinuria and albuminuria.

5.4 Podocyte-specific gene deletion of AC α subunit increased permeability to albumin in isolated glomeruli

More evidences were collected by measuring glomerular permeability to albumin of WT/WT, *Asah1^{fl/fl}/WT*, and *Asah1^{fl/fl}/Podo^{Cre}* mice. Glomeruli were isolated in an isotonic HBSS solution containing 6% BSA (Fig. 29A). Following a rapid change in the concentration of the bath from 6% BSA to 4% BSA, an oncotic gradient of ~ 9 mmHg was generated. This oncotic gradient drove water into the glomerular capillaries, which leads to reduction of the concentration and fluorescence intensity of the FITC-dextran in the glomerular capillaries. This oncotic pressure-dependent fluid movement within glomeruli can be used for measurement of glomerular filtration membrane permeability. As shown in Fig. 29B and 29C, the intensities of fluorescence in glomeruli isolated from WT/WT and *Asah1^{fl/fl}/WT* mice were remarkably decreased after a rapid change of the concentration of the bath from 6% BSA to 4% BSA, indicating the movement of water into glomerular capillaries of WT/WT and *Asah1^{fl/fl}/WT* mice and normal permeability with barrier for movement of oncotic molecules. On the other hand, there were almost no changes in intensities of fluorescence in glomeruli isolated from *Asah1^{fl/fl}/Podo^{Cre}* mice after formation of the oncotic gradient, which indicates increased glomerular permeability to albumin of *Asah1^{fl/fl}/Podo^{Cre}* mice because oncotic molecules are balanced across the glomerular filtration membrane or capillaries to lose driving force for water to move into capillaries. These data further confirm that podocyte-specific gene deletion of AC α

subunit in mice leads to podocyte dysfunction to produce hyperpermeability damage and glomerular injury.

5.5 Undetectable glomerular sclerosis in *Asah1^{fl/fl}/Podo^{Cre}* mice

By periodic acid Schiff staining, morphological examinations showed no remarkable sclerotic changes such as mesangial expansion, collapse of glomerular capillaries, and hypercellularity, in glomeruli of *Asah1^{fl/fl}/Podo^{Cre}* mice (Fig. 30A). There was no significant increase in glomerular damage index of *Asah1^{fl/fl}/Podo^{Cre}* mice compared with WT/WT mice (Fig. 30B). Together, these results indicate that podocyte-specific gene deletion of AC α subunit may induce minimal change disease (MCD), a nephrotic syndrome without glomerular morphological changes under light microscope.

5.6 Hypoalbuminemia and edema induced by podocyte-specific gene deletion of AC α subunit

Given the clinical signs of minimal change disease are proteinuria, hypoalbuminemia, and edema, measurements of serum albumin levels and hematocrits of WT/WT and *Asah1^{fl/fl}/Podo^{Cre}* mice were performed to diagnose the podocytopathy induced by podocyte-specific gene deletion of AC α subunit. As shown in Fig. 31A, when mouse age reached 8 weeks, *Asah1^{fl/fl}/Podo^{Cre}* mice had severe hypoalbuminemia compared with WT/WT mice. Correspondingly, when mice became 12-week-old, hematocrits of *Asah1^{fl/fl}/Podo^{Cre}* mice were significantly lower compared with WT/WT mice. These results indicate that edema occurs in *Asah1^{fl/fl}/Podo^{Cre}* mice.

5.7 Ultrastructural changes of podocytes in *Asah1^{fl/fl}/Podo^{Cre}* mice

Based on previous studies, three hallmarks of MCD include a diffuse loss of foot processes, vacuolation, and the appearance of microvilli in podocytes, but there is no loss of podocyte cell body from glomerular filtration membrane. Using transmission electron microscopy, we found that *Asah1^{fl/fl}/Podo^{Cre}* mice had critical foot process effacement, vacuolation, and formation of microvilli in podocytes compared with WT/WT mice (Fig. 32), which showed typical ultrastructural pathological changes in podocytes of MCD patients or animals.

5.8 Resistance of podocytopathy in *Asah1^{fl/fl}/Podo^{Cre}* mice to corticosteroid treatment

Considering that corticosteroids are the most often prescribed medication for MCD patients, dexamethasone (DEX), a type of corticosteroid, was i.p. injected to *Asah1^{fl/fl}/Podo^{Cre}* mice daily for 4 weeks. As shown in Fig. 33, albuminuria in *Asah1^{fl/fl}/Podo^{Cre}* mice was not attenuated by DEX treatment, indicating the steroid resistance of MCD in *Asah1^{fl/fl}/Podo^{Cre}* mice. Based on results from *in vitro* cell studies, podocyte-specific gene deletion of AC α subunit may inhibit lysosome function, leading to autophagic deficiency and podocyte dysfunction due to induction of dedifferentiation. Therefore, we tested whether daily i.p. injection of rapamycin, an activator of entire autophagy process including formation of autophagosomes and their flux, can attenuate MCD in *Asah1^{fl/fl}/Podo^{Cre}* mice. It was found that rapamycin treatment for 4 weeks also failed to decrease albuminuria in *Asah1^{fl/fl}/Podo^{Cre}* mice (Fig. 34).

5.9 Dystroglycans in *Asah1^{fl/fl}/Podo^{Cre}* mice

In previous studies, it has been found that reduction of dystroglycans (DGs), a class of adhesion proteins, in glomeruli is a hallmark of MCD, which can be reversed if foot processes are reconstituted due to treatment or removal of pathogenic factors (143). Some studies have

shown that the staining of DGs in glomeruli can differentiate patients with a diagnosis of MCD at renal biopsy into groups sensitive or resistant to corticosteroid therapy. It is possible that MCD is sensitive to corticosteroid treatment when expressions of both α -DG and β -DG in glomeruli are reduced. In contrast, if β -DG is reduced and α -DG is comparable to normal, the MCD patients or animals are resistant to corticosteroid treatment (144). For diagnosis, we detected expressions of DGs in glomeruli by immunohistochemistry. As shown in Fig. 35, remarkable reduction of β -DG in glomeruli was found in *Asah1^{fl/fl}/Podo^{Cre}* mice compared with WT/WT mice. However, there were no significant changes in the expression of α -DG in glomeruli between WT/WT and *Asah1^{fl/fl}/Podo^{Cre}* mice. These results indicate that podocyte-specific gene deletion of AC α subunit may induce steroid-resistant MCD.

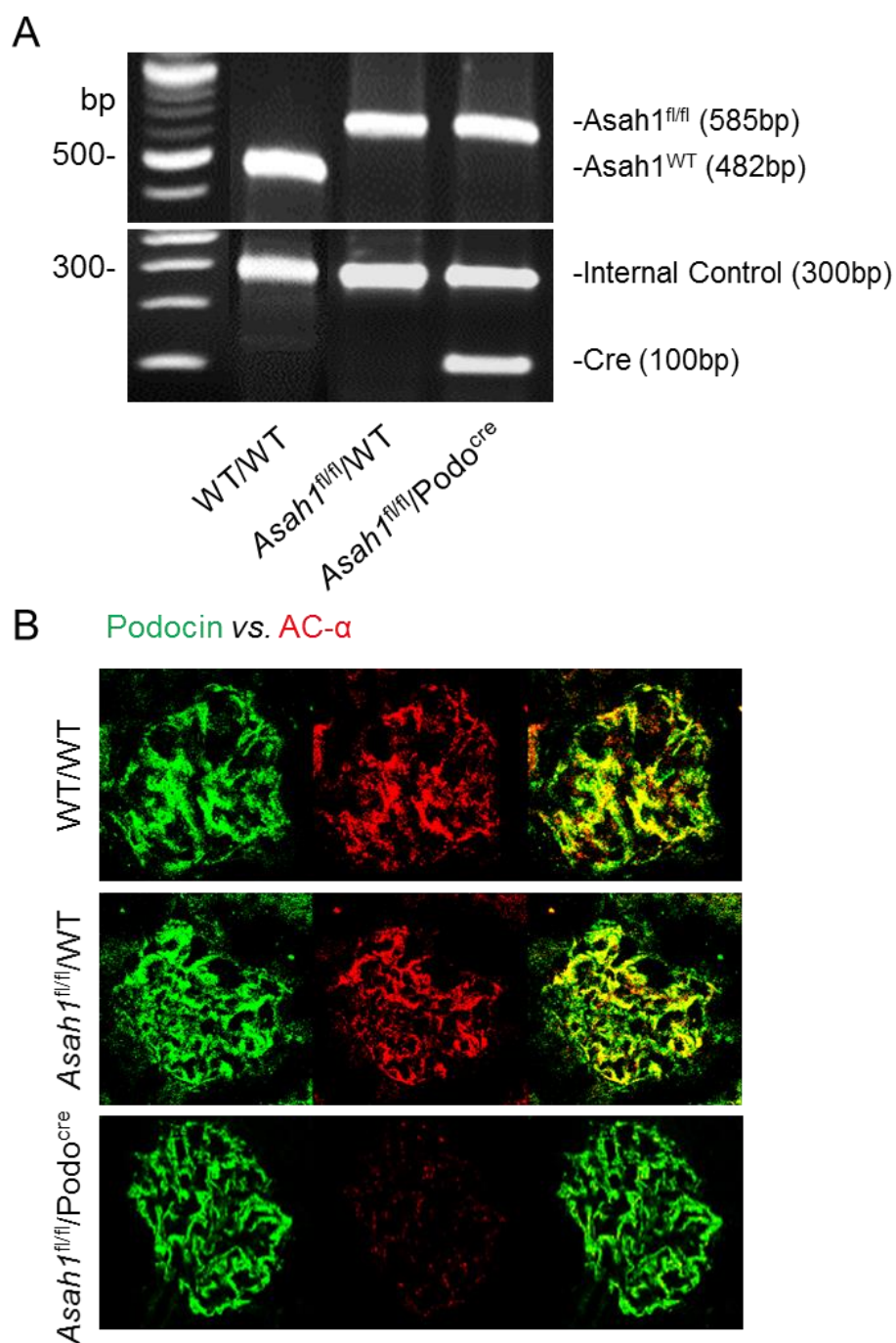
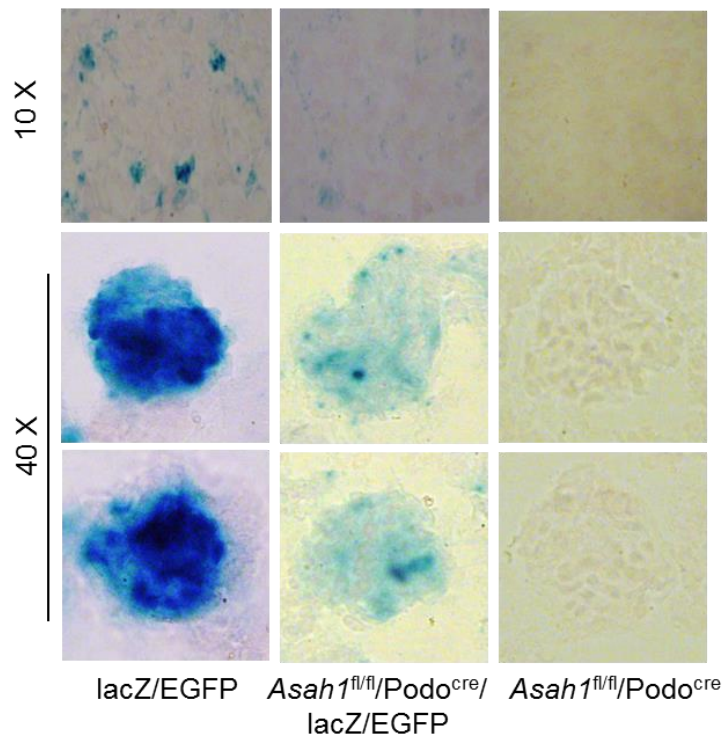


Fig. 24. Characterization of *Asah1*^{fl/fl}/Podo^{Cre} mice. A. Representative gel documents showing detection of floxed *Asah1* gene and Cre recombinase gene by PCR Genotyping. B. Representative images showing the colocalization of podocin (green fluorescence) and AC α subunit (red fluorescence) in glomeruli of different groups of mice (n=6). Cre: Cre recombinase; AC- α : AC α subunit.

A



B

EGFP vs. Podocin

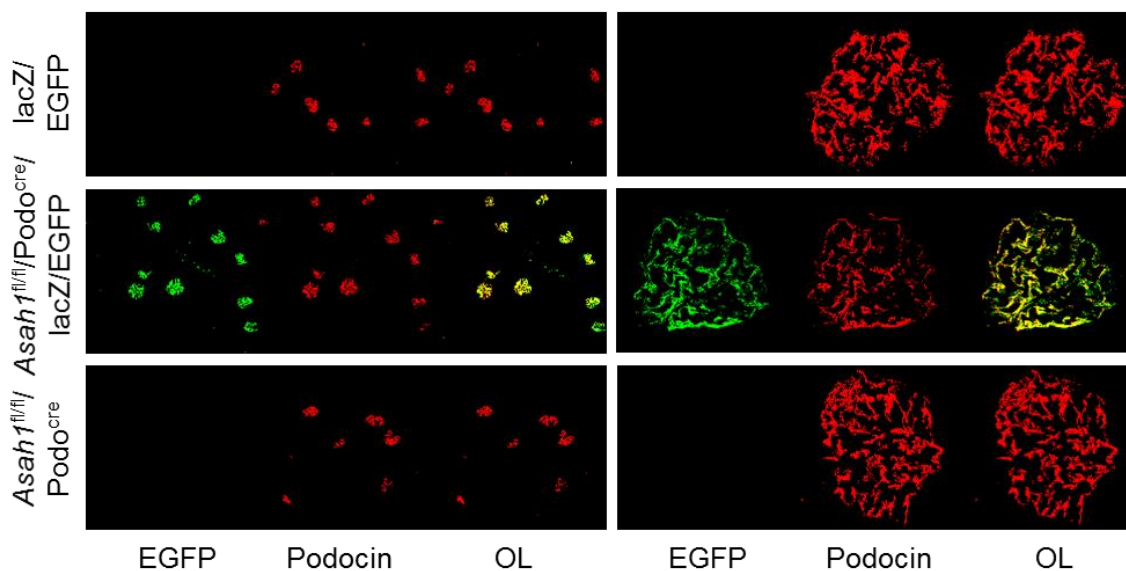


Fig. 25. Confirmation of podocyte-specific expression of Cre recombinase. A. Representative images of enzymatic X-gal staining in which dark blue staining in glomeruli indicates β -galactosidase expression. B. Representative images showing the colocalization of EGFP (green fluorescence) and podocin (red fluorescence) in glomeruli of different groups of mice (n=6). OL: overlay.

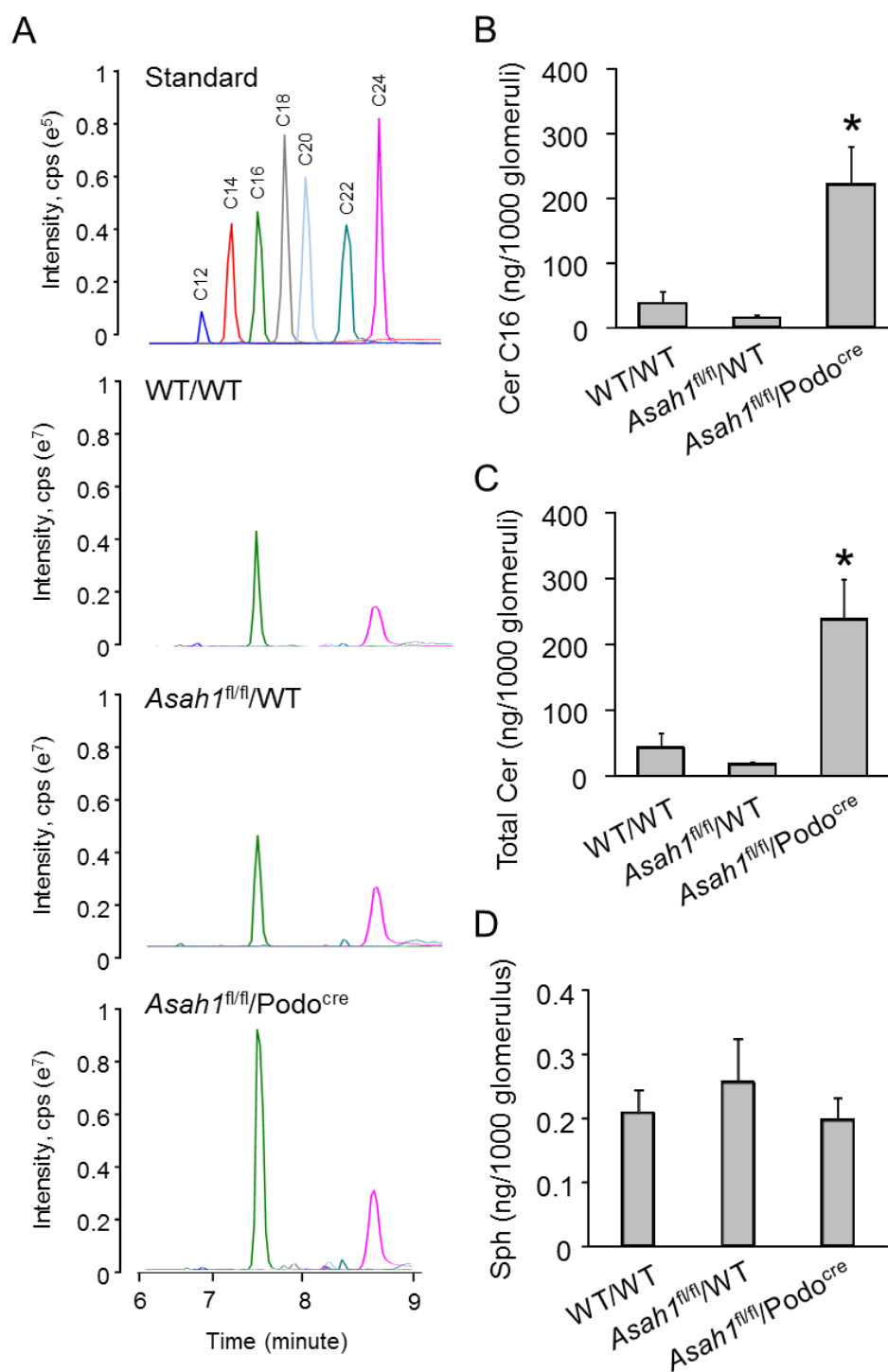


Fig. 26. Ceramide accumulation in glomeruli of *Asah1^{fl/fl}/Podo^{Cre}* mice. A. Representative multiple reaction monitoring chromatography of ceramides separated by liquid chromatography tandem mass spectrometry. B. Summarized data showing the levels of C16 ceramide, total ceramide, and sphingosine in isolated glomeruli of different groups of mice (n=5-6). * $P < 0.05$ vs. WT/WT group. Cer: ceramide; Sph: sphingosine.

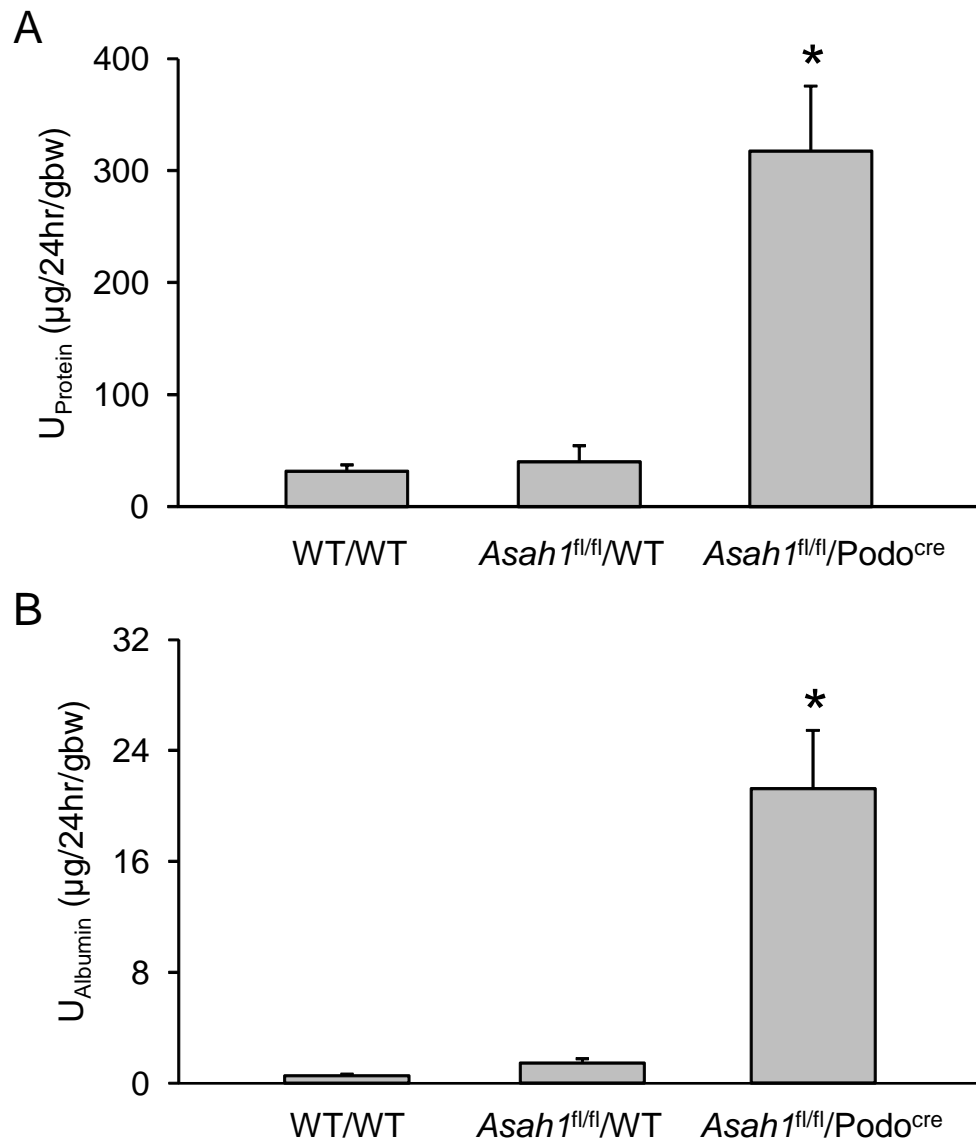


Fig. 27. Severe proteinuria and albuminuria in *Asah1*^{fl/fl}/Podo^{Cre} mice. A. Detection of severe proteinuria in *Asah1*^{fl/fl}/Podo^{Cre} mice compared with WT/WT and *Asah1*^{fl/fl}/WT mice (n=7-15). B. Detection of severe albuminuria in *Asah1*^{fl/fl}/Podo^{Cre} mice compared with WT/WT and *Asah1*^{fl/fl}/WT mice (n=7-10). * P<0.05 vs. WT/WT group.

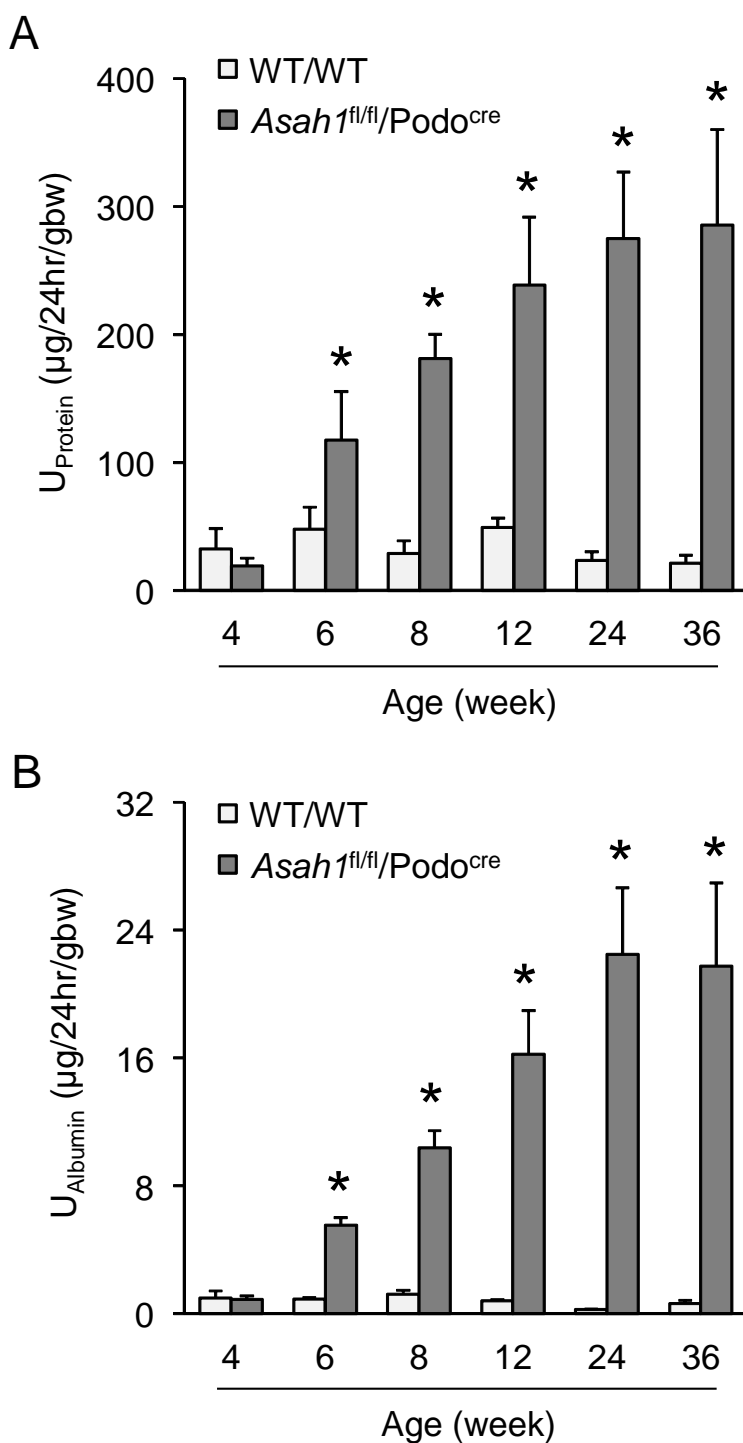


Fig. 28. Development of proteinuria and albuminuria in *Asah1*^{fl/fl}/*Podo*^{Cre} mice. A. Urinary protein excretion of WT/WT and *Asah1*^{fl/fl}/*Podo*^{Cre} mice at different ages (n=3-15). B. Urinary albumin excretion of WT/WT and *Asah1*^{fl/fl}/*Podo*^{Cre} mice at different ages (n=3-12). * P<0.05 vs. WT/WT group.

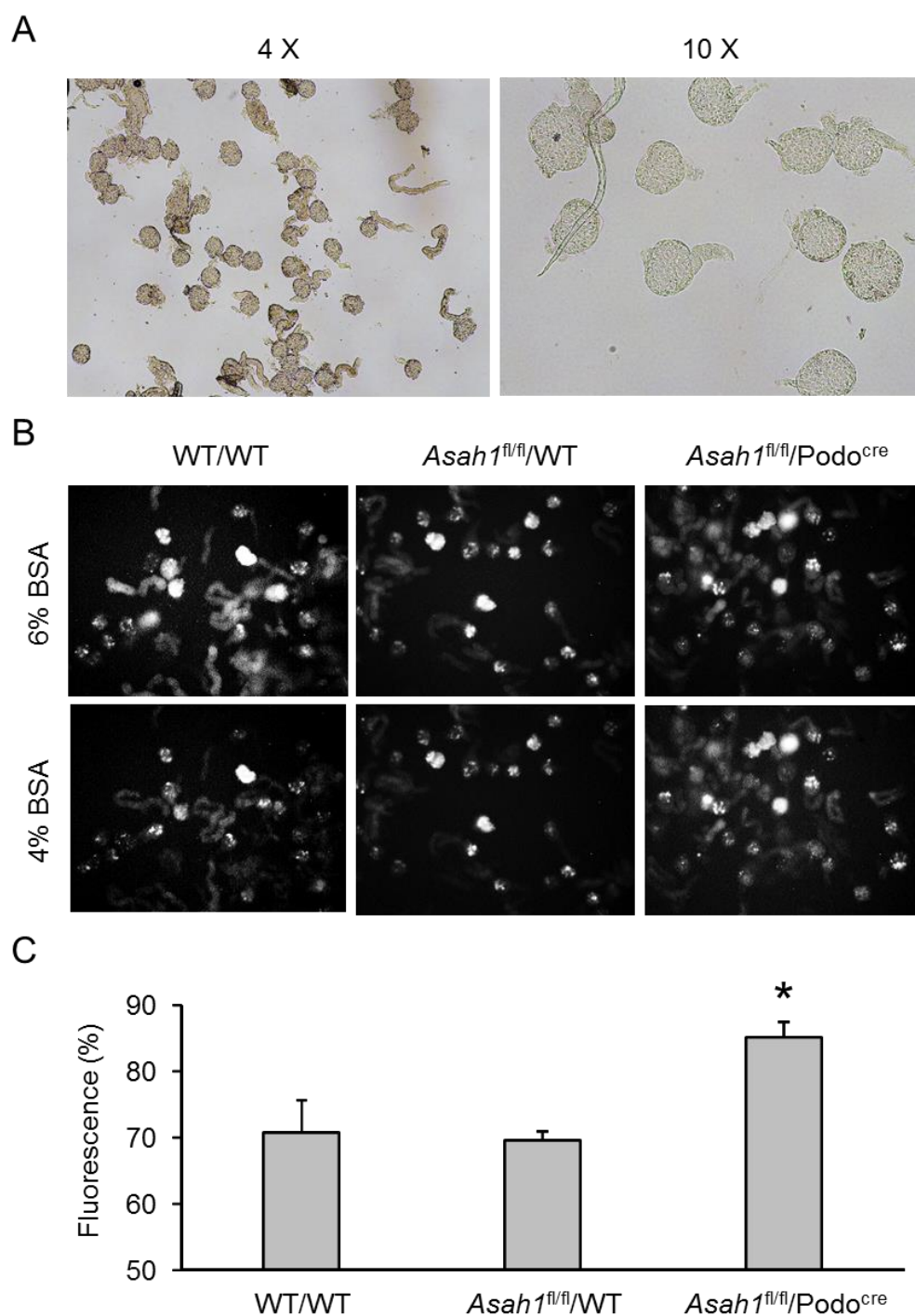


Fig. 29. Glomerular permeability to albumin increased in *Asah1*^{fl/fl}/Podo^{Cre} mice. A. Representative images of isolated glomeruli. B. Representative images showing glomerular fluorescence intensities before and after changes of oncotic pressure of different groups of mice. C. Summarized data showing responses to different oncotic gradient (n=4-6). * P<0.05 vs. WT/WT group.

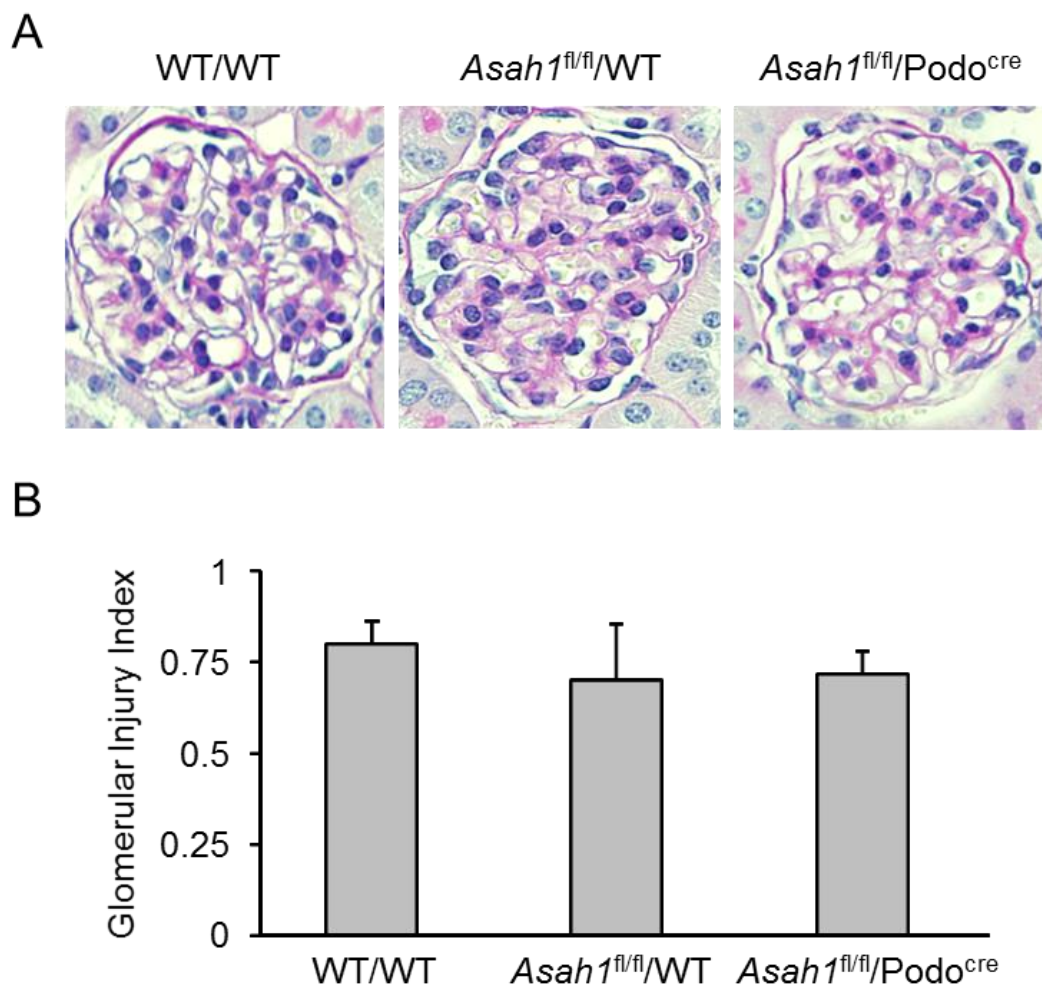


Fig. 30. Undetectable glomerular morphological changes in *Asah1*^{fl/fl}/Podo^{Cre} mice under light microscope. A. Representative images showing the glomerular morphological changes (periodic acid-Schiff staining) of different groups of mice. B. Summarized data of glomerular damage indexes of different groups of mice (n=8).

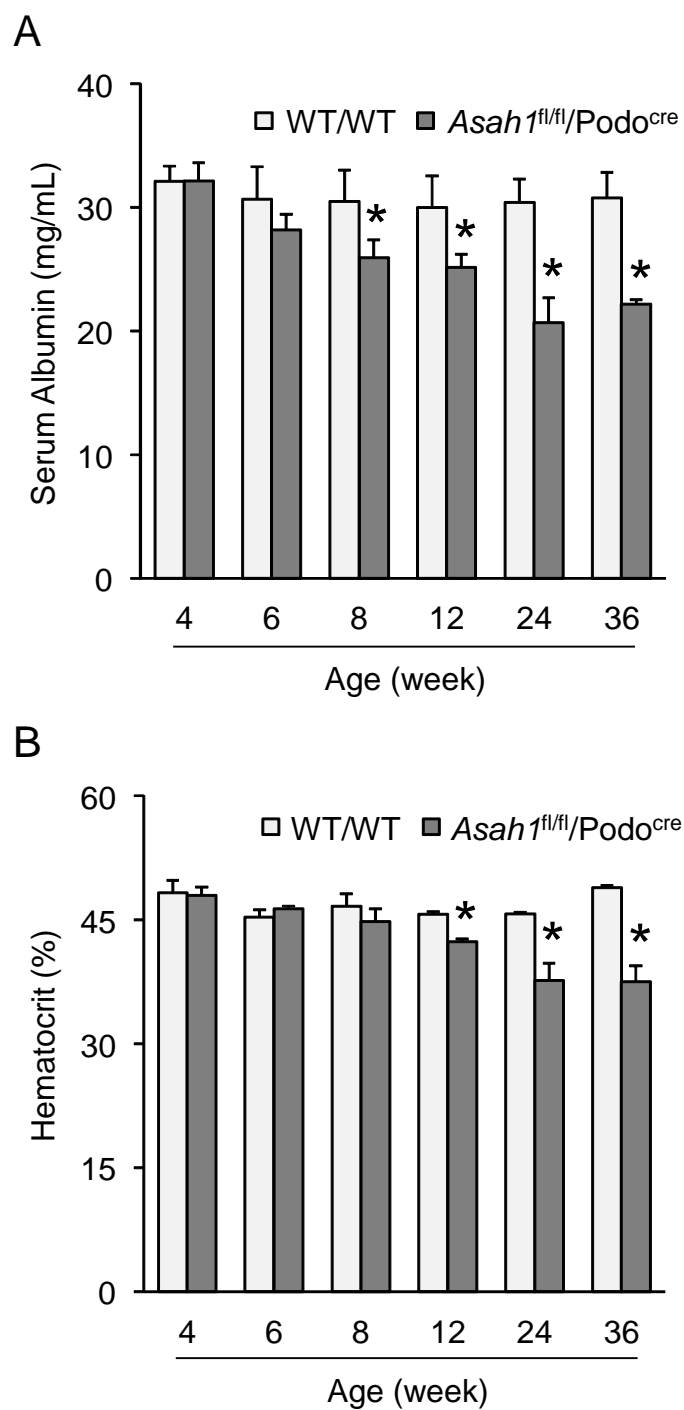


Fig. 31. Hypoalbuminemia and edema in *Asah1*^{fl/fl}/*Podo*^{Cre} mice. A. Serum albumin levels of WT/WT and *Asah1*^{fl/fl}/*Podo*^{Cre} mice at different ages (n=3-7). B. Hematocrits of WT/WT and *Asah1*^{fl/fl}/*Podo*^{Cre} mice at different ages (n=3-9). * P<0.05 vs. WT/WT group.

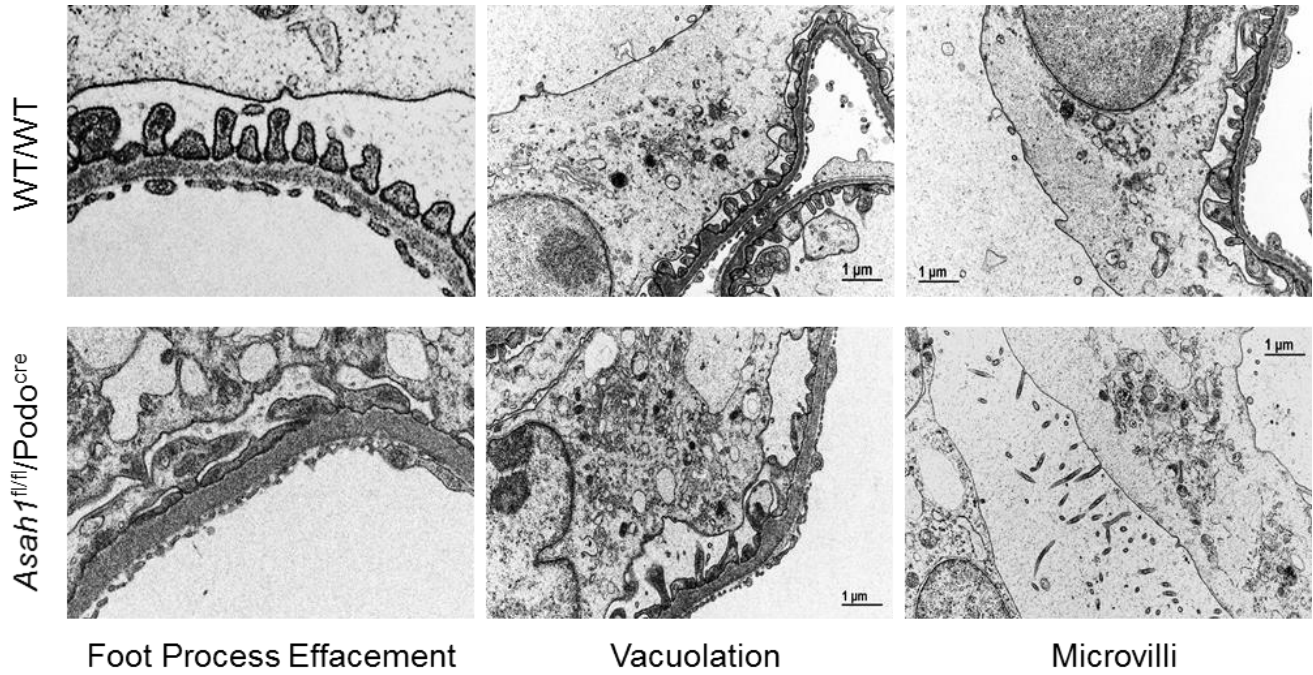


Fig. 32. Ultrastructural changes of podocytes in *Asah1^{fl/fl}/Podo^{Cre}* mice. Representative images showing ultrastructural changes in podocytes of *Asah1^{fl/fl}/Podo^{Cre}* mice compared with WT/WT mice (n=3).

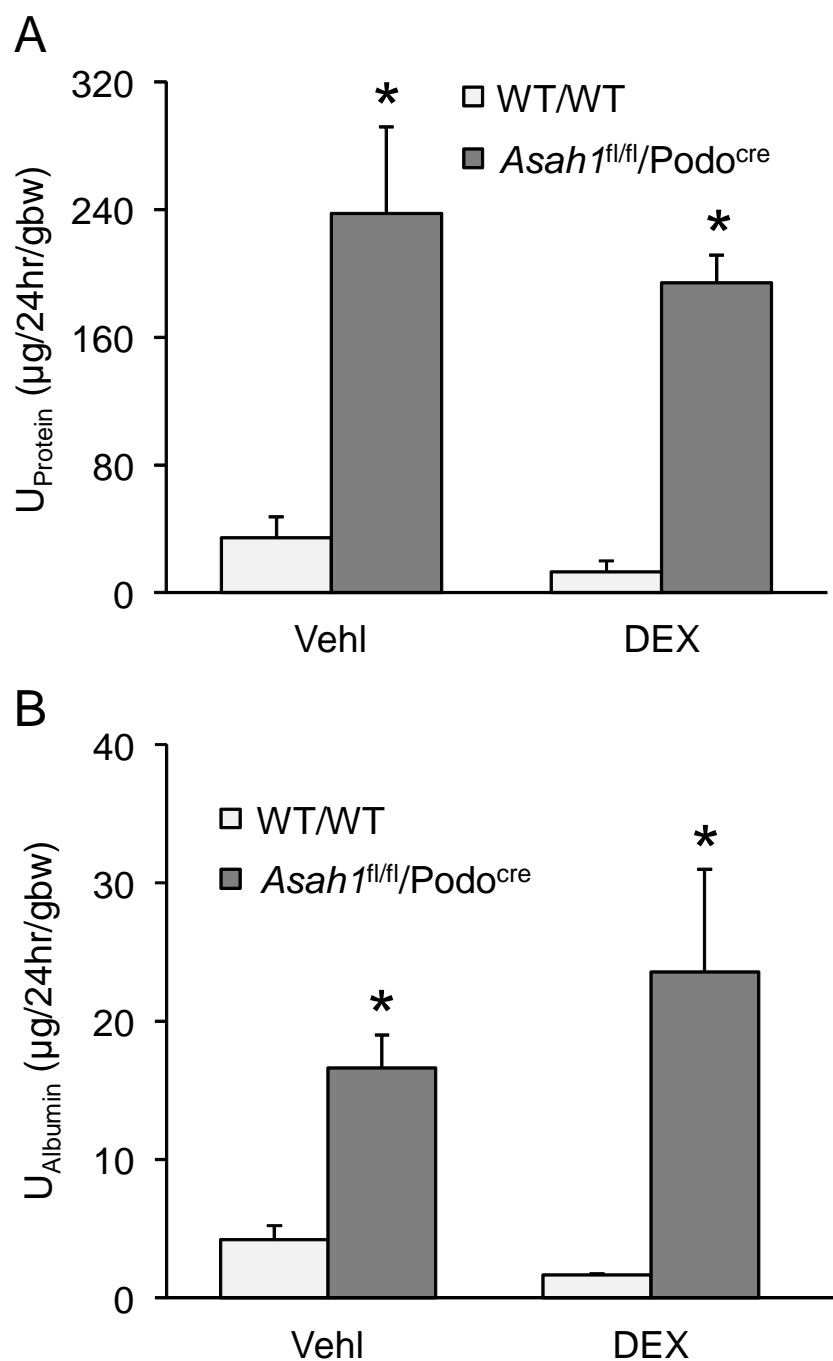


Fig. 33. Resistance of podocytopathy in *Asah1*^{fl/fl}/*Podo*^{Cre} mice to dexamethasone treatment. A. Urinary protein excretion of WT/WT and *Asah1*^{fl/fl}/*Podo*^{Cre} mice treated with vehicle or DEX (n=3-6). B. Urinary albumin excretion of WT/WT and *Asah1*^{fl/fl}/*Podo*^{Cre} mice treated with vehicle or DEX (n=3-6). * P<0.05 vs. WT/WT-Vehl group. Vehl: vehicle; DEX: dexamethasone.

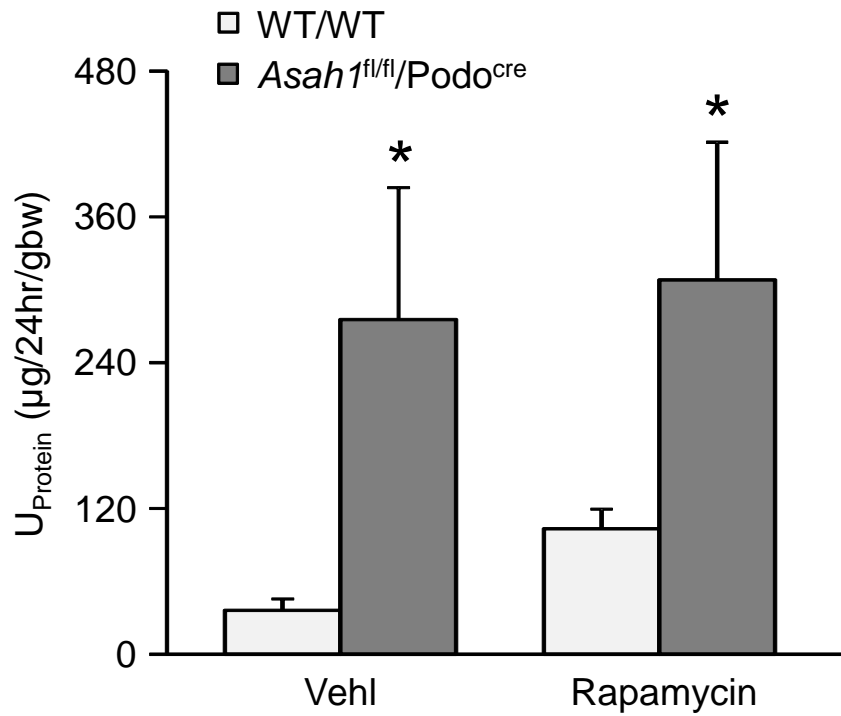


Fig. 34. Resistance of podocytopathy in *Asah1*^{fl/fl}/*Podo*^{Cre} mice to rapamycin treatment. Urinary protein excretion of WT/WT and *Asah1*^{fl/fl}/*Podo*^{Cre} mice treated with vehicle or DEX (n=3-6). * P<0.05 vs. WT/WT-Veh1 group. Veh1: vehicle.

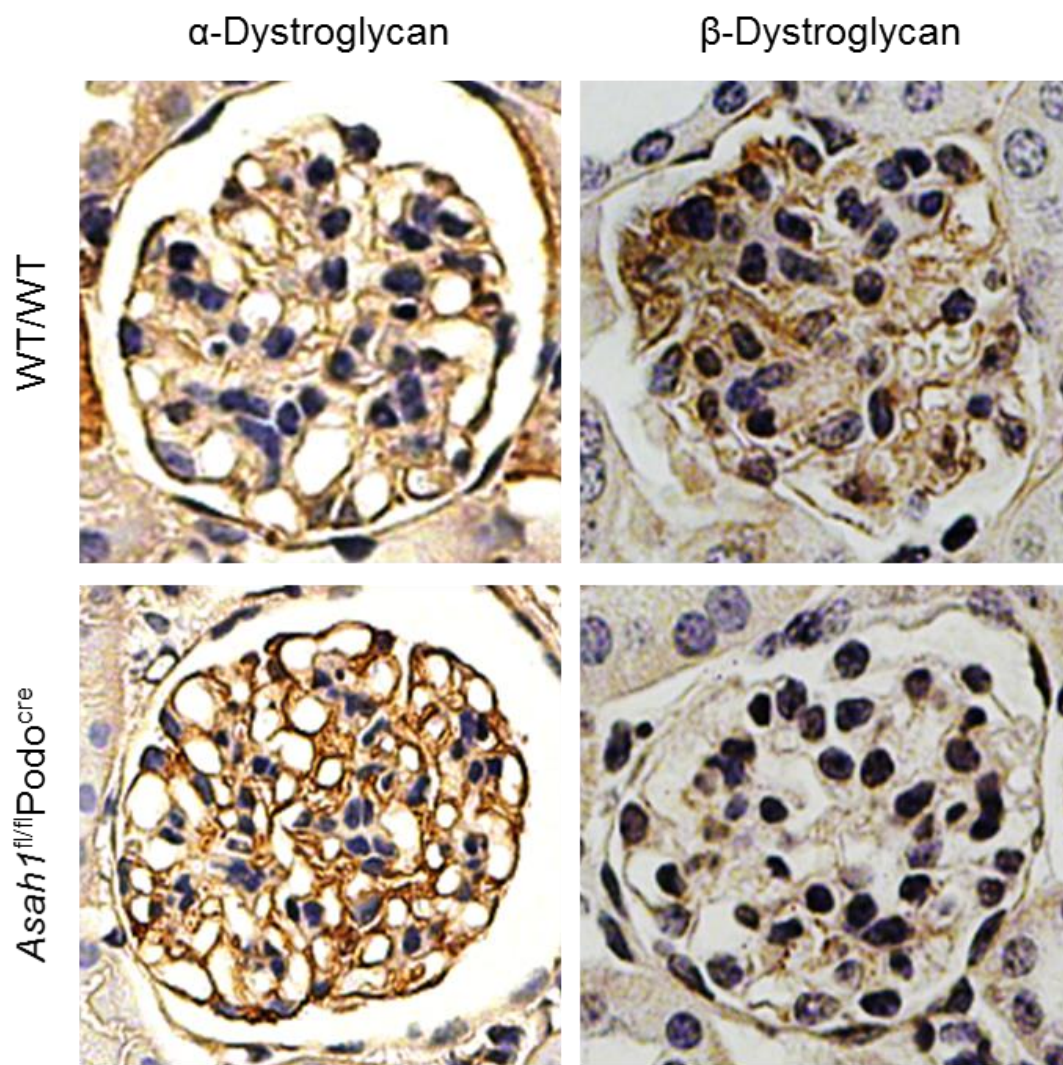


Fig. 35. Dystroglycans in *Asah1*^{fl/fl}/*Podo*^{Cre} mice. Representative immunohistochemical staining of α -dystroglycan and β -dystroglycan in glomeruli of WT/WT and *Asah1*^{fl/fl}/*Podo*^{Cre} mice (n=3).

CHAPTER SIX

DISCUSSION

6.1 Enhanced podocyte dedifferentiation associated with autophagic deficiency due to lysosome dysfunction

The major goals of our first series of studies were to determine whether lysosome dysfunction-induced podocyte dedifferentiation is attributed to the accumulation of autophagosome and p62, which are degraded by autophagic process and to explore the mechanisms by which accumulation of p62 exerts its action as a signaling hub to activate or enhance dedifferentiation in podocytes. It was found that lysosome function inhibition with a low dose of lysosomal V-ATPase inhibitor, Baf A1 (5 nM) or by silencing V-ATPase gene remarkably enhanced podocyte dedifferentiation, which was accompanied by autophagosome accumulation due to the deficient autophagic flux. This enhancement of dedifferentiation in podocytes was significantly attenuated by inhibition of the autophagosome formation with Sp-1, suggesting that autophagosome accumulation in podocytes contributes to enhanced dedifferentiation induced by lysosome dysfunction. We further explored the signaling mechanisms activating or enhancing podocyte dedifferentiation associated with lysosome dysfunction. Given that p62 was found significantly increased during lysosome dysfunction and resulting deficiency of autophagic flux, several signaling pathways regulated via p62 were tested including Nrf2-mediated redox signaling, NF- κ B-dependent transcriptional regulation, and CDK1-mediated phosphorylation of p62 as an intracellular controller of cell mitosis exit. Our results indicate that reduction of CDK1-mediated p62 phosphorylation and consequent speeding

exit of cell mitosis are a critical molecular mechanism mediating podocyte dedifferentiation during lysosome dysfunction.

It has been reported that podocytes in glomeruli of mammalian animals are highly differentiated and therefore the maintenance of functional and structural integrity of these cells during their long time surviving are much dependent upon the autophagic process, which includes the formation and degradation of autophagosomes (89). This led us to hypothesize that lysosome dysfunction and consequent derangement of autophagic flux may be an important mechanism activating or enhancing dedifferentiation in podocytes, leading to podocyte injury and glomerular sclerosis. This hypothesis was tested in the present study by inhibition of lysosome function using V-ATPase inhibitor, Baf A1 (Baf A1) and specific V-ATPase siRNA. We indeed demonstrated that inhibition of lysosome function by Baf A1 and V-ATPase siRNA significantly enhanced dedifferentiation in podocytes, which was comparable to that produced by a well-established dedifferentiation inducer, TGF- β (15, 145) or by inhibition or knocking down of CD38, an enzyme for production of an endogenous regulator of lysosome function, NAADP (88, 89). To our knowledge, these results represent the first experimental evidence that inhibition of lysosomal V-ATPase activity or its gene silencing activated or enhanced podocyte dedifferentiation. In previous studies, some molecular mechanisms have been proposed to activate dedifferentiation in other cell or tissue types, which are similar to those regulating oncogenic properties in neoplastic cells such as proliferation, resistance to apoptosis and angiogenesis through transcription factors (26). However, these mechanisms are found mainly related to ubiquitination, namely, the covalent link of the small 76-amino acid protein ubiquitin to target proteins, which serves as a signal for many proteins to be degraded by the proteasomes

(26). Although lysosomal degradation of some signaling proteins may be one of mechanisms responsible for dedifferentiation, little is known so far how lysosome dysfunction induces dedifferentiation in many cell types including podocytes. In this regard, some previous studies demonstrated that Raf and TGF- β may work together to promote lysosomal degradation of E-cadherin instead of its recycling in tumor cells, resulting in dedifferentiation and tumor progression (146). Despite these observations of lysosomal degradation of signaling proteins in dedifferentiation, it remains unknown how lysosomal degradation of signaling proteins activates dedifferentiation. In particular, it is interesting to know whether the reversal of differentiation induced by autophagy, a process fine controlled by lysosome function, contributes to dedifferentiation in podocytes. If so, we need to test what is the triggering mechanism.

We first examined whether enhanced dedifferentiation during lysosome dysfunction is associated with deficient autophagy, in particular, the autophagic flux, given the important role of lysosomes in this process. It was demonstrated that autophagosome and p62, a scaffold protein also in autophagic process, were largely accumulated in podocytes by Baf A1 or silencing of v-ATPase gene, suggesting that lysosome function inhibition leads to abnormal autophagic flux and thereby reduces autophagic degradation of ubiquitinated cargoes and functional substrates involved in the autophagic process such as p62 (133, 147-149). We also demonstrated that inhibition of autophagosome formation by Sp-1 significantly attenuated the enhancement of dedifferentiation induced by lysosome dysfunction induced by Baf A1 and V-ATPase siRNA. To our knowledge, these results provide the first evidence that autophagosome accumulation may serve as a critical mechanism activating or enhancing dedifferentiation in podocytes. In some previous studies, autophagy was shown to be critical for the invasion of tumor cells, which is

associated with the induction of dedifferentiation and activation of TGF- β /Smad3-dependent signaling pathway (150). In addition, the autophagy process and the autophagy-mediated lysosomal degradation of SNAI/Snail and TWIST, two master inducers of the dedifferentiation process have been reported to mediate the effects of death effector domain-containing DNA-binding protein (DEDD) to alter tumor growth and metastasis, suggesting that autophagy is involved in dedifferentiation and subsequent growth or metastasis of tumors (151, 152).

After confirmation of deficient autophagic flux as an important process, we went on to address how Baf A1-induced accumulation of autophagosome initiated dedifferentiation in podocytes. It has been reported that p62 as a signaling hub regulates cell proliferation and many other activities (153, 154) and that in tumor cells, p62 is required for cell transformation (153, 155, 156). Interestingly, the genetic inactivation of key autophagy molecules, such as Atg7, results in p62 accumulation and hepatotoxicity, which leads to the generation of liver tumors (153, 155), suggesting the important association of autophagic process of p62 with tumorigenesis or cell transdifferentiation. We tested the role of 3 pathways regulated p62 in podocyte dedifferentiation, which include NF- κ B, Nrf2 and cyclin-dependent kinases (CDKs). Using selective inhibitor or siRNAs, we found that inhibition of NF- κ B and Nrf2 signaling pathways had no effect on Baf A1-induced dedifferentiation in podocytes, suggesting that both pathways are not involved in this podocytes transdifferentiation induced by lysosome dysfunction. However, inhibition of CDK1 activity or silencing its gene produced podocyte dedifferentiation without effect on the level of p62. In the presence of CDK1 inhibitor or siRNA, Baf-induced podocyte dedifferentiation was markedly attenuated by 60%, which was accompanied by significantly reduced phosphorylation of p62 in these podocytes. These results suggest that

CDK1 phosphorylation exerts an important regulatory role on podocyte dedifferentiation and that reduced CDK1 phosphorylation may result in enhancement of this dedifferentiation. To our knowledge, there have been no reports on the role of CDK1-mediated p62 phosphorylation in the regulation of podocytes differentiation or transdifferentiation. Our results provide direct evidence that this CDK1-mediated mechanism critically contributes to dedifferentiation activation. In studies using other cell types, CDKs were demonstrated to regulate the progression of mammalian cells through the various phases of the cell cycle (157). Among these CDKs, CDK1 controls transit through the late S/G2 phase and early mitosis phase of the cell cycle (158, 159), which may be associated with p62 phosphorylation at residues T269 and S272 (160, 161). In cancer cells, expression of a nonphosphorylatable p62 mutant displayed higher tumorigenic properties than the same cells expressing wild-type p62 (161). Moreover, p62 phosphorylation has been shown to play an important role in the stabilization of cyclin B1, which interacts with CDK1 to specifically regulate the entry into mitosis (161). Our findings together with these previous results provide strong evidence that reduced phosphorylation of p62 due to inhibition of CDK1 during lysosome dysfunction leads to a faster exit from cell mitosis and thereby enhances dedifferentiation in podocytes, which is resulted from accumulation of p62 induced by deranged autophagic flux.

In summary, the first series of studies revealed a new triggering mechanism of podocyte dedifferentiation during lysosome dysfunction, which is characterized by deranged autophagic flux, p62 accumulation and associated reduction of p62 phosphorylation. This dysregulation of p62 and its CDK1-dependent phosphorylation may represent a novel early event leading to podocyte dysfunction, which may initiate podocytes injury and ultimately result in

glomerulosclerosis during lysosome dysfunction. These results may direct toward the development of new therapeutic strategies targeting phosphorylation of p62 for prevention or treatment of glomerular sclerosis associated with lysosome dysfunction and deficient autophagy under different pathological conditions such as hypercholesterolemia, hyperhomocysteinemia or diabetes mellitus.

6.2 Deficient lysosome trafficking in response to altered ceramide metabolism and associated inhibition of TRPML1 channel activity

The major goals of our second series of studies were to determine whether dysfunction of AC leads to deficient lysosome trafficking in podocytes and to explore the mechanisms by which AC controls lysosome trafficking with a focus on the regulation of TRPML1 channel activity by AC. It was found that inhibition of AC with a selective AC inhibitor, Carmofur, remarkably inhibited lysosome trafficking and fusion to autophagosomes or MVBs in podocytes. This inhibition of lysosome trafficking in podocytes was significantly attenuated by activation of AC with genistein or addition of sphingosine, suggesting that production of sphingosine by AC contributes to lysosome trafficking in podocytes. We further explored the molecular mechanisms mediating lysosome trafficking dependent on AC activity. Given that Ca^{2+} release plays an essential role in lysosome trafficking through dynein-microtubule system and TRPML1 has been confirmed to be a lysosomal Ca^{2+} channel, we tested whether AC contributes to lysosome trafficking through activation of TRPML1 channel. Our results indicate that reduction of AC activity and consequent inhibition of TRPML1 channel are a critical molecular mechanism mediating lysosome dysfunction or blunted lysosome trafficking in podocytes.

It has been reported that lysosomes have trafficking function and lysosome trafficking is a main regulatory mechanism of autophagic flux, which may depend upon the Ca^{2+} release from lysosomes (96-102). It is well known that Ca^{2+} enters lysosomal compartment by $\text{H}^+/\text{Ca}^{2+}$ exchange under resting condition and is released through transient receptor potential-mucolipin-1 (TRPML1) channels in response to endogenously produced NAADP (103, 107, 108, 117, 118) or other factors like PIPs (PI(3,5)P2) and irons (109, 111, 119). More recently, lysosomal TRPML1 channel activity regulated by sphingolipids has been shown to be a key mechanism determining lysosome trafficking (112, 121). This led us to hypothesize that dysfunction of AC, a lysosomal enzyme for ceramide metabolism, may inhibit TRPML1 channel activity and consequent Ca^{2+} release from lysosomes, leading to lysosome dysfunction and autophagic deficiency in podocytes. This hypothesis was tested in the present study by inhibition of AC function using a selective AC inhibitor, carmofur. We demonstrated that inhibition of AC function by carmofur significantly attenuated lysosome trafficking and fusion to autophagosomes or MVBs in podocytes, which was comparable to that produced by a well-established V-ATPase inhibitor, Baf A1 or by inhibition or knocking down of CD38, an enzyme for production of an endogenous agonist of TRPML1 channel, NAADP (89). To our knowledge, these results represent the first experimental evidence that inhibition of lysosomal AC activity blocked lysosome trafficking in podocyte.

In previous studies, some molecular mechanisms have been proposed to be involved in lysosome trafficking, such as CD38-NAADP-TRPML1 system (89, 141, 142), dynein-microtubule system (162), vesicle-associated membrane protein 2 (VAMP-2) (163), and dysferlin C2A domain (164). Recent studies in our laboratory have found that activation of ASM

contributes to lysosome trafficking in coronary arterial endothelial cells (CAECs) (134, 135) and coronary arterial smooth muscle cells (CASMCs) (136). However, the mechanism mediating the role of ASM in lysosome trafficking and autophagic flux remains unknown. In this regard, some previous studies demonstrated that sphingolipids control lysosome trafficking via regulation of TRPML1 channel activity in cells transfected with TRPML1 channel plasmids (112, 121). It was found that sphingomyelin inhibited TRPML1 channel activity while sphingosine enhanced TRPML1 channel activation induced by its stimulator. On the other hand, ceramide had no effects on TRPML1 channel activity. In the present study, it is interesting to know whether the metabolism of ceramide to sphingosine, a process fine controlled by lysosomal AC, contributes to TRPML1 channel activation and consequent lysosome trafficking in podocytes.

To test our hypothesis, we examined whether inhibition of AC activity is associated with dysfunction of TRPML1 channel in podocytes by GCaMP3 Ca^{2+} imaging. It was demonstrated that the selective AC inhibitor, Carmofur, totally blocked ML-SA1-induced Ca^{2+} release through TRPML1 channel, suggesting that normal function of AC is essential for TRPML1 channel activity. We also demonstrated that addition of sphingosine to the external solution, the product of ceramide metabolism by AC, significantly increased Ca^{2+} release through TRPML1 channel compared with treatment with sphingosine-1-phosphate (S1P). Since sphingomyelin and C16 ceramide, the substrate of AC, are impermeable to plasma membrane, we used whole-lysosome patch clamp recording to further confirm the roles of different sphingolipids in TRPML1 channel activity. We found that ML-SA1-induced Ca^{2+} release through TRPML1 channel from lysosome was blocked by sphingomyelin. However, sphingosine as the product of ceramide metabolism by AC remarkably enhanced ML-SA1-induced TRPML1 channel activation. It was found that

ceramide had no effects on ML-SA1-induced Ca^{2+} release through TRPML1 channel. To our knowledge, these results provide the first evidence that ceramide metabolism by AC may serve as a critical mechanism mediating TRPML1 channel activation in podocytes. It has been reported that lysosomal accumulation of SM by ASM deficiency inhibits the activity of TRPML1 and thereby blocks the lysosomal Ca^{2+} -dependent membrane trafficking (112). A target protein regulated by lysosomal Ca^{2+} is dynein, a multi-subunit microtubule motor protein complex, which is responsible for nearly all minus-end microtubule-based transport of vesicles within eukaryotic cells and is recently implicated in lysosome and autophagosome (AP) trafficking to meet and form autophagolysosomes (ALPs) (165, 166). Inhibition or loss of dynein function abolished lysosome fusion with APs and increases the number of APs in glioma, or neuronal cells, and in CASMCs (166, 167). These previous studies have suggested that ASM-regulated lysosomal trafficking function may be associated with the level of lysosomal SM via regulating TRPML1/lysosomal Ca^{2+} /dynein signaling axis. Recent studies in our lab have also demonstrated that ASM is critical for the fusion of lysosome and autophagosome. The control of lysosome trafficking and fusion by ASM is essential to a normal autophagic flux (136). In addition, ASM was found to be essential for lysosomal trafficking, membrane fusion and formation of membrane raft (MR) redox signaling platforms (134, 135). However, none of these studies have elucidated the mechanisms mediating the role of ASM in lysosome trafficking. In the present study, we have demonstrated different effects of various sphingolipids on TRPML1 channel activity, which may define the molecular mechanism for control of lysosome trafficking by both ASM and AC.

In summary, the second series of studies revealed a new molecular mechanism mediating lysosome trafficking in podocytes, which is characterized by signaling via AC-dependent ceramide metabolism and TRPML1 channel activation. The hydrolysis of ceramide by AC may play an essential role in governing TRPML1 channel activity and thereby contributes to lysosome trafficking and fusion to autophagosome in podocytes. These results may direct toward the development of new therapeutic strategies targeting AC for prevention or treatment of podocyte dedifferentiation or dysfunction associated with lysosome dysfunction and deficient autophagy under different pathological conditions.

6.3 Podocytopathy and albuminuria induced by podocyte-specific gene knockout of AC α subunit

The major goal of our third series of studies was to determine whether podocyte-specific gene knockout of AC α subunit induces podocyte dedifferentiation or dysfunction, leading to glomerular injury and diseases. For this purpose, *Asah1^{fl/fl}/Podo^{Cre}* mice were generated. We first confirmed remarkable accumulation of ceramide in glomeruli of *Asah1^{fl/fl}/Podo^{Cre}* mice. Our data showed that podocyte-specific gene knockout of AC α subunit induces severe proteinuria and albuminuria. Glomerular permeability to albumin was remarkably increased in *Asah1^{fl/fl}/Podo^{Cre}* mice. However, glomerular morphological changes were undetectable under light microscope, which indicate that podocyte-specific gene knockout of AC α subunit and ceramide accumulation only in podocyte may induce minimal change disease (MCD). More features of MCD, such as hypoalbuminemia and edema, were also confirmed in *Asah1^{fl/fl}/Podo^{Cre}* mice. By transmission electron microscopy, ultrastructural changes of podocyte were found in *Asah1^{fl/fl}/Podo^{Cre}* mice, which included diffuse foot process effacement, vacuolation, and

microvillus formation. In treatment experiments of MCD, we confirmed the resistance to corticosteroid of MCD in *Asah1^{fl/fl}/Podo^{Cre}* mice. Our results indicate that AC activity is essential for maintaining the integrity and function of podocytes and lack of AC activity is an important inducer of podocyte dysfunction and glomerular injury, which may be a new pathogenic mechanism of proteinuria or MCD.

Acid ceramidase (AC) was identified by Gatt in 1963 (168), but it was purified in 1995, which was first isolated from human urine (169). AC is the lipid hydrolase responsible for the degradation of ceramide into sphingosine and free fatty acids within lysosomes. Farber disease is a lysosomal storage disease caused by the inherited deficiency of AC activity (170). In most cases, the disease is diagnosed early in life with typical symptoms including deformed joints, subcutaneous nodules, and progressive hoarseness (171). In 2002, the global AC knockout mouse model was created by Li et al. (172), but it could not be used for physiological studies because some insertional mutagenesis of the mouse AC gene leads to early embryonic lethality in homozygotes. In addition, AC not only hydrolyzes ceramide into sphingosine, but also can synthesize ceramide from sphingosine and free fatty acids *in vitro* and *in situ* under certain conditions (173). This "reverse" enzymatic activity occurs at a distinct pH from the hydrolysis ("forward") reaction (6.0 vs. 4.5, respectively), suggesting that the enzyme may have diverse functions within cells dependent on its subcellular location and the local pH. Since AC α subunit is primarily responsible for posttranslational positioning of AC to lysosomes, gene deletion of AC α subunit may totally blocked the normal function of lysosomal AC. In the present study, *Asah1^{fl/fl}/Podo^{Cre}* mouse colony was the first mouse model, in which we could study the role of AC activity in the integrity and function of podocytes. Given the *in vitro* evidences in the present

study, we tested whether podocyte-specific deficiency of AC activity induces podocyte dysfunction, leading to glomerular injury and proteinuria.

After characterization of podocyte-specific gene deletion of AC α subunit, we first examined whether podocyte-specific deficiency of AC activity results in ceramide accumulation in glomeruli of *Asah1^{fl/fl}/Podo^{Cre}* mice. It was found that podocyte-specific deficiency of AC activity induced significant increase in ceramide in glomeruli of *Asah1^{fl/fl}/Podo^{Cre}* mice. On the other hand, sphingosine as the product of ceramide metabolism by AC had no changes in *Asah1^{fl/fl}/Podo^{Cre}* mice compared with WT/WT and *Asah1^{fl/fl}/WT* mice. We further tested whether podocyte-specific gene deletion of AC α subunit leads to podocyte injury and associated proteinuria. It was demonstrated that *Asah1^{fl/fl}/Podo^{Cre}* mice had serious proteinuria and albuminuria compared with WT/WT and *Asah1^{fl/fl}/WT* mice, suggesting that gene deletion of AC α subunit induced severe podocyte injury. *In vitro* experiment using isolated glomeruli demonstrated that glomerular permeability to albumin were remarkably increased in *Asah1^{fl/fl}/Podo^{Cre}* mice compared with WT/WT and *Asah1^{fl/fl}/WT* mice. To our knowledge, these data for the first time showed that lysosomal AC activity is essential for maintenance of the functional integrity of podocytes and glomeruli. In this regard, previous studies have reported that ceramide is implicated in the regulation of renal function, which is mainly considered as a potent regulator of cell proliferation, activation, and apoptosis (174). However, this lipid mediator has shown to mediate the detrimental or pathogenic actions of many different injury factors in different cells and tissues (174-176). For example, we have demonstrated by pharmacological and genetic interventions that ceramide contributes to the development of chronic glomerular injury associated with hyperhomocysteinemia (hHcys) and obesity (177,

178). Recent studies in our lab have reported that overproduction of ceramide by ASM activation contributes to podocyte injury and glomerular sclerosis during hHcys and obesity (93-95). The NADPH-dependent superoxide production and consequent NLRP3 inflammasome activation may be the molecular mechanism mediating podocyte injury and glomerular sclerosis induced by ASM activation and ceramide accumulation. These pathological changes were remarkably attenuated in global ASM gene knockout mice compared with WT/WT mice. The present study further increase our knowledge that AC gene defect or deficiency of AC activity even only in podocyte is involved in the development of podocyte injury.

With interesting results obtained in our functional studies, we went on to examine whether glomerular sclerosis was developed in *Asah1^{fl/fl}/Podo^{Cre}* mice. Surprisingly, glomerular morphological changes were undetectable in *Asah1^{fl/fl}/Podo^{Cre}* mice under light microscope. These results indicate that minimal change disease (MCD) may occur in *Asah1^{fl/fl}/Podo^{Cre}* mice because MCD is defined as a type of nephrotic syndrome characterized by albuminuria, but histopathologically lacking global or even focal segmental glomerular sclerotic changes under light microscope. Another feature of MCD is foot process (FP) effacement or flattening process of podocyte as seen by electron microscopy (179). To further confirm the development of MCD in *Asah1^{fl/fl}/Podo^{Cre}* mice, we measured serum albumin levels and hematocrits in WT/WT and *Asah1^{fl/fl}/Podo^{Cre}* mice. As another classical MCD feature, obvious hypoalbuminemia and edema were observed in *Asah1^{fl/fl}/Podo^{Cre}* mice, but not in WT/WT mice. By transmission electron microscopy, diffuse foot process effacement, vacuolation, and microvillus formation were observed in *Asah1^{fl/fl}/Podo^{Cre}* mice, but not in WT/WT mice. Together, these results firmly confirm that podocyte-specific deletion leads to MCD in mice. To our knowledge, so far this is

the only study that links deficient AC activity and associated ceramide accumulation to the development of MCD, which may be novel pathogenic mechanisms for MCD and a novel therapeutic therapy targeting AC deficiency may be a future research direction.

With respect to the pathogenesis and pathophysiology, podocyte injury in MCD may be idiopathic, genetic, or reactive (144). The major clinical distinction among subgroups of this category is the responsiveness to glucocorticoid therapy. It has been reported that idiopathic and reactive forms of MCD may be generally steroid sensitive. Steroid-resistant forms have a similar morphology but worse outcome and likely have distinct etiologies. In this regard, idiopathic MCD is typically steroid sensitive, particularly in children. Medications that are effective in treating reactive MCD may affect the cellular immune system. Cell-mediated immunity has been invoked as an etiologic factor in the development of reactive MCD (180). Three genetic forms of genetic MCD have been identified. Steroid-resistant MCD that presents in infancy or childhood with autosomal recessive inheritance may be caused by mutations in *NPHS2*, encoding podocin. Autosomal dominant nephrotic syndrome, presenting as focal segmental glomerular sclerosis (FSGS) or less commonly as MCD, has been linked to a nearby locus on chromosome 19q, for which the gene remains unidentified (181, 182). Recently, MCD was reported in a patient with limb girdle muscular dystrophy type 2B, which is caused by mutations in dysferlin (*DYSF*) (183). To confirm which subtype of MCD was developed in *Asah1^{fl/fl}/Podo^{Cre}* mice, dexamethasone (DEX) as a medical corticosteroid was used to treat these mice and their littermates. It was found that DEX had no protective effects on any functional and structural changes in podocytes and glomerular in *Asah1^{fl/fl}/Podo^{Cre}* mice after treatment for 4 weeks. It seems that MCD in *Asah1^{fl/fl}/Podo^{Cre}* mice may be resistant to steroid treatment, which is

consistent with genetic MCD. It is possible that AC deficiency interfered with podocin synthesis leading to MCD as shown by mutations of NPHS2. In addition, it has been reported that the staining for dystroglycan may segregate patients with a diagnosis of MCD at renal biopsy into one group of patients with a high likelihood of favorable response to corticosteroid therapy and another group of patients with poor response to the steroid therapy (143, 144). To further confirm whether steroid-resistant MCD was developed in *Asah1^{fl/fl}/Podo^{Cre}* mice, we detected the expression of dystroglycans in glomeruli by immunohistochemistry. It was found that β -dystroglycan was remarkably decreased in glomeruli of *Asah1^{fl/fl}/Podo^{Cre}* mice compared with WT/WT mice. On the other hand, there were no significant changes in glomerular α -dystroglycan between WT/WT mice and *Asah1^{fl/fl}/Podo^{Cre}* mice. Such results with decreased β -dystroglycans and unchanged α -dystroglycan indeed indicate the occurrence of corticosteroid resistant MCD in *Asah1^{fl/fl}/Podo^{Cre}* mice.

In previous studies, ceramide has been shown to block insulin action by inhibiting insulin signal transduction in cultured adipocytes or myotubes (184-187). Moreover, intracellular levels of ceramide are elevated in rodent or human skeletal muscles made insulin resistant by either obesity (188, 189) or acute lipid infusion (190). By contrast, exercise training, which improves insulin sensitivity, markedly decreases muscle ceramide levels in both rats and humans (191-193). Recently, it has been reported that saturated FFA-induced ceramide accumulation contributes to the development of saturated fat-induced muscle insulin resistance (194). Overexpression of AC can protect cells from the inhibitory effects of palmitate and other long-chain saturated FFAs on insulin signaling. It is possible that podocyte-specific gene deletion of AC α subunit may induce insulin resistance in podocytes, leading to podocyte injury even at

normal blood glucose level, which is similar to pathological changes at early stage of Type 2 diabetes. Such podocyte injury due to enhanced insulin resistance has been reported in studies by podocyte-specific deletion of insulin receptor. This possibility will be explored in our future studies.

In summary, the third series of studies revealed that podocyte-specific gene deletion of AC α subunit may be a potential triggering mechanism of corticosteroid-resistant MCD, which is characterized by albuminuria, hypoalbuminemia, edema, undetectable glomerular morphological changes under light microscope, and podocyte effacement or projection flattening. These results reveal a novel pathogenic mechanism for MCD and may direct toward the development of new therapeutic strategies for treatment of MCD by targeting dysfunction of AC deficiency and associated ceramide.

REFERENCES

1. Appel, D., D. B. Kershaw, B. Smeets, G. Yuan, A. Fuss, B. Frye, M. Elger, W. Kriz, J. Floege, and M. J. Moeller. 2009. Recruitment of podocytes from glomerular parietal epithelial cells. *J Am Soc Nephrol* **20**: 333-343.
2. Romagnani, P., and G. Remuzzi. 2013. Renal progenitors in non-diabetic and diabetic nephropathies. *Trends Endocrinol Metab* **24**: 13-20.
3. Romagnani, P., L. Lasagni, and G. Remuzzi. 2013. Renal progenitors: an evolutionary conserved strategy for kidney regeneration. *Nat Rev Nephrol* **9**: 137-146.
4. Ronconi, E., C. Sagrinati, M. L. Angelotti, E. Lazzeri, B. Mazzinghi, L. Ballerini, E. Parente, F. Becherucci, M. Gacci, M. Carini, E. Maggi, M. Serio, G. B. Vannelli, L. Lasagni, S. Romagnani, and P. Romagnani. 2009. Regeneration of glomerular podocytes by human renal progenitors. *J Am Soc Nephrol* **20**: 322-332.
5. Sagrinati, C., G. S. Netti, B. Mazzinghi, E. Lazzeri, F. Liotta, F. Frosali, E. Ronconi, C. Meini, M. Gacci, R. Squecco, M. Carini, L. Gesualdo, F. Francini, E. Maggi, F. Annunziato, L. Lasagni, M. Serio, S. Romagnani, and P. Romagnani. 2006. Isolation and characterization of multipotent progenitor cells from the Bowman's capsule of adult human kidneys. *J Am Soc Nephrol* **17**: 2443-2456.
6. Ohse, T., M. R. Vaughan, J. B. Kopp, R. D. Krofft, C. B. Marshall, A. M. Chang, K. L. Hudkins, C. E. Alpers, J. W. Pippin, and S. J. Shankland. 2010. De novo expression of podocyte proteins in parietal epithelial cells during experimental glomerular disease. *Am J Physiol Renal Physiol* **298**: F702-711.
7. Zhang, J., K. M. Hansen, J. W. Pippin, A. M. Chang, Y. Taniguchi, R. D. Krofft, S. G. Pickering, Z. H. Liu, C. K. Abrass, and S. J. Shankland. 2012. De novo expression of podocyte

proteins in parietal epithelial cells in experimental aging nephropathy. *Am J Physiol Renal Physiol* **302**: F571-580.

8. Zhang, J., J. W. Pippin, M. R. Vaughan, R. D. Krofft, Y. Taniguchi, P. Romagnani, P. J. Nelson, Z. H. Liu, and S. J. Shankland. 2012. Retinoids augment the expression of podocyte proteins by glomerular parietal epithelial cells in experimental glomerular disease. *Nephron Exp Nephrol* **121**: e23-37.

9. Zhang, J., J. W. Pippin, R. D. Krofft, S. Naito, Z. H. Liu, and S. J. Shankland. 2013. Podocyte repopulation by renal progenitor cells following glucocorticoids treatment in experimental FSGS. *Am J Physiol Renal Physiol* **304**: F1375-1389.

10. Sell, S. 1993. Cellular origin of cancer: dedifferentiation or stem cell maturation arrest? *Environ Health Perspect* **101 Suppl 5**: 15-26.

11. May, C. J., M. Saleem, and G. I. Welsh. 2014. Podocyte dedifferentiation: a specialized process for a specialized cell. *Front Endocrinol (Lausanne)* **5**: 148.

12. Little, M. H., and A. P. McMahon. 2012. Mammalian kidney development: principles, progress, and projections. *Cold Spring Harb Perspect Biol* **4**.

13. Andrews, P. M., and A. K. Coffey. 1980. In vitro studies of kidney glomerular epithelial cells. *Scan Electron Microsc*: 179-191.

14. Ghiggeri, G. M., M. Gigante, and A. Di Donato. 2013. Constitutional Nephtrin Deficiency in Conditionally Immortalized Human Podocytes Induced Epithelial-Mesenchymal Transition, Supported by beta-Catenin/NF-kappa B Activation: A Consequence of Cell Junction Impairment? *Int J Nephrol* **2013**: 457490.

15. Li, Y., Y. S. Kang, C. Dai, L. P. Kiss, X. Wen, and Y. Liu. 2008. Epithelial-to-mesenchymal transition is a potential pathway leading to podocyte dysfunction and proteinuria. *Am J Pathol* **172**: 299-308.
16. Sunamoto, M., M. Husain, J. C. He, E. J. Schwartz, and P. E. Klotman. 2003. Critical role for Nef in HIV-1-induced podocyte dedifferentiation. *Kidney Int* **64**: 1695-1701.
17. He, J. C., M. Husain, M. Sunamoto, V. D. D'Agati, M. E. Klotman, R. Iyengar, and P. E. Klotman. 2004. Nef stimulates proliferation of glomerular podocytes through activation of Src-dependent Stat3 and MAPK1,2 pathways. *J Clin Invest* **114**: 643-651.
18. Husain, M., V. D. D'Agati, J. C. He, M. E. Klotman, and P. E. Klotman. 2005. HIV-1 Nef induces dedifferentiation of podocytes in vivo: a characteristic feature of HIVAN. *AIDS* **19**: 1975-1980.
19. Yadav, A., S. Vallabu, D. Kumar, G. Ding, D. N. Charney, P. N. Chander, and P. C. Singhal. 2010. HIVAN phenotype: consequence of epithelial mesenchymal transdifferentiation. *Am J Physiol Renal Physiol* **298**: F734-744.
20. Herman-Edelstein, M., M. C. Thomas, V. Thallas-Bonke, M. Saleem, M. E. Cooper, and P. Kantharidis. 2011. Dedifferentiation of immortalized human podocytes in response to transforming growth factor-beta: a model for diabetic podocytopathy. *Diabetes* **60**: 1779-1788.
21. Herman-Edelstein, M., T. Weinstein, and U. Gafter. 2013. TGFbeta1-dependent podocyte dysfunction. *Curr Opin Nephrol Hypertens* **22**: 93-99.
22. Sam, R., L. Wanna, K. P. Gudehithlu, S. L. Garber, G. Dunea, J. A. Arruda, and A. K. Singh. 2006. Glomerular epithelial cells transform to myofibroblasts: early but not late removal of TGF-beta1 reverses transformation. *Transl Res* **148**: 142-148.

23. Li, S. Y., P. H. Huang, A. H. Yang, D. C. Tarng, W. C. Yang, C. C. Lin, J. W. Chen, G. Schmid-Schonbein, and S. J. Lin. 2014. Matrix metalloproteinase-9 deficiency attenuates diabetic nephropathy by modulation of podocyte functions and dedifferentiation. *Kidney Int* **86**: 358-369.
24. Sweetwyne, M. T., A. Gruenwald, T. Niranjana, R. Nishinakamura, L. J. Strobl, and K. Susztak. 2015. Notch1 and Notch2 in Podocytes Play Differential Roles During Diabetic Nephropathy Development. *Diabetes* **64**: 4099-4111.
25. Li, Z., H. Yin, S. Hao, L. Wang, J. Gao, X. Tan, and Z. Yang. 2016. miR-200 family promotes podocyte differentiation through repression of RSAD2. *Sci Rep* **6**: 27105.
26. Kang, Y. S., Y. Li, C. Dai, L. P. Kiss, C. Wu, and Y. Liu. 2010. Inhibition of integrin-linked kinase blocks podocyte epithelial-mesenchymal transition and ameliorates proteinuria. *Kidney Int* **78**: 363-373.
27. Dai, H. Y., M. Zheng, L. L. Lv, R. N. Tang, K. L. Ma, D. Liu, M. Wu, and B. C. Liu. 2012. The roles of connective tissue growth factor and integrin-linked kinase in high glucose-induced phenotypic alterations of podocytes. *J Cell Biochem* **113**: 293-301.
28. Tang, R., C. Yang, J. L. Tao, Y. K. You, N. An, S. M. Li, H. L. Wu, and H. F. Liu. 2011. Epithelial-mesenchymal transdifferentiation of renal tubular epithelial cells induced by urinary proteins requires the activation of PKC-alpha and betaI isozymes. *Cell Biol Int* **35**: 953-959.
29. Zhang, C., M. Xia, K. M. Boini, C. X. Li, J. M. Abais, X. X. Li, L. A. Laperle, and P. L. Li. 2011. Epithelial-to-mesenchymal transition in podocytes mediated by activation of NADPH oxidase in hyperhomocysteinemia. *Pflugers Arch* **462**: 455-467.

30. Dai, H., Y. Zhang, L. Yuan, J. Wu, L. Ma, and H. Shi. 2016. CTGF mediates high-glucose induced epithelial-mesenchymal transition through activation of beta-catenin in podocytes. *Ren Fail* **38**: 1711-1716.
31. Wang, C., X. Liu, Z. Ke, Y. Tang, C. C. Li, C. M. Li, Z. Ye, J. Zhang, and T. Lou. 2012. Mesangial medium from IgA nephropathy patients induces podocyte epithelial-to-mesenchymal transition through activation of the phosphatidyl inositol-3-kinase/Akt signaling pathway. *Cell Physiol Biochem* **29**: 743-752.
32. Lv, Z., M. Hu, J. Zhen, J. Lin, Q. Wang, and R. Wang. 2013. Rac1/PAK1 signaling promotes epithelial-mesenchymal transition of podocytes in vitro via triggering beta-catenin transcriptional activity under high glucose conditions. *Int J Biochem Cell Biol* **45**: 255-264.
33. Guo, J., N. Xia, L. Yang, S. Zhou, Q. Zhang, Y. Qiao, and Z. Liu. 2014. GSK-3beta and vitamin D receptor are involved in beta-catenin and snail signaling in high glucose-induced epithelial-mesenchymal transition of mouse podocytes. *Cell Physiol Biochem* **33**: 1087-1096.
34. Xing, L., Q. Liu, S. Fu, S. Li, L. Yang, S. Liu, J. Hao, L. Yu, and H. Duan. 2015. PTEN Inhibits High Glucose-Induced Phenotypic Transition in Podocytes. *J Cell Biochem* **116**: 1776-1784.
35. Chen, T., L. Y. Zheng, W. Xiao, D. Gui, X. Wang, and N. Wang. 2015. Emodin ameliorates high glucose induced-podocyte epithelial-mesenchymal transition in-vitro and in-vivo. *Cell Physiol Biochem* **35**: 1425-1436.
36. Liu, L., W. Fu, J. Xu, L. Shao, and Y. Wang. 2015. Effect of BMP7 on podocyte transdifferentiation and Smad7 expression induced by hyperglycemia. *Clin Nephrol* **84**: 95-99.
37. Du, M., Q. Wang, W. Li, X. Ma, L. Wu, F. Guo, S. Zhao, F. Huang, H. Wang, and G. Qin. 2016. Overexpression of FOXO1 ameliorates the podocyte epithelial-mesenchymal

transition induced by high glucose in vitro and in vivo. *Biochem Biophys Res Commun* **471**: 416-422.

38. Wan, J., P. Li, D. W. Liu, Y. Chen, H. Z. Mo, B. G. Liu, W. J. Chen, X. Q. Lu, J. Guo, Q. Zhang, Y. J. Qiao, Z. S. Liu, and G. R. Wan. 2016. GSK-3beta inhibitor attenuates urinary albumin excretion in type 2 diabetic db/db mice, and delays epithelial-to-mesenchymal transition in mouse kidneys and podocytes. *Mol Med Rep* **14**: 1771-1784.

39. Wang, Z., M. Wei, M. Wang, L. Chen, H. Liu, Y. Ren, K. Shi, and H. Jiang. 2014. Inhibition of macrophage migration inhibitory factor reduces diabetic nephropathy in type II diabetes mice. *Inflammation* **37**: 2020-2029.

40. Sun, L. N., Z. X. Chen, X. C. Liu, H. Y. Liu, G. J. Guan, and G. Liu. 2014. Curcumin ameliorates epithelial-to-mesenchymal transition of podocytes in vivo and in vitro via regulating caveolin-1. *Biomed Pharmacother* **68**: 1079-1088.

41. Peng, R., L. Zhou, Y. Zhou, Y. Zhao, Q. Li, D. Ni, Y. Hu, Y. Long, J. Liu, Z. Lyu, Z. Mao, Y. Yuan, L. Huang, H. Zhao, G. Li, and Q. Zhou. 2015. MiR-30a Inhibits the Epithelial--Mesenchymal Transition of Podocytes through Downregulation of NFATc3. *Int J Mol Sci* **16**: 24032-24047.

42. Kumar, P. A., G. I. Welsh, G. Raghu, R. K. Menon, M. A. Saleem, and G. B. Reddy. 2016. Carboxymethyl lysine induces EMT in podocytes through transcription factor ZEB2: Implications for podocyte depletion and proteinuria in diabetes mellitus. *Arch Biochem Biophys* **590**: 10-19.

43. Lu, T. C., J. C. He, and P. E. Klotman. 2007. Podocytes in HIV-associated nephropathy. *Nephron Clin Pract* **106**: c67-71.

44. Barisoni, L., W. Kriz, P. Mundel, and V. D'Agati. 1999. The dysregulated podocyte phenotype: a novel concept in the pathogenesis of collapsing idiopathic focal segmental glomerulosclerosis and HIV-associated nephropathy. *J Am Soc Nephrol* **10**: 51-61.
45. Nagata, M., K. Nakayama, Y. Terada, S. Hoshi, and T. Watanabe. 1998. Cell cycle regulation and differentiation in the human podocyte lineage. *Am J Pathol* **153**: 1511-1520.
46. Barisoni, L., M. Mokrzycki, L. Sablay, M. Nagata, H. Yamase, and P. Mundel. 2000. Podocyte cell cycle regulation and proliferation in collapsing glomerulopathies. *Kidney Int* **58**: 137-143.
47. Husain, M., G. L. Gusella, M. E. Klotman, I. H. Gelman, M. D. Ross, E. J. Schwartz, A. Cara, and P. E. Klotman. 2002. HIV-1 Nef induces proliferation and anchorage-independent growth in podocytes. *J Am Soc Nephrol* **13**: 1806-1815.
48. Zuo, Y., T. Matsusaka, J. Zhong, J. Ma, L. J. Ma, Z. Hanna, P. Jolicoeur, A. B. Fogo, and I. Ichikawa. 2006. HIV-1 genes vpr and nef synergistically damage podocytes, leading to glomerulosclerosis. *J Am Soc Nephrol* **17**: 2832-2843.
49. Reidy, K., H. M. Kang, T. Hostetter, and K. Susztak. 2014. Molecular mechanisms of diabetic kidney disease. *J Clin Invest* **124**: 2333-2340.
50. Kato, H., A. Gruenwald, J. H. Suh, J. H. Miner, L. Barisoni-Thomas, M. M. Taketo, C. Faul, S. E. Millar, L. B. Holzman, and K. Susztak. 2011. Wnt/beta-catenin pathway in podocytes integrates cell adhesion, differentiation, and survival. *J Biol Chem* **286**: 26003-26015.
51. Dai, C., D. B. Stolz, L. P. Kiss, S. P. Monga, L. B. Holzman, and Y. Liu. 2009. Wnt/beta-catenin signaling promotes podocyte dysfunction and albuminuria. *J Am Soc Nephrol* **20**: 1997-2008.

52. Gill, P. S., and C. S. Wilcox. 2006. NADPH oxidases in the kidney. *Antioxid Redox Signal* **8**: 1597-1607.
53. Jiang, F. 2009. NADPH oxidase in the kidney: a Janus in determining cell fate. *Kidney Int* **75**: 135-137.
54. McCully, K. S. 2009. Chemical pathology of homocysteine. IV. Excitotoxicity, oxidative stress, endothelial dysfunction, and inflammation. *Ann Clin Lab Sci* **39**: 219-232.
55. Upchurch, G. R., Jr., G. N. Welch, A. J. Fabian, J. E. Freedman, J. L. Johnson, J. F. Keaney, Jr., and J. Loscalzo. 1997. Homocyst(e)ine decreases bioavailable nitric oxide by a mechanism involving glutathione peroxidase. *J Biol Chem* **272**: 17012-17017.
56. Upchurch, G. R., Jr., G. N. Welch, A. J. Fabian, A. Pigazzi, J. F. Keaney, Jr., and J. Loscalzo. 1997. Stimulation of endothelial nitric oxide production by homocyst(e)ine. *Atherosclerosis* **132**: 177-185.
57. Li, C. X., M. Xia, W. Q. Han, X. X. Li, C. Zhang, K. M. Boini, X. C. Liu, and P. L. Li. 2011. Reversal by growth hormone of homocysteine-induced epithelial-to-mesenchymal transition through membrane raft-redox signaling in podocytes. *Cell Physiol Biochem* **27**: 691-702.
58. Li, C., M. Xia, J. M. Abais, X. Liu, N. Li, K. M. Boini, and P. L. Li. 2013. Protective role of growth hormone against hyperhomocysteinemia-induced glomerular injury. *Naunyn Schmiedebergs Arch Pharmacol* **386**: 551-561.
59. Levine, B., and G. Kroemer. 2008. Autophagy in the pathogenesis of disease. *Cell* **132**: 27-42.
60. Ravikumar, B., S. Sarkar, J. E. Davies, M. Futter, M. Garcia-Arencibia, Z. W. Green-Thompson, M. Jimenez-Sanchez, V. I. Korolchuk, M. Lichtenberg, S. Luo, D. C. Massey, F. M.

- Menzies, K. Moreau, U. Narayanan, M. Renna, F. H. Siddiqi, B. R. Underwood, A. R. Winslow, and D. C. Rubinsztein. 2010. Regulation of mammalian autophagy in physiology and pathophysiology. *Physiol Rev* **90**: 1383-1435.
61. Wirawan, E., T. Vanden Berghe, S. Lippens, P. Agostinis, and P. Vandenabeele. 2012. Autophagy: for better or for worse. *Cell Res* **22**: 43-61.
62. Rubinsztein, D. C., G. Marino, and G. Kroemer. 2011. Autophagy and aging. *Cell* **146**: 682-695.
63. Klionsky, D. J., J. M. Cregg, W. A. Dunn, Jr., S. D. Emr, Y. Sakai, I. V. Sandoval, A. Sibirny, S. Subramani, M. Thumm, M. Veenhuis, and Y. Ohsumi. 2003. A unified nomenclature for yeast autophagy-related genes. *Dev Cell* **5**: 539-545.
64. Levine, B., and D. J. Klionsky. 2004. Development by self-digestion: molecular mechanisms and biological functions of autophagy. *Dev Cell* **6**: 463-477.
65. Reggiori, F., and D. J. Klionsky. 2002. Autophagy in the eukaryotic cell. *Eukaryot Cell* **1**: 11-21.
66. Wang, C. W., and D. J. Klionsky. 2003. The molecular mechanism of autophagy. *Mol Med* **9**: 65-76.
67. Bampton, E. T., C. G. Goemans, D. Niranjana, N. Mizushima, and A. M. Tolkovsky. 2005. The dynamics of autophagy visualized in live cells: from autophagosome formation to fusion with endo/lysosomes. *Autophagy* **1**: 23-36.
68. Chen, Y., and D. J. Klionsky. 2011. The regulation of autophagy - unanswered questions. *J Cell Sci* **124**: 161-170.
69. Criollo, A., J. M. Vicencio, E. Tasdemir, M. C. Maiuri, S. Lavandro, and G. Kroemer. 2007. The inositol trisphosphate receptor in the control of autophagy. *Autophagy* **3**: 350-353.

70. Ghavami, S., M. Eshragi, S. R. Ande, W. J. Chazin, T. Klonisch, A. J. Halayko, K. D. McNeill, M. Hashemi, C. Kerkhoff, and M. Los. 2010. S100A8/A9 induces autophagy and apoptosis via ROS-mediated cross-talk between mitochondria and lysosomes that involves BNIP3. *Cell Res* **20**: 314-331.
71. Hoyer-Hansen, M., L. Bastholm, P. Szyniarowski, M. Campanella, G. Szabadkai, T. Farkas, K. Bianchi, N. Fehrenbacher, F. Elling, R. Rizzuto, I. S. Mathiasen, and M. Jaattela. 2007. Control of macroautophagy by calcium, calmodulin-dependent kinase kinase-beta, and Bcl-2. *Mol Cell* **25**: 193-205.
72. Kim, J. S., T. Nitta, D. Mohuczy, K. A. O'Malley, L. L. Moldawer, W. A. Dunn, Jr., and K. E. Behrns. 2008. Impaired autophagy: A mechanism of mitochondrial dysfunction in anoxic rat hepatocytes. *Hepatology* **47**: 1725-1736.
73. Marino, G., A. F. Fernandez, S. Cabrera, Y. W. Lundberg, R. Cabanillas, F. Rodriguez, N. Salvador-Montoliu, J. A. Vega, A. Germana, A. Fueyo, J. M. Freije, and C. Lopez-Otin. 2010. Autophagy is essential for mouse sense of balance. *J Clin Invest* **120**: 2331-2344.
74. Pankiv, S., T. H. Clausen, T. Lamark, A. Brech, J. A. Bruun, H. Outzen, A. Overvatn, G. Bjorkoy, and T. Johansen. 2007. p62/SQSTM1 binds directly to Atg8/LC3 to facilitate degradation of ubiquitinated protein aggregates by autophagy. *J Biol Chem* **282**: 24131-24145.
75. Scott, R. C., O. Schuldiner, and T. P. Neufeld. 2004. Role and regulation of starvation-induced autophagy in the Drosophila fat body. *Dev Cell* **7**: 167-178.
76. Singh, R., Y. Xiang, Y. Wang, K. Baikati, A. M. Cuervo, Y. K. Luu, Y. Tang, J. E. Pessin, G. J. Schwartz, and M. J. Czaja. 2009. Autophagy regulates adipose mass and differentiation in mice. *J Clin Invest* **119**: 3329-3339.
77. Vellai, T. 2009. Autophagy genes and ageing. *Cell Death Differ* **16**: 94-102.

78. Vessoni, A. T., A. R. Muotri, and O. K. Okamoto. 2012. Autophagy in stem cell maintenance and differentiation. *Stem Cells Dev* **21**: 513-520.
79. Vazquez, P., A. I. Arroba, F. Cecconi, E. J. de la Rosa, P. Boya, and F. de Pablo. 2012. Atg5 and Ambra1 differentially modulate neurogenesis in neural stem cells. *Autophagy* **8**: 187-199.
80. Zhang, J., J. Liu, Y. Huang, J. Y. Chang, L. Liu, W. L. McKeehan, J. F. Martin, and F. Wang. 2012. FRS2alpha-mediated FGF signals suppress premature differentiation of cardiac stem cells through regulating autophagy activity. *Circ Res* **110**: e29-39.
81. Zhang, J., J. Liu, L. Liu, W. L. McKeehan, and F. Wang. 2012. The fibroblast growth factor signaling axis controls cardiac stem cell differentiation through regulating autophagy. *Autophagy* **8**: 690-691.
82. Tra, T., L. Gong, L. P. Kao, X. L. Li, C. Grandela, R. J. Devenish, E. Wolvetang, and M. Prescott. 2011. Autophagy in human embryonic stem cells. *PLoS ONE* **6**: e27485.
83. Mizushima, N., A. Yamamoto, M. Hatano, Y. Kobayashi, Y. Kabeya, K. Suzuki, T. Tokuhiya, Y. Ohsumi, and T. Yoshimori. 2001. Dissection of autophagosome formation using Apg5-deficient mouse embryonic stem cells. *J Cell Biol* **152**: 657-668.
84. Yue, Z., S. Jin, C. Yang, A. J. Levine, and N. Heintz. 2003. Beclin 1, an autophagy gene essential for early embryonic development, is a haploinsufficient tumor suppressor. *Proc Natl Acad Sci U S A* **100**: 15077-15082.
85. Fimia, G. M., A. Stoykova, A. Romagnoli, L. Giunta, S. Di Bartolomeo, R. Nardacci, M. Corazzari, C. Fuoco, A. Ucar, P. Schwartz, P. Gruss, M. Piacentini, K. Chowdhury, and F. Cecconi. 2007. Ambra1 regulates autophagy and development of the nervous system. *Nature* **447**: 1121-1125.

86. Qu, X., Z. Zou, Q. Sun, K. Luby-Phelps, P. Cheng, R. N. Hogan, C. Gilpin, and B. Levine. 2007. Autophagy gene-dependent clearance of apoptotic cells during embryonic development. *Cell* **128**: 931-946.
87. Asanuma, K., I. Tanida, I. Shirato, T. Ueno, H. Takahara, T. Nishitani, E. Kominami, and Y. Tomino. 2003. MAP-LC3, a promising autophagosomal marker, is processed during the differentiation and recovery of podocytes from PAN nephrosis. *FASEB J* **17**: 1165-1167.
88. Boini, K. M., M. Xia, J. Xiong, C. Li, L. P. Payne, and P. L. Li. 2012. Implication of CD38 gene in podocyte epithelial-to-mesenchymal transition and glomerular sclerosis. *J Cell Mol Med* **16**: 1674-1685.
89. Xiong, J., M. Xia, M. Xu, Y. Zhang, J. M. Abais, G. Li, C. R. Riebling, J. K. Ritter, K. M. Boini, and P. L. Li. 2013. Autophagy maturation associated with CD38-mediated regulation of lysosome function in mouse glomerular podocytes. *J Cell Mol Med* **17**: 1598-1607.
90. Liu, F., X. Li, C. Lu, A. Bai, J. Bielawski, A. Bielawska, B. Marshall, P. V. Schoenlein, I. O. Lebedyeva, and K. Liu. 2016. Ceramide activates lysosomal cathepsin B and cathepsin D to attenuate autophagy and induces ER stress to suppress myeloid-derived suppressor cells. *Oncotarget* **7**: 83907-83925.
91. Teixeira, V., T. C. Medeiros, R. Vilaca, J. Ferreira, P. Moradas-Ferreira, and V. Costa. 2016. Ceramide signaling targets the PP2A-like protein phosphatase Sit4p to impair vacuolar function, vesicular trafficking and autophagy in *Isc1p* deficient cells. *Biochim Biophys Acta* **1861**: 21-33.
92. Futerman, A. H., and Y. A. Hannun. 2004. The complex life of simple sphingolipids. *EMBO Rep* **5**: 777-782.

93. Boini, K. M., M. Xia, C. Li, C. Zhang, L. P. Payne, J. M. Abais, J. L. Poklis, P. B. Hylemon, and P. L. Li. 2011. Acid sphingomyelinase gene deficiency ameliorates the hyperhomocysteinemia-induced glomerular injury in mice. *Am J Pathol* **179**: 2210-2219.
94. Boini, K. M., M. Xia, J. M. Abais, M. Xu, C. X. Li, and P. L. Li. 2012. Acid sphingomyelinase gene knockout ameliorates hyperhomocysteinemic glomerular injury in mice lacking cystathionine-beta-synthase. *PLoS ONE* **7**: e45020.
95. Boini, K. M., M. Xia, S. Koka, T. W. Gehr, and P. L. Li. 2016. Instigation of NLRP3 inflammasome activation and glomerular injury in mice on the high fat diet: role of acid sphingomyelinase gene. *Oncotarget* **7**: 19031-19044.
96. Aubin, I., C. P. Adams, S. Opsahl, D. Septier, C. E. Bishop, N. Auge, R. Salvayre, A. Negre-Salvayre, M. Goldberg, J. L. Guenet, and C. Poirier. 2005. A deletion in the gene encoding sphingomyelin phosphodiesterase 3 (Smpd3) results in osteogenesis and dentinogenesis imperfecta in the mouse. *Nat Genet* **37**: 803-805.
97. Guse, A. H. 2012. Linking NAADP to ion channel activity: a unifying hypothesis. *Sci Signal* **5**: pe18.
98. Mullins, C., and J. S. Bonifacino. 2001. The molecular machinery for lysosome biogenesis. *Bioessays* **23**: 333-343.
99. Nojima, H., C. M. Freeman, R. M. Schuster, L. Japtok, B. Kleuser, M. J. Edwards, E. Gulbins, and A. B. Lentsch. 2016. Hepatocyte exosomes mediate liver repair and regeneration via sphingosine-1-phosphate. *J Hepatol* **64**: 60-68.
100. Pankajakshan, D., T. O. Makinde, R. Gaurav, M. Del Core, G. Hatzoudis, I. Pipinos, and D. K. Agrawal. 2012. Successful transfection of genes using AAV-2/9 vector in swine coronary and peripheral arteries. *J Surg Res* **175**: 169-175.

101. Piccin, A., W. G. Murphy, and O. P. Smith. 2007. Circulating microparticles: pathophysiology and clinical implications. *Blood Rev* **21**: 157-171.
102. Schieder, M., K. Rotzer, A. Bruggemann, M. Biel, and C. A. Wahl-Schott. 2010. Characterization of two-pore channel 2 (TPCN2)-mediated Ca²⁺ currents in isolated lysosomes. *J Biol Chem* **285**: 21219-21222.
103. Churchill, G. C., Y. Okada, J. M. Thomas, A. A. Genazzani, S. Patel, and A. Galione. 2002. NAADP mobilizes Ca(2+) from reserve granules, lysosome-related organelles, in sea urchin eggs. *Cell* **111**: 703-708.
104. Kinnear, N. P., C. N. Wyatt, J. H. Clark, P. J. Calcraft, S. Fleischer, L. H. Jeyakumar, G. F. Nixon, and A. M. Evans. 2008. Lysosomes co-localize with ryanodine receptor subtype 3 to form a trigger zone for calcium signalling by NAADP in rat pulmonary arterial smooth muscle. *Cell Calcium* **44**: 190-201.
105. Zhang, F., S. Jin, F. Yi, and P. L. Li. 2009. TRP-ML1 functions as a lysosomal NAADP-sensitive Ca²⁺ release channel in coronary arterial myocytes. *J Cell Mol Med* **13**: 3174-3185.
106. Zhang, F., and P. L. Li. 2007. Reconstitution and characterization of a nicotinic acid adenine dinucleotide phosphate (NAADP)-sensitive Ca²⁺ release channel from liver lysosomes of rats. *J Biol Chem* **282**: 25259-25269.
107. Zhang, F., M. Xia, and P. L. Li. 2010. Lysosome-dependent Ca(2+) release response to Fas activation in coronary arterial myocytes through NAADP: evidence from CD38 gene knockouts. *Am J Physiol Cell Physiol* **298**: C1209-1216.
108. Zhang, F., G. Zhang, A. Y. Zhang, M. J. Koeberl, E. Wallander, and P. L. Li. 2006. Production of NAADP and its role in Ca²⁺ mobilization associated with lysosomes in coronary arterial myocytes. *Am J Physiol Heart Circ Physiol* **291**: H274-282.

109. Dong, X. P., D. Shen, X. Wang, T. Dawson, X. Li, Q. Zhang, X. Cheng, Y. Zhang, L. S. Weisman, M. Delling, and H. Xu. 2010. PI(3,5)P(2) controls membrane trafficking by direct activation of mucolipin Ca(2+) release channels in the endolysosome. *Nat Commun* **1**: 38.
110. Glunde, K., S. E. Guggino, M. Solaiyappan, A. P. Pathak, Y. Ichikawa, and Z. M. Bhujwala. 2003. Extracellular acidification alters lysosomal trafficking in human breast cancer cells. *Neoplasia* **5**: 533-545.
111. Li, X., N. Rydzewski, A. Hider, X. Zhang, J. Yang, W. Wang, Q. Gao, X. Cheng, and H. Xu. 2016. A molecular mechanism to regulate lysosome motility for lysosome positioning and tubulation. *Nat Cell Biol* **18**: 404-417.
112. Shen, D., X. Wang, X. Li, X. Zhang, Z. Yao, S. Dibble, X. P. Dong, T. Yu, A. P. Lieberman, H. D. Showalter, and H. Xu. 2012. Lipid storage disorders block lysosomal trafficking by inhibiting a TRP channel and lysosomal calcium release. *Nat Commun* **3**: 731.
113. Trajkovic, K., A. S. Dhaunchak, J. T. Goncalves, D. Wenzel, A. Schneider, G. Bunt, K. A. Nave, and M. Simons. 2006. Neuron to glia signaling triggers myelin membrane exocytosis from endosomal storage sites. *J Cell Biol* **172**: 937-948.
114. Dong, X. P., X. Wang, D. Shen, S. Chen, M. Liu, Y. Wang, E. Mills, X. Cheng, M. Delling, and H. Xu. 2009. Activating mutations of the TRPML1 channel revealed by proline-scanning mutagenesis. *J Biol Chem* **284**: 32040-32052.
115. Kim, H. J., A. A. Soyombo, S. Tjon-Kon-Sang, I. So, and S. Muallem. 2009. The Ca(2+) channel TRPML3 regulates membrane trafficking and autophagy. *Traffic* **10**: 1157-1167.
116. Lloyd-Evans, E., A. J. Morgan, X. He, D. A. Smith, E. Elliot-Smith, D. J. Sillence, G. C. Churchill, E. H. Schuchman, A. Galione, and F. M. Platt. 2008. Niemann-Pick disease type C1 is

a sphingosine storage disease that causes deregulation of lysosomal calcium. *Nat Med* **14**: 1247-1255.

117. Dell'Angelica, E. C., C. Mullins, S. Caplan, and J. S. Bonifacino. 2000. Lysosome-related organelles. *FASEB J* **14**: 1265-1278.

118. Galione, A. 2006. NAADP, a new intracellular messenger that mobilizes Ca²⁺ from acidic stores. *Biochem Soc Trans* **34**: 922-926.

119. Dong, X. P., X. Cheng, E. Mills, M. Delling, F. Wang, T. Kurz, and H. Xu. 2008. The type IV mucopolipidosis-associated protein TRPML1 is an endolysosomal iron release channel. *Nature* **455**: 992-996.

120. Li, P. L., Y. Zhang, J. M. Abais, J. K. Ritter, and F. Zhang. 2013. Cyclic ADP-Ribose and NAADP in Vascular Regulation and Diseases. *Messenger (Los Angel)* **2**: 63-85.

121. Piccoli, E., M. Nadai, C. M. Caretta, V. Bergonzini, C. Del Vecchio, H. R. Ha, L. Bigler, D. Dal Zoppo, E. Faggin, A. Pettenazzo, R. Orlando, C. Salata, A. Calistri, G. Palu, and A. Baritussio. 2011. Amiodarone impairs trafficking through late endosomes inducing a Niemann-Pick C-like phenotype. *Biochem Pharmacol* **82**: 1234-1249.

122. Bruggemann, A., M. George, M. Klau, M. Beckler, J. Steindl, J. C. Behrends, and N. Fertig. 2003. High quality ion channel analysis on a chip with the NPC technology. *Assay Drug Dev Technol* **1**: 665-673.

123. Schieder, M., K. Rotzer, A. Bruggemann, M. Biel, and C. Wahl-Schott. 2010. Planar patch clamp approach to characterize ionic currents from intact lysosomes. *Sci Signal* **3**: pl3.

124. Cang, C., Y. Zhou, B. Navarro, Y. J. Seo, K. Aranda, L. Shi, S. Battaglia-Hsu, I. Nissim, D. E. Clapham, and D. Ren. 2013. mTOR regulates lysosomal ATP-sensitive two-pore Na⁽⁺⁾ channels to adapt to metabolic state. *Cell* **152**: 778-790.

125. Kostyuk, P. G., O. A. Krishtal, and V. I. Pidoplichko. 1975. Effect of internal fluoride and phosphate on membrane currents during intracellular dialysis of nerve cells. *Nature* **257**: 691-693.
126. Moeller, M. J., I. A. Kovari, and L. B. Holzman. 2000. Evaluation of a new tool for exploring podocyte biology: mouse *Nphs1* 5' flanking region drives LacZ expression in podocytes. *J Am Soc Nephrol* **11**: 2306-2314.
127. Savin, V. J., R. Sharma, H. B. Lovell, and D. J. Welling. 1992. Measurement of albumin reflection coefficient with isolated rat glomeruli. *J Am Soc Nephrol* **3**: 1260-1269.
128. Savin, V. J., and D. A. Terreros. 1981. Filtration in single isolated mammalian glomeruli. *Kidney Int* **20**: 188-197.
129. Fan, F., C. C. Chen, J. Zhang, C. M. Schreck, E. A. Roman, J. M. Williams, T. Hirata, M. Sharma, D. A. Beard, V. J. Savin, and R. J. Roman. 2015. Fluorescence dilution technique for measurement of albumin reflection coefficient in isolated glomeruli. *Am J Physiol Renal Physiol* **309**: F1049-1059.
130. Xia, M., S. M. Conley, G. Li, P. L. Li, and K. M. Boini. 2014. Inhibition of hyperhomocysteinemia-induced inflammasome activation and glomerular sclerosis by NLRP3 gene deletion. *Cell Physiol Biochem* **34**: 829-841.
131. Abais, J. M., M. Xia, G. Li, T. W. Gehr, K. M. Boini, and P. L. Li. 2014. Contribution of endogenously produced reactive oxygen species to the activation of podocyte NLRP3 inflammasomes in hyperhomocysteinemia. *Free Radic Biol Med* **67**: 211-220.
132. Raij, L., S. Azar, and W. Keane. 1984. Mesangial immune injury, hypertension, and progressive glomerular damage in Dahl rats. *Kidney Int* **26**: 137-143.

133. Bitto, A., C. A. Lerner, T. Nacarelli, E. Crowe, C. Torres, and C. Sell. 2014. P62/SQSTM1 at the interface of aging, autophagy, and disease. *Age (Dordr)* **36**: 9626.
134. Bao, J. X., M. Xia, J. L. Poklis, W. Q. Han, C. Brimson, and P. L. Li. 2010. Triggering role of acid sphingomyelinase in endothelial lysosome-membrane fusion and dysfunction in coronary arteries. *Am J Physiol Heart Circ Physiol* **298**: H992-H1002.
135. Li, X., W. Q. Han, K. M. Boini, M. Xia, Y. Zhang, and P. L. Li. 2013. TRAIL death receptor 4 signaling via lysosome fusion and membrane raft clustering in coronary arterial endothelial cells: evidence from ASM knockout mice. *J Mol Med (Berl)* **91**: 25-36.
136. Li, X., M. Xu, A. L. Pitzer, M. Xia, K. M. Boini, P. L. Li, and Y. Zhang. 2014. Control of autophagy maturation by acid sphingomyelinase in mouse coronary arterial smooth muscle cells: protective role in atherosclerosis. *J Mol Med (Berl)* **92**: 473-485.
137. Alvarez-Erviti, L., Y. Seow, A. H. Schapira, C. Gardiner, I. L. Sargent, M. J. Wood, and J. M. Cooper. 2011. Lysosomal dysfunction increases exosome-mediated alpha-synuclein release and transmission. *Neurobiol Dis* **42**: 360-367.
138. Vingtdeux, V., M. Hamdane, A. Loyens, P. Gele, H. Drobeck, S. Begard, M. C. Galas, A. Delacourte, J. C. Beauvillain, L. Buee, and N. Sergeant. 2007. Alkalizing drugs induce accumulation of amyloid precursor protein by-products in luminal vesicles of multivesicular bodies. *J Biol Chem* **282**: 18197-18205.
139. Hasegawa, T., M. Konno, T. Baba, N. Sugeno, A. Kikuchi, M. Kobayashi, E. Miura, N. Tanaka, K. Tamai, K. Furukawa, H. Arai, F. Mori, K. Wakabayashi, M. Aoki, Y. Itoyama, and A. Takeda. 2011. The AAA-ATPase VPS4 regulates extracellular secretion and lysosomal targeting of alpha-synuclein. *PLoS ONE* **6**: e29460.

140. Samie, M., X. Wang, X. Zhang, A. Goschka, X. Li, X. Cheng, E. Gregg, M. Azar, Y. Zhuo, A. G. Garrity, Q. Gao, S. Slaugenhaupt, J. Pickel, S. N. Zolov, L. S. Weisman, G. M. Lenk, S. Titus, M. Bryant-Geneviev, N. Southall, M. Juan, M. Ferrer, and H. Xu. 2013. A TRP channel in the lysosome regulates large particle phagocytosis via focal exocytosis. *Dev Cell* **26**: 511-524.
141. Zhang, F., M. Xu, W. Q. Han, and P. L. Li. 2011. Reconstitution of lysosomal NAADP-TRP-ML1 signaling pathway and its function in TRP-ML1(-/-) cells. *Am J Physiol Cell Physiol* **301**: C421-430.
142. Zhang, Y., M. Xu, M. Xia, X. Li, K. M. Boini, M. Wang, E. Gulbins, P. H. Ratz, and P. L. Li. 2014. Defective autophagosome trafficking contributes to impaired autophagic flux in coronary arterial myocytes lacking CD38 gene. *Cardiovasc Res* **102**: 68-78.
143. Regele, H. M., E. Fillipovic, B. Langer, H. Poczewki, I. Kraxberger, R. E. Bittner, and D. Kerjaschki. 2000. Glomerular expression of dystroglycans is reduced in minimal change nephrosis but not in focal segmental glomerulosclerosis. *J Am Soc Nephrol* **11**: 403-412.
144. Barisoni, L., H. W. Schnaper, and J. B. Kopp. 2007. A proposed taxonomy for the podocytopathies: a reassessment of the primary nephrotic diseases. *Clin J Am Soc Nephrol* **2**: 529-542.
145. Linares, J. F., R. Amanchy, K. Greis, M. T. Diaz-Meco, and J. Moscat. 2011. Phosphorylation of p62 by cdk1 controls the timely transit of cells through mitosis and tumor cell proliferation. *Mol Cell Biol* **31**: 105-117.
146. Voutsadakis, I. A. 2012. Ubiquitination and the Ubiquitin-Proteasome System as regulators of transcription and transcription factors in epithelial mesenchymal transition of cancer. *Tumour Biol* **33**: 897-910.

147. Janda, E., M. Nevolo, K. Lehmann, J. Downward, H. Beug, and M. Grieco. 2006. Raf plus TGFbeta-dependent EMT is initiated by endocytosis and lysosomal degradation of E-cadherin. *Oncogene* **25**: 7117-7130.
148. Johansen, T., and T. Lamark. 2011. Selective autophagy mediated by autophagic adapter proteins. *Autophagy* **7**: 279-296.
149. Matsumoto, G., K. Wada, M. Okuno, M. Kurosawa, and N. Nukina. 2011. Serine 403 phosphorylation of p62/SQSTM1 regulates selective autophagic clearance of ubiquitinated proteins. *Mol Cell* **44**: 279-289.
150. Komatsu, M., S. Waguri, M. Koike, Y. S. Sou, T. Ueno, T. Hara, N. Mizushima, J. Iwata, J. Ezaki, S. Murata, J. Hamazaki, Y. Nishito, S. Iemura, T. Natsume, T. Yanagawa, J. Uwayama, E. Warabi, H. Yoshida, T. Ishii, A. Kobayashi, M. Yamamoto, Z. Yue, Y. Uchiyama, E. Kominami, and K. Tanaka. 2007. Homeostatic levels of p62 control cytoplasmic inclusion body formation in autophagy-deficient mice. *Cell* **131**: 1149-1163.
151. Li, J., B. Yang, Q. Zhou, Y. Wu, D. Shang, Y. Guo, Z. Song, Q. Zheng, and J. Xiong. 2013. Autophagy promotes hepatocellular carcinoma cell invasion through activation of epithelial-mesenchymal transition. *Carcinogenesis* **34**: 1343-1351.
152. Lv, Q., F. Hua, and Z. W. Hu. 2012. DEDD, a novel tumor repressor, reverses epithelial-mesenchymal transition by activating selective autophagy. *Autophagy* **8**: 1675-1676.
153. Lv, Q., W. Wang, J. Xue, F. Hua, R. Mu, H. Lin, J. Yan, X. Lv, X. Chen, and Z. W. Hu. 2012. DEDD interacts with PI3KC3 to activate autophagy and attenuate epithelial-mesenchymal transition in human breast cancer. *Cancer Res* **72**: 3238-3250.
154. Moscat, J., and M. T. Diaz-Meco. 2012. p62: a versatile multitasker takes on cancer. *Trends Biochem Sci* **37**: 230-236.

155. Moscat, J., and M. T. Diaz-Meco. 2009. p62 at the crossroads of autophagy, apoptosis, and cancer. *Cell* **137**: 1001-1004.
156. Nezis, I. P., and H. Stenmark. 2012. p62 at the interface of autophagy, oxidative stress signaling, and cancer. *Antioxid Redox Signal* **17**: 786-793.
157. Inami, Y., S. Waguri, A. Sakamoto, T. Kouno, K. Nakada, O. Hino, S. Watanabe, J. Ando, M. Iwadate, M. Yamamoto, M. S. Lee, K. Tanaka, and M. Komatsu. 2011. Persistent activation of Nrf2 through p62 in hepatocellular carcinoma cells. *J Cell Biol* **193**: 275-284.
158. Malumbres, M., and M. Barbacid. 2005. Mammalian cyclin-dependent kinases. *Trends Biochem Sci* **30**: 630-641.
159. Nigg, E. A. 2001. Mitotic kinases as regulators of cell division and its checkpoints. *Nat Rev Mol Cell Biol* **2**: 21-32.
160. Wang, Z., M. Fan, D. Candas, T. Q. Zhang, L. Qin, A. Eldridge, S. Wachsmann-Hogiu, K. M. Ahmed, B. A. Chromy, D. Nantajit, N. Duru, F. He, M. Chen, T. Finkel, L. S. Weinstein, and J. J. Li. 2014. Cyclin B1/Cdk1 coordinates mitochondrial respiration for cell-cycle G2/M progression. *Dev Cell* **29**: 217-232.
161. Ye, X., and R. D. Sloboda. 1997. Molecular characterization of p62, a mitotic apparatus protein required for mitotic progression. *J Biol Chem* **272**: 3606-3614.
162. Xu, M., X. X. Li, Y. Chen, A. L. Pitzer, Y. Zhang, and P. L. Li. 2014. Enhancement of dynein-mediated autophagosome trafficking and autophagy maturation by ROS in mouse coronary arterial myocytes. *J Cell Mol Med* **18**: 2165-2175.
163. Han, W. Q., M. Xia, C. Zhang, F. Zhang, M. Xu, N. J. Li, and P. L. Li. 2011. SNARE-mediated rapid lysosome fusion in membrane raft clustering and dysfunction of bovine coronary arterial endothelium. *Am J Physiol Heart Circ Physiol* **301**: H2028-2037.

164. Han, W. Q., M. Xia, M. Xu, K. M. Boini, J. K. Ritter, N. J. Li, and P. L. Li. 2012. Lysosome fusion to the cell membrane is mediated by the dysferlin C2A domain in coronary arterial endothelial cells. *J Cell Sci* **125**: 1225-1234.
165. Jahreiss, L., F. M. Menzies, and D. C. Rubinsztein. 2008. The itinerary of autophagosomes: from peripheral formation to kiss-and-run fusion with lysosomes. *Traffic* **9**: 574-587.
166. Yamamoto, M., S. O. Suzuki, and M. Himeno. 2010. The effects of dynein inhibition on the autophagic pathway in glioma cells. *Neuropathology* **30**: 1-6.
167. Xu, M., X. X. Li, J. Xiong, M. Xia, E. Gulbins, Y. Zhang, and P. L. Li. 2013. Regulation of autophagic flux by dynein-mediated autophagosomes trafficking in mouse coronary arterial myocytes. *Biochim Biophys Acta* **1833**: 3228-3236.
168. Gatt, S. 1963. Enzymic Hydrolysis and Synthesis of Ceramides. *J Biol Chem* **238**: 3131-3133.
169. Bernardo, K., R. Hurwitz, T. Zenk, R. J. Desnick, K. Ferlinz, E. H. Schuchman, and K. Sandhoff. 1995. Purification, characterization, and biosynthesis of human acid ceramidase. *J Biol Chem* **270**: 11098-11102.
170. Sugita, M., J. T. Dulaney, and H. W. Moser. 1972. Ceramidase deficiency in Farber's disease (lipogranulomatosis). *Science* **178**: 1100-1102.
171. Park, J. H., and E. H. Schuchman. 2006. Acid ceramidase and human disease. *Biochim Biophys Acta* **1758**: 2133-2138.
172. Li, C. M., J. H. Park, C. M. Simonaro, X. He, R. E. Gordon, A. H. Friedman, D. Ehleiter, F. Paris, K. Manova, S. Hepbildikler, Z. Fuks, K. Sandhoff, R. Kolesnick, and E. H. Schuchman. 2002. Insertional mutagenesis of the mouse acid ceramidase gene leads to early embryonic

lethality in homozygotes and progressive lipid storage disease in heterozygotes. *Genomics* **79**: 218-224.

173. Okino, N., X. He, S. Gatt, K. Sandhoff, M. Ito, and E. H. Schuchman. 2003. The reverse activity of human acid ceramidase. *J Biol Chem* **278**: 29948-29953.

174. Williams, K. J., and I. Tabas. 1995. The response-to-retention hypothesis of early atherogenesis. *Arterioscler Thromb Vasc Biol* **15**: 551-561.

175. Ueda, N., G. P. Kaushal, and S. V. Shah. 2000. Apoptotic mechanisms in acute renal failure. *Am J Med* **108**: 403-415.

176. Coroneos, E., M. Martinez, S. McKenna, and M. Kester. 1995. Differential regulation of sphingomyelinase and ceramidase activities by growth factors and cytokines. Implications for cellular proliferation and differentiation. *J Biol Chem* **270**: 23305-23309.

177. Yi, F., A. Y. Zhang, N. Li, R. W. Muh, M. Fillet, A. F. Renert, and P. L. Li. 2006. Inhibition of ceramide-redox signaling pathway blocks glomerular injury in hyperhomocysteinemic rats. *Kidney Int* **70**: 88-96.

178. Boini, K. M., C. Zhang, M. Xia, J. L. Poklis, and P. L. Li. 2010. Role of sphingolipid mediator ceramide in obesity and renal injury in mice fed a high-fat diet. *J Pharmacol Exp Ther* **334**: 839-846.

179. Churg, J., R. Habib, and R. H. White. 1970. Pathology of the nephrotic syndrome in children: a report for the International Study of Kidney Disease in Children. *Lancet* **760**: 1299-1302.

180. Shalhoub, R. J. 1974. Pathogenesis of lipid nephrosis: a disorder of T-cell function. *Lancet* **2**: 556-560.

181. Vats, A., A. Nayak, D. Ellis, P. S. Randhawa, D. N. Finegold, K. L. Levinson, and R. E. Ferrell. 2000. Familial nephrotic syndrome: clinical spectrum and linkage to chromosome 19q13. *Kidney Int* **57**: 875-881.
182. Winn, M. P., P. J. Conlon, K. L. Lynn, M. K. Farrington, T. Creazzo, A. F. Hawkins, N. Daskalakis, S. Y. Kwan, S. Ebersviller, J. L. Burchette, M. A. Pericak-Vance, D. N. Howell, J. M. Vance, and P. B. Rosenberg. 2005. A mutation in the TRPC6 cation channel causes familial focal segmental glomerulosclerosis. *Science* **308**: 1801-1804.
183. Izzedine, H., I. Brocheriou, B. Eymard, M. Le Charpentier, N. B. Romero, G. Lenaour, E. Bourry, and G. Deray. 2006. Loss of podocyte dysferlin expression is associated with minimal change nephropathy. *Am J Kidney Dis* **48**: 143-150.
184. Schmitz-Peiffer, C., D. L. Craig, and T. J. Biden. 1999. Ceramide generation is sufficient to account for the inhibition of the insulin-stimulated PKB pathway in C2C12 skeletal muscle cells pretreated with palmitate. *J Biol Chem* **274**: 24202-24210.
185. Summers, S. A., L. A. Garza, H. Zhou, and M. J. Birnbaum. 1998. Regulation of insulin-stimulated glucose transporter GLUT4 translocation and Akt kinase activity by ceramide. *Mol Cell Biol* **18**: 5457-5464.
186. Stratford, S., K. L. Hoehn, F. Liu, and S. A. Summers. 2004. Regulation of insulin action by ceramide: dual mechanisms linking ceramide accumulation to the inhibition of Akt/protein kinase B. *J Biol Chem* **279**: 36608-36615.
187. Powell, D. J., E. Hajduch, G. Kular, and H. S. Hundal. 2003. Ceramide disables 3-phosphoinositide binding to the pleckstrin homology domain of protein kinase B (PKB)/Akt by a PKCzeta-dependent mechanism. *Mol Cell Biol* **23**: 7794-7808.

188. Adams, J. M., 2nd, T. Pratipanawatr, R. Berria, E. Wang, R. A. DeFronzo, M. C. Sullards, and L. J. Mandarino. 2004. Ceramide content is increased in skeletal muscle from obese insulin-resistant humans. *Diabetes* **53**: 25-31.
189. Turinsky, J., D. M. O'Sullivan, and B. P. Bayly. 1990. 1,2-Diacylglycerol and ceramide levels in insulin-resistant tissues of the rat in vivo. *J Biol Chem* **265**: 16880-16885.
190. Straczkowski, M., I. Kowalska, A. Nikolajuk, S. Dzienis-Straczkowska, I. Kinalska, M. Baranowski, M. Zendzian-Piotrowska, Z. Brzezinska, and J. Gorski. 2004. Relationship between insulin sensitivity and sphingomyelin signaling pathway in human skeletal muscle. *Diabetes* **53**: 1215-1221.
191. Dobrzyn, A., and J. Gorski. 2002. Ceramides and sphingomyelins in skeletal muscles of the rat: content and composition. Effect of prolonged exercise. *Am J Physiol Endocrinol Metab* **282**: E277-285.
192. Helge, J. W., A. Dobrzyn, B. Saltin, and J. Gorski. 2004. Exercise and training effects on ceramide metabolism in human skeletal muscle. *Exp Physiol* **89**: 119-127.
193. Dobrzyn, A., M. Knapp, and J. Gorski. 2004. Effect of acute exercise and training on metabolism of ceramide in the heart muscle of the rat. *Acta Physiol Scand* **181**: 313-319.
194. Chavez, J. A., W. L. Holland, J. Bar, K. Sandhoff, and S. A. Summers. 2005. Acid ceramidase overexpression prevents the inhibitory effects of saturated fatty acids on insulin signaling. *J Biol Chem* **280**: 20148-20153.

VITA

1. PERSONAL INFORMATION:

1.1 Name: Guangbi Li

1.2 Birthday: 01/21/1991, Birth Place: Wuhan, Hubei, China

1.3 Home Address:

300 West Franklin Street, 1103E

Richmond, VA 23220

Phone: 804-709-7146

1.4 Office Address:

MMRB, 3rd Floor, Room 3055

1220 East Broad Street

Richmond, VA 23298

Phone: 804-828-4791

Fax: 804-828-4794

E-mail: guangbi.li@vcuhealth.org

2. EDUCATION:

2009–2013: B.A. Bioengineering, Wuchang Institute of Science and Technology

2014-2015: M.S. Pharmacology & Toxicology, VCU

2015- : Ph.D. Pharmacology & Toxicology, VCU

3. ORAL PRESENTATION:

Pannexin-1 channel activity and associated ATP release in podocytes in response to adipokines.
(04/26/2017 FASEB meeting 2017).

4. PUBLICATIONS:

4.1 Published Research Papers:

- 1 Xiong J, Xia M, Xu M, Zhang Y, Abais JM, Li G, Riebling CR, Ritter JK, Boini KM, Li PL. Autophagy maturation associated with CD38-mediated regulation of lysosome function in mouse glomerular podocytes. *J Cell Mol Med.* 17(12):1598-607, 2013. PMCID: PMC3914646
- 2 Abais JM, Xia M, Li G, Gehr T, Boini KM, Li PL. Contribution of endogenously produced reactive oxygen species to the activation of podocyte NLRP3 inflammasomes in hyperhomocysteinemia. *Free Radic Biol Med.* 16;67C:211-220, 2014. PMCID: PMC3945111
- 3 Boini KM, Xia M, Abais JM, Li G, Pitzer AL, Gehr TW, Zhang Y, Li PL. Activation of inflammasomes in podocyte injury of mice on the high fat diet: effects of ASC gene deletion and silencing. *Biochim Biophys Acta.* 1843(5):836-45, 2014. PMCID: PMC3986924
- 4 Abais JM, Xia M, Li G, Chen Y, Conley SM, Gehr TW, Boini KM, Li PL. Nod-like receptor protein 3 (NLRP3) inflammasome activation and podocyte injury via

- thioredoxin-interacting protein during hyperhomocysteinemia. *J Biol Chem.* 289(39):27159-27168, 2014. PMID: PMC4175351
- 5 Xia M, Conley SM, Li G, Li PL, Boini KM. Inhibition of hyperhomocysteinemia-induced inflammasome activation and glomerular sclerosis by NLRP3 gene deletion. *Cell Physiol Biochem.* 34(3):829-841, 2014. PMID: PMC4864609
- 6 Li G, Li CX, Xia M, Ritter JK, Gehr TW, Boini KM, Li PL. Enhanced epithelial-to-mesenchymal transition associated with lysosome dysfunction in podocytes: role of p62/Sequestosome 1 as a signaling hub. *Cell Physiol Biochem.* 35(5):1773-86, 2015. PMID: PMC4391077
- 7 Ritter JK, Li G, Xia M, Boini K. Anandamide and its metabolites: what are their roles in the kidney? *Front Biosci (Schol Ed).* 8:264-77, 2016. PMID: 27100705
- 8 Li G, Xia M, Abais JM, Boini K, Li PL, Ritter JK. Protective action of anandamide and its COX-2 metabolite against homocysteine-induced NLRP3 inflammasome activation and injury in podocytes. *J Pharmacol Exp Ther.* 358(1):61-70, 2016. PMID: PMC4931881
- 9 Bao J, Li G, Yuan X, Gulbins E, Li PL. Contribution of p62 to phenotype transition of coronary arterial myocytes with defective autophagy. *Cell Physiol Biochem.* 41(2):555-568, 2017. PMID: 28214847
- 10 Li G, Chen Z, Zhang Q, Abais JM, Conley SM, Gehr TW, Ritter JK, Li PL. NLRP3 inflammasome as a novel target for docosahexaenoic acid metabolites to abrogate glomerular injury. *J Lipid Res.* 58(6):1080-1090, 2017. PMID: PMC5454504
[Available on 2018-06-01]

- 11 Ahmad A, Daneva Z, Li G, Dempsey S, Li N, Poklis JL, Li PL, Ritter J. Stimulation of diuresis and salt excretion by renomedullary infusion of a dual inhibitor of fatty acid amide hydrolase and monoacylglycerol lipase. *Am J Physiol Renal Physiol.* 313(5):F1068-F1076, 2017. PMID: 28768662
- 12 Bhat O, Yuan X, Li G, Lee R, Li PL. Sphingolipids and redox signaling in renal regulation and chronic kidney diseases. *Antioxid Redox Signal.* 2017. PMID: 29121774

4.2 Papers in preparation:

1. Li G, Zhang Q, Kidd JM, Gehr TW, Ritter JK, Li PL. Inhibition of pannexin-1 channel activity in podocytes by adiponectin: role of acid ceramidase activation.
2. Li G, Lohner H, Dempsey S, Yuan X, Zhang Q, Hong J, Poklis J, Ritter JK, Li PL. Podocyte-specific deletion of *Asah1* gene produced podocytopathy without sclerotic pathology: a potential mouse model for steroid-insensitive minimal change disease.

4.3 Abstracts:

1. Boini KM, Xia M, Li G, Abais JM and Li PL. Enhanced dedifferentiation and injury in mouse podocytes lacking CD38 gene. *FASEB J* 28:691.4, 2014
2. Bao JX, Li G, Li X, Pitzer A, Zhang Y, Li PL. Contribution of p62 to the phenotype transition of coronary arterial myocytes from mice lacking CD38 gene. *The FASEB Journal.* 29:783.11. 2015.
3. Li G, Li CX, Xia M, Abais JM, Boini KM, Ritter JK, Li PL. Enhanced epithelial-to-mesenchymal transition associated with lysosome dysfunction in podocytes: role of p62/Sequestosome 1 as a signaling hub. *The FASEB Journal.* 29:938.9. 2015.

4. Boini KM, Xia M, Conley SM, Li G, Gehr TW, Li PL. Prevention of high fat-induced podocyte injury and glomerular sclerosis in mice lacking Nod-like receptor protein 3: role of inflammasome extinction. *The FASEB Journal*. 29:808.12, 2015.
5. Boini KM, Xia M, Conley SM, Li G, Koka S, Gehr TW, Li PL. Contribution of high mobility group box 1 to hyperhomocysteinemia-induced podocyte injury and glomerular sclerosis. *Hypertension*. 66: AP017, 2015.
6. Conley SM, Chen Z, Li G, Gehr TW, Boini KM, Li PL. NLRP3 inflammasome as a novel target for docosahexaenoic acid and its metabolites to abrogate glomerular injury during hyperhomocysteinemia. *The FASEB Journal*. 30:701.1. 2016.
7. Xia M, Li G, Conley SM, Meng N, Boini KM, Ritter JK, Li PL. Prostamide-mediated protective action of anandamide on Nlrp3 inflammasome activation in glomeruli of mice with hyperhomocysteinemia. *The FASEB Journal*. 30:739.14. 2016.
8. Li G, Zhang Q, Ritter JK, Li PL. Pannexin-1 channel activity and associated ATP release in podocytes in response to adipokines. *The FASEB Journal*. 31:991.9. 2017.
9. Li G, Boini KM, Gehr TW, Li PL. Albuminuria and Podocytopathy Induced by Podocyte-Specific Deletion of Acid Ceramidase α Subunit. *Am Soc Nephrol*. 2017.